COMPUTATIONAL MECHANISTIC STUDIES ON THE TRANSITION METAL CATALYZED ACTIVATION OF CARBON DIOXIDE

Rositha Kuniyil

UNIVERSITAT ROVIRA i VIRGILI

Computational Mechanistic Studies on the Transition Metal Catalyzed Activation of Carbon Dioxide

ROSITHA KUNIYIL

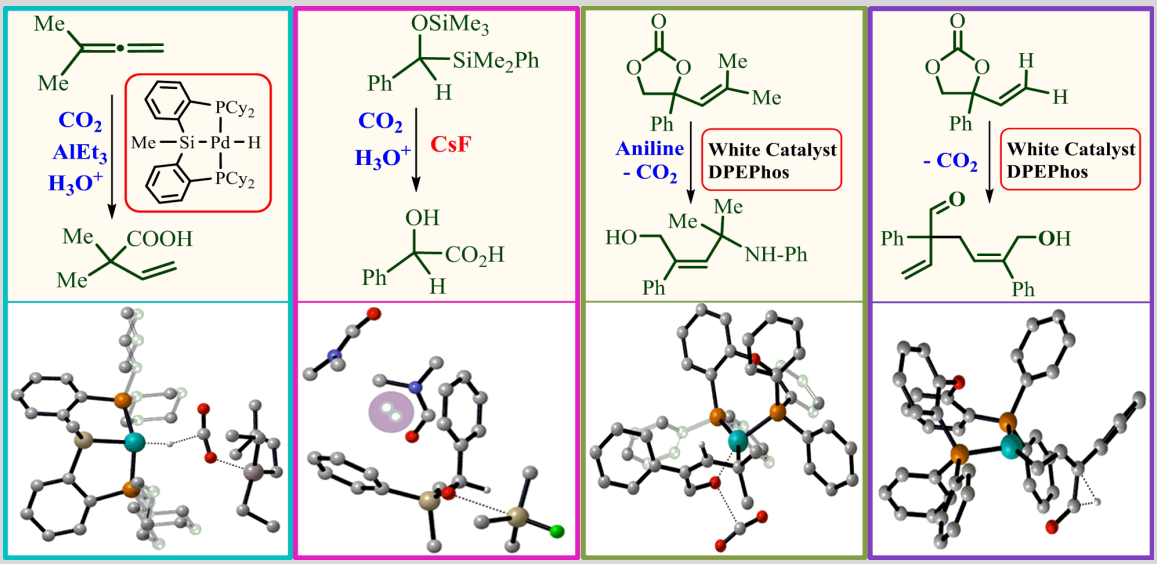

DOCTORAL THESIS
2017

Rositha Kuniyil

Computational Mechanistic Studies on the Transition Metal Catalyzed Activation of Carbon Dioxide

DOCTORAL THESIS

Supervised by

Prof. Feliu Maseras

Institute of Chemical Research of Catalonia

Tarragona

2017

ICIQ- Institut Català d'Investigació Química

Avgda, Països Catalans 16,

43007 Tarragona (Spain)

Prof. Feliu Maseras, Group Leader at the Institute of Chemical Research of Catalonia,

I STATE that the present study, entitled "Computational Mechanistic Studies on the Transition Metal Catalyzed Activation of Carbon Dioxide", presented by Rositha Kuniyil for the award of the degree of Doctor, has been carried out under my supervision in my group at the Institute of Chemical Research of Catalonia and that it fulfils all the requirements to be eligible for the International Doctor Distinction

Tarragona, September 27, 2017

Doctoral Thesis Supervisor

Prof. Feliu Maseras

Acknowledgement

The last five years of my stay in ICIQ as a graduate research student has indeed been a memorable and pleasant experience in my life. I would like to acknowledge and extend my heartfelt gratitude to the following persons who have made the completion of this research work possible.

I would like to first thank my supervisor Prof. Feliu Maseras for being my mentor, guide and co-worker. He has played different roles at different times and helped me in learning different aspects of computational chemistry. He has always shown confidence in my work, which has helped me in moving ahead in difficult times. His passion for research, belief in his students, commitment to his work, and a desire for perfection have inspired me and I have tried to imbibe some of these qualities and would continue to do so in every aspect of my future endeavors. I would also like to acknowledge ICIQ for providing excellent research facilities and great infrastructure, without which the thesis would not have taken the present form. I am also grateful to Spanish ministry for providing me the FPU fellowship for last 4 years. Many thanks for Prof. Nuria Lopez and Prof. Carles Bo for their advice and kindness. I will never forget the help and support which has been provided by Nuria Vendrell and Martin Gumbau during my stay here.They both have made my life much easier in these 4 years.

I am lucky to meet many colleagues at ICIQ during my PhD years. They have helped me tremendously during my stay. First I would like to thank Dr. Maria Besora, who has been extremely kind in sparing her precious time to help and support me. I specially thank Victor, Ignacio, Mauro, Angel, Adiran and Shaofei for all the help they have provided during my entire stay here. Also I extend my sincere gratitude towards rodrigo and miquel for listening to me and helping me to confront the difficult situations. Thanks are extended to the past members of our lab Max, Guillem, Luca and Charles.

I would like to thank CARISMA-COST organization for providing me the fellowship for my short stay visit at Heriot-Watt University. I

would like to express my heartfelt thankfulness to Prof. Stuart Macgregor for his hospitality during my entire stay in his group during winter 2015. Those 3 months were a substancial learning period for me and got to meet great personalities. In particular Tobi, Nasir, Nick and Dave for helping me with everything while I was there and for sharing good times during my stay.

I will be always greatful for Prof. Arjan Kleij and Dr.Wusheng Guo for the awesome collaboration work. I have always been motivated by the enthusiasm and passion of both of them towards their work.

I have been fortunate enough to be a part of the computational chemistry group at IIT Bombay for my master´s thesis where I have learned the basics of computational chemistry. I am truly indebted to Prof. R. B. Sunoj for giving all the motivation, freedom and guidance during my stay there. Words are beyond to express my thanks towards each member in that lab. Garima has helped me in several ways, for which I am extremely grateful to her. I always cherish the moment I spend with Athira, Dilna, Nithya, Naidu, Bhaskar, Anju, Hemanth, Akhilesh, Rajeev, Vibin and Abhishek at IIT Bombay. Discussions with them on scientific issues have been helpful for my research work in several ways

I would like to express my gratitude to my teachers Prof. Basheer and Ashraf for all the inspiration to pursue a career in science.

I was always under the impression that words are sufficient to express one'e gratitude. However, I really feel at loss of words to thank my mom, dad and grandma. I owe them my entire life and whatever little I have been able to achieve till now. While, my parents helped me to begin my graduate studies, Noufal provided unconditional support in completing this journey and start a new one. I am fortunate to have a life partner who is so passionate about science, understand and appreciates my research and encourages me to work toward my future endeavors.

Lastly, I would like to thank God Almighty for pouring His kindness on me throughout my life.

Table of Contents

List of Figures

List of Schemes

List of Tables

Abstract

The activation and conversion of carbon dioxide into organic products have attracted researchers over the years despite the high thermodynamical stability and kinetical inertness of this molecule. Although the use of CO_2 as a chemical feedstock is unlikely to reduce its atmospheric concentration significantly, it may provide access to high-value products from a sustainable and green source. The achievements over the past ten years in this field of transition metal-catalyzed activation of CO_2 are remarkable. With the rise of new synthetic strategies for the CO_2 activation, comes the need for mechanistic studies which can help the rationalization of the outcomes and thus enable improvements in the design of future reaction schemes. In this regard, computational chemistry has proven over time to be a powerful tool to gain mechanistic information. In particular the computation of reaction pathways using Density Functional Theory (DFT) methods is an established method for mechanistic elucidation of regio- and stereoselective reactions.

In this thesis we set out to study the reaction mechanism for a number of transition metal-catalyzed reactions related to the activation of carbon dioxide. We chose a few landmark carboxylation reactions and also the conversion of cyclic carbonates, which are one of the important initial products from CO_2 activation. We applied DFT methods combined with tools such as microkinetic modeling to clarify the mechanisms. A detailed background for this work can be found in chapter 1, where we present an overview of the progress that has been made in the area of the transition metal catalyzed activation of carbon dioxide including a few of the previous DFT-based studies. Chapter 2 describes the theoretical tools used throughout the thesis.

In chapter 3, the reaction mechanism of palladium-catalyzed allene carboxylation reaction was studied. The insertion of allene and CO_2 with the assistance of $AlEt_3$ is elucidated. The role of $AlEt_3$ in the system beyond transmetallating agent is addressed and explained.

In chapter 4, we studied the reaction mechanism of carbon dioxide with siloxy silane. The importance of the presence of the seemingly innocent counterions in reaction mechanism was explained. The interaction of the cationic counterions with the aprotic solvent was also found to play a role.

In chapter 5, we studied two reactions of cyclic vinyl carbonates involving a decarboxylative approach catalyzed by palladium complexes. In the first part, we analyzed the conversion of cyclic vinyl carbonates to allylic amines by using aniline as the nucleophile. The stereocontrolling transition states were examined and the selectivity of the process was found to depend on the formation of a six-membered palladacyclic intermediate. In the second part of chapter 5 we studied the behavior of the same catalytic system in the absence of the nucleophilic amine. It was found that the cyclic carbonate reactant can generate a nucleophilic intermediate in situ that can undergo a similar reactivity. Two different products, containing one or two units of reactant can be formed, and we were able to reproduce the selectivity of the process with the use of DFT calculations and microkinetic modeling.

Chapter 1

Introduction

1.1 Carbon Dioxide

Carbon dioxide, the most oxidized form of carbon, is thermodynamically stable and kinetically inert. It is a colourless odourless gas consisting of a carbon atom covalently bound to two oxygen atoms. It is a linear molecule with 16 valence electrons. It does not have a dipole moment due to its symmetry, but the two C-O bonds are polarized. The two oxygen atoms are nucleophilic and the carbon atom is electrophilic. Although the molecule is quite inert, its chemistry is mostly dominated by the electrophilicity of its carbon center. It is a weak electrophile, with a mild affinity toward nucleophiles and electron-donating reagents. There are three resonance structures possible for CO_2 as shown in Figure 1.1.

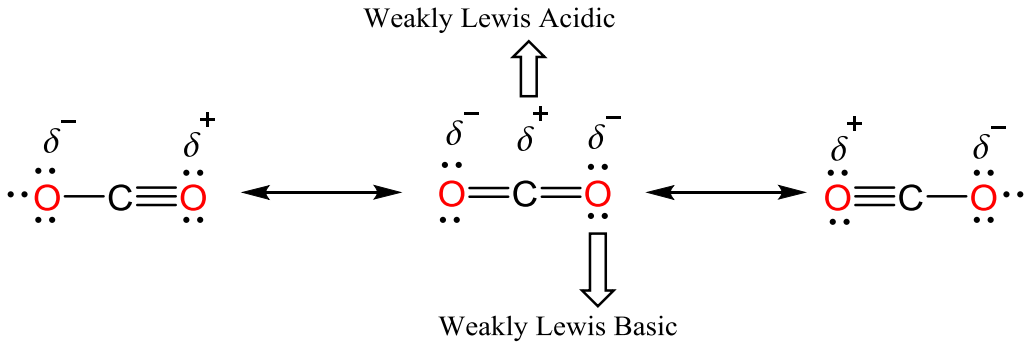

Figure 1.1. Main resonance structures for CO_2

The activation and conversion of carbon dioxide into organic products have attracted researchers over the years (1). Carbon dioxide is very stable, and thus special conditions are required to make the reaction thermodynamically feasible. Energy rich reagents can be used. Strong nucleophilic organometallic complexes, olefins, epoxides, amines, hydrogen, etc are applied and converted to oxidized low-energy products such as carboxylic acids, carbonates, carbamates, methanol, ethanol, formic acid etc (2). External energy inputs may be also applied, such as light (photoirradiation) (3) and electricity (electrolysis) (4).

Apart from the thermodynamical problem, there is also a kinetic

problem, as carbon dioxide is difficult to activate. Catalysis by transition metal complexes plays an important role in these conversions. In this case, the reactivity mainly proceeds through binding to the transition metal center. CO_2 activation is in fact the rate determining step in most of its reported reactions.

1.2 Utilisation of CO_2 as a C1 Feedstock

To date, approximately 90% of all carbon atoms in industrial chemical synthesis derive from natural gas and petroleum, 9% from coal and only 1% from renewable resources (5). This is especially troublesome when taking into account the dwindling of petroleum feedstocks. Carbon dioxide is a renewable, inexpensive, abundant and non-toxic C1 feedstock which can potentially serve as a useful building block for the organic synthesis and industrial applications. Although the use of CO_2 as a chemical feedstock is unlikely to reduce its atmospheric concentration significantly, it may provide access to high-value products from a sustainable and green source. Only 1% of the total abundance of CO_2 on earth is currently being used for chemical synthesis (6), so there is a large potential for application without a shortage of raw material in the foreseeable furture.

The extended use of carbon dioxide is hindered because its capture and storage is expensive. The Kolbe–Schmitt reaction and carboxylation reactions using Grignard reagents are well-known chemical fixations of carbon dioxide from the early days of chemistry; these non-catalytic reactions have many limitations for practical application (7). Catalytic reactions are considered to be essential for widening and deepening the synthetic utility of CO_2. The transformation of alternative, yet unreactive, carbon sources originating from the carbon cycle is an important goal of catalysis. Effective catalytic systems have developed to tackle the unfavorable kinetics for the reduction of CO_2 to formic acid, formaldehyde, methanol, methylamines, methane and CO (8). Currently, CO_2 is employed in the chemical industry for the production of bulk

chemicals, such as urea, salicylic acid, cyclic carbonates, and polypropylene carbonates. Tremendous efforts have been devoted by the scientific community for the activation and utilization of CO_2 to attain and implement the sustainable chemistry. As a result, over the years a plethora of methods have been developed for the transformation of CO_2 into value added products. The transition metal catalyzed activation of CO_2 is of particular interest. The achievements over the past ten years in this field of transition metal catalyzed activation of CO_2 are remarkably noteworthy.

Transition metal catalysis makes possible a number of selective and atom-economical transformations of CO_2. The basic ideas of several of the transformations were long known but have undergone substantial refinements over the past few decades. In the past, highly reactive nucleophiles such as organolithium and Grignard reagents were typically utilized for the activation of CO_2 to deal with its low electrophilicity. These were not so convenient because of sensitivity towards moisture and low tolerance with respect to useful functional groups such as ketones, esters, aldehydes, nitriles etc. They have been replaced by less reactive organometallic reagents and other nucleophiles. The biggest challenge was the incorporation of these excellent nucleophiles into the system. This was accomplished by using proper complexes of transition metals with various ligands which enhance the nucleophilicity. As C-C bonds are dominant in organic chemistry, the formation of C-C bonds with CO_2 is of prominent utility and has been a clear target.

1.3 Coordination Mode in Transition Metal Complexes

The coordination of carbon dioxide to the metal is the basis of its “activation”. Understanding the mode of coordination is thus important, and the topic has been analyzed through many stoichiometric experiments (9). In principle, five chelating modes are possible when one metal center reacts with a single molecule of carbon dioxide (see Figure 1.2). In mode I, a metallacarboxylate complex is formed, with a M-C bond being

formed by electron transfer from an electron-rich metal center to the carbon atom of carbon dioxide. In mode II, a three-membered metallacycle complex is formed. This is characterized by the electron transfer from the metal center to carbon atom and from the oxygen atom to the transition metal. In mode III, coordination of the C-O double bond to the metal center occurs, resulting in the the formation of π-complexes. These three modes generally lead to activation of the CO_2 molecule. The transfer of electrons from metal center to carbon will populate the LUMO of carbon dioxide, which will lose its linearity and adopt a bent structure.

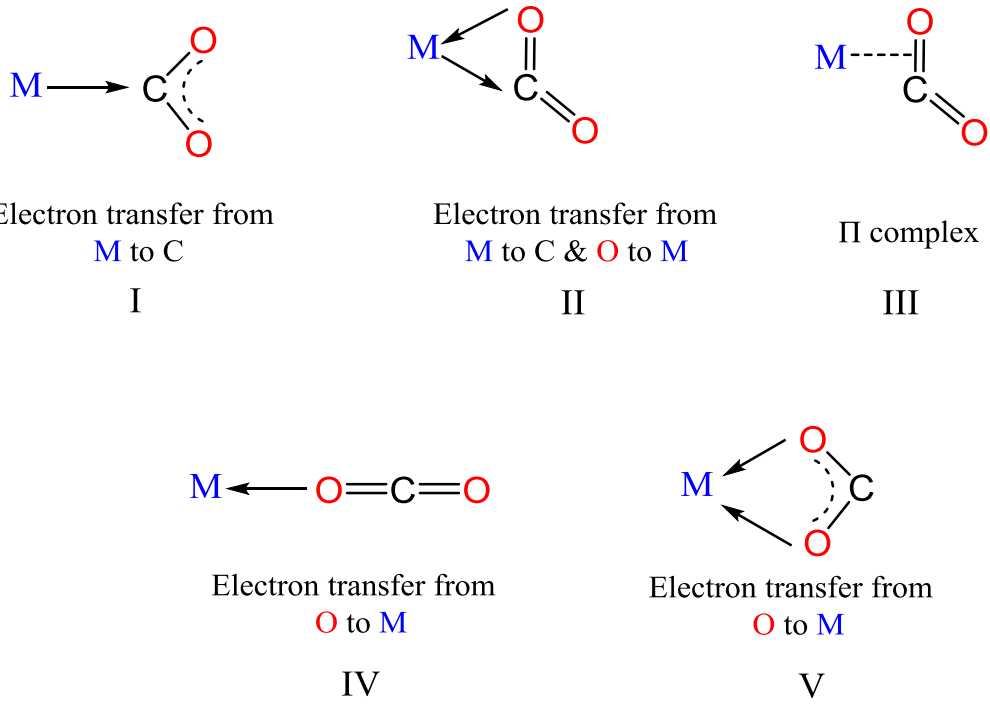

Figure 1.2. Possible coordination modes for CO_2 with metal

Modes IV and V are presented for the sake of completion, although they do not participate usually in carbon dioxide activation. The end-on coordination in mode IV is associated to the weak interaction between the lone pair of one of the oxygen atoms and the metal center. In mode V there is a bidentate coordination of two oxygen atoms to the metal center.

In these two modes, it is the HOMO of carbon dioxide that plays the main role, as elecrons are transferred to the metal center. LUMO is basically empty which keeps the linearity of the CO_2 molecule as such.

The most common coordination mode in complexes active for carbon dioxide activation is mode I, with σ bonding of the metal to the carbon atom. This requires a particular type of transition metal complexes with high electron density in the metal and low oxidation state.

The first isolated and characterised metal complex with CO_2 as a ligand was prepared by Aresta and co-workers. In 1975, they synthesised $Ni(CO_2)(PCy_3)_2$ (Cy = cyclohexyl) complex by treating $Ni(PCy_3)_3$ or $\{Ni(PCy_3)_2\}_2N_2$ with CO_2 in toluene at room temperature as shown in Scheme 1.1. The electron rich Ni(0) was coordinated to the central atom of CO_2 in η^2 form . This was the first demonstration that an electron-rich metal could activate CO_2 (10).

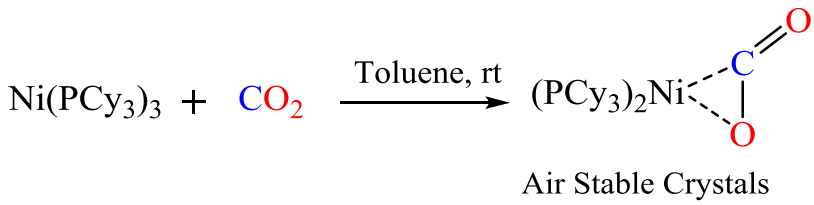

Scheme 1.1: First reported transition metal complex with CO_2 as a ligand by Aresta and co-workers

1.4 Transition Metal-Catalysed Activation of CO_2

1.4.1 Formation of Carboxylic Acids

Carboxylic acids are important structural units that are frequently found in a vast array of natural products, and they are highly versatile starting materials for the preparation of biologically active compounds and other fine chemicals (11). Even though there are well-established conventional procedures for the preparation of carboxylic acids such as the oxidation

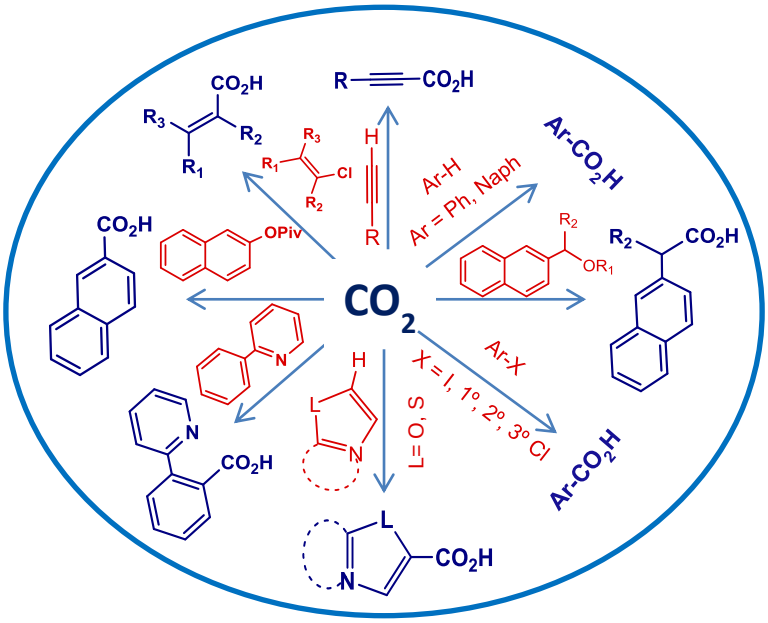
CO2
Ar-H
Ar = Ph, Naph
Ar-CO2H
Ar-X
X = I, 1°, 2°, 3° Cl
L= O, S
Ar-CO2H
R-CO2H
OPiv
OR1
Cl

A

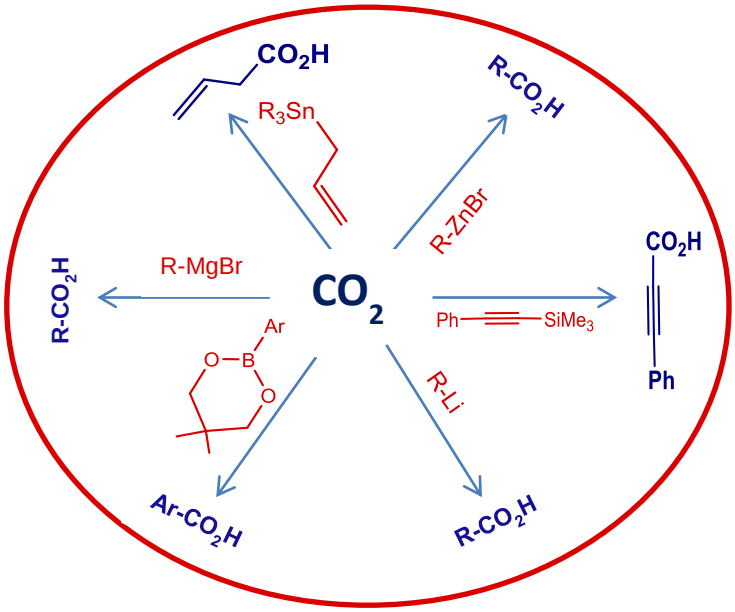
CO2
R3Sn
R-CO2H
R-ZnBr
R-MgBr
R-CO2H
Ph—SiMe3
Ar
R-Li
Ar-CO2H
R-CO2H
Ph

B

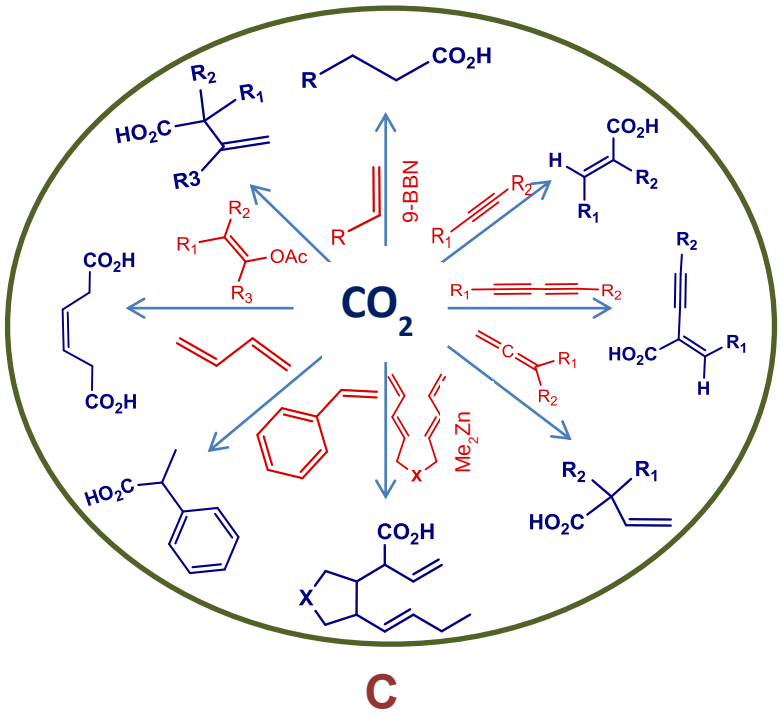

Scheme 1.2. Selected set of carboxylation reactions (i) A: Insertion of CO_2 into the sp3-, sp2-, sp- C-H bonds, C-Halogen bonds and C-O bond (ii) B: Carboxylation of organometallic reagents such as organozinc, organotin, organoboranes, organomagnesium, organo-lithium and organosilanes (iii) C: Reductive carboxylation of olefins

of alcohols or aldehydes and the hydrolysis of nitriles and related derivatives (12), a formally simple method for accessing carboxylic acids is *via* CO_2 activation (13). In recent years, substantial advances in the field of CO_2 based carboxylic acid preparation have allowed the use of relatively less reactive coupling partners such as unactivated organic (pseudo) halides, (hetero)aromatics and allylic/benzylic compounds. Scheme 1.2 shows how first-row transition metals (Fe, Co, Ni and Cu), second-row transition metals (Ru, Rh, Pd and Ag) and third-row transition metals (Ir, Pt and Au) have been used for the insertion of CO_2 into the sp^3, sp^2 and sp C-H

bonds (14), C-Halogen bonds, C-O bonds (15) and nucleophilic organometallic reagents (organozinc, organotin, organoboranes, and organosilanes) (16) and reductive carboxylation of olefins (17).

1.4.2. Formation of Cyclic Carbonates

Another successful application of CO_2 activation in the synthesis of materials is the catalytic production of industrially important cyclic carbonates such as ethylene carbonate (EC), propylene carbonate (PC) or polycarbonates by the cycloaddition reaction with the corresponding epoxides. These compounds have high commercial interest (18). A variety of metal complexes have been shown to catalyze these reactions. This includes Al–, Cr–, and Co– porphyrin complexes, mono-and bimetallic Al–, Co–, and Cr–salen (salen =N, N'-ethylenebis (salicylimine)) complexes (19). Recently, the first example of an iron-catalysed copolymerization of propylene oxide/CO_2 and glycidyl phenyl ether/CO_2 has been reported (20). Aziridine, which is the nitrogen equivalent of cyclic epoxide, can also react with CO_2 to form cyclic carbamate, which is the N equivalent of cyclic carbonates (21). The cycloaddition of certain olefins can also form cyclic carbonates by utilizing CO_2 as shown in Scheme1.3 (22).

A number of these compounds especially 5-member cyclic carbonates have a wide range of applications. For instance, in the manufacture of CDs, DVDs, eyeglasses, aircraft windows, use as green solvents, aprotic polar solvents, additives to gasoline, thickeners for cosmetics and electrolytes for lithium batteries (23). Cyclic carbonates are moreover used as reactive intermediates for the synthesis of several value added products, as they are cheap, readily available and nontoxic. They can react with aliphatic and aromatic amines, alcohols, thiols, and carboxylic acids (24). Five-member cyclic carbonates such as ethylene carbonate and

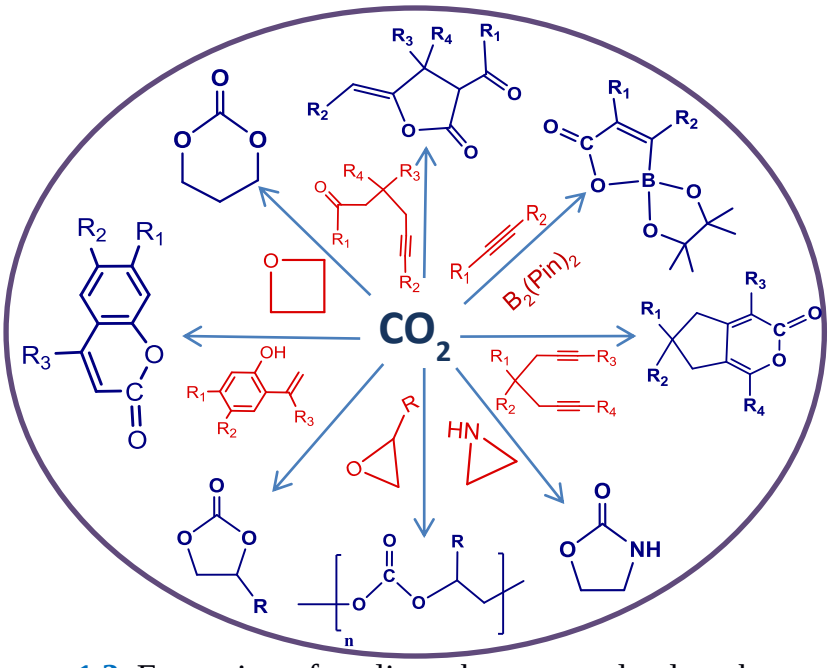

Scheme 1.3. Formation of cyclic carbonates and polycarbonates using CO_2

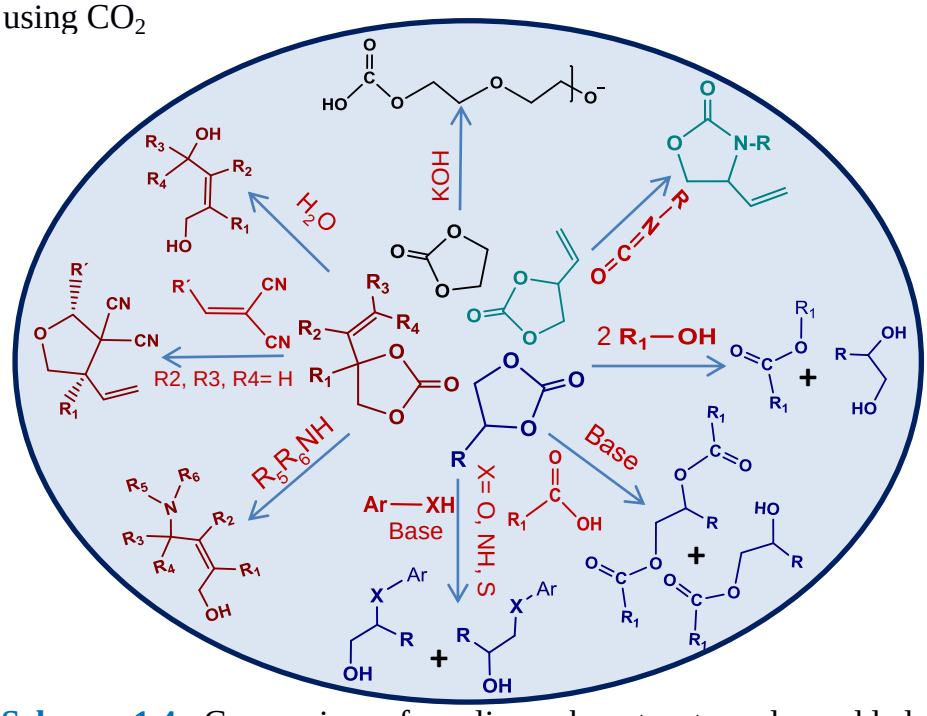

Scheme 1.4. Conversion of cyclic carbonates to value added products

propylene carbonate are very useful for ring-opening polymerization. Allyl surrogates, which have a wide range of application in synthetic chemistry, can be prepared in situ by the decarboxylative approach from cyclic vinyl carbonates. Scheme 1.4 shows how these allyl surrogates can further undergo cycloaddition reactions with imines, isocyanates, formaldehyde or Michael acceptors and also react with nucleophiles such as water, or amine (25).

1.4.3. Reductive Functionalization of Carbon Dioxide

Significant progress has taken place also in the last two decades for CO_2 reduction. Scheme 1.5 shows how several routes have been explored for the synthesis of formic acids and derivatives, methanol, hydrocarbons, formaldehyde, ethanol, methylamines, methane, CO, dialkoxymethane ether, N-formylation of amines and hydrocarbons (26).

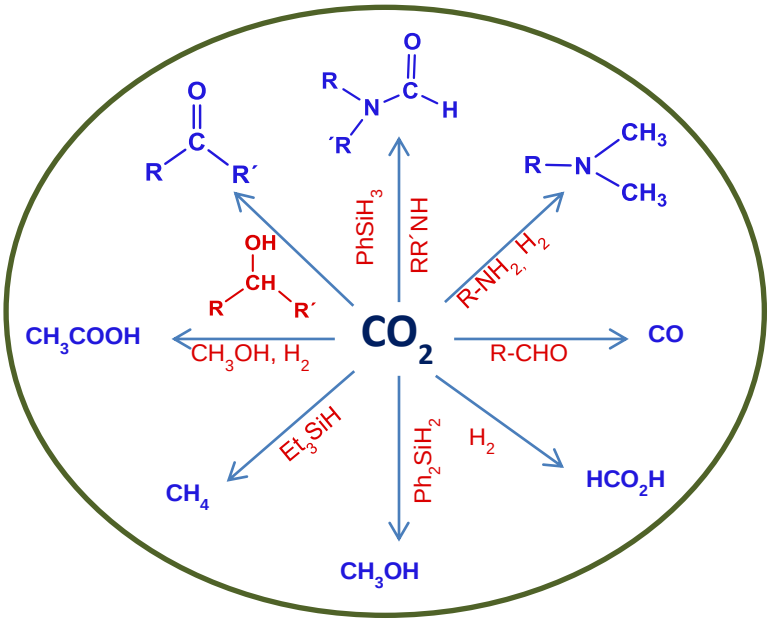

Scheme 1.5. Reduction of CO_2 giving high value products

Most of the reactions include the use of dihydrogen which is considered to be a renewable reducing agent. This method has an important appeal as a procedure for the dihydrogen storage. Some of these products are excellent fuels in internal combustion engines and few of them are useful as raw materials for industrial applications.

1.5. Computational Approach for Mechanistic studies on CO_2 Activation

One of the leading goals in contemporary chemical catalysis is to improve the efficiency of existing catalytic protocols. This goal can be facilitated by improved mechanistic understanding. Combined experimental and computational approaches are now being adopted to decipher mechanisms of increasing order of complexity. Over the years, computational chemistry methods have witnessed a steady growth. Our group has been actively involved in this field of research for many years (27). The ever increasing computing technology has enabled incorporation of the effect of medium and other external perturbations in the usual scheme of things. Increased reliability of *ab initio* and density functional computations has helped to achieve valuable insights into the structure, property and reactivities of molecules and materials. In the present decade, the synergy between theory and experiments has become more evident than ever before. Knowledge of the stereoelectronic factors operating in the key transition states of the reaction can provide valuable inputs in the design of new catalytic processes. Computational chemistry has been also applied to the study of the mechanism of CO_2 activation reactions (28). We highlight in what follows some studies we consider particularly representative.

Yates and co-workers reported the study summarized in Figure 1.3 on the copper-catalyzed formation of carboxylate compounds from heteroarenes. They found that the coordination of

a nitrogen atom in the heteroarene compound could assist the cleavage of the adjacent C–H bond (Figure 1.3), leading to the

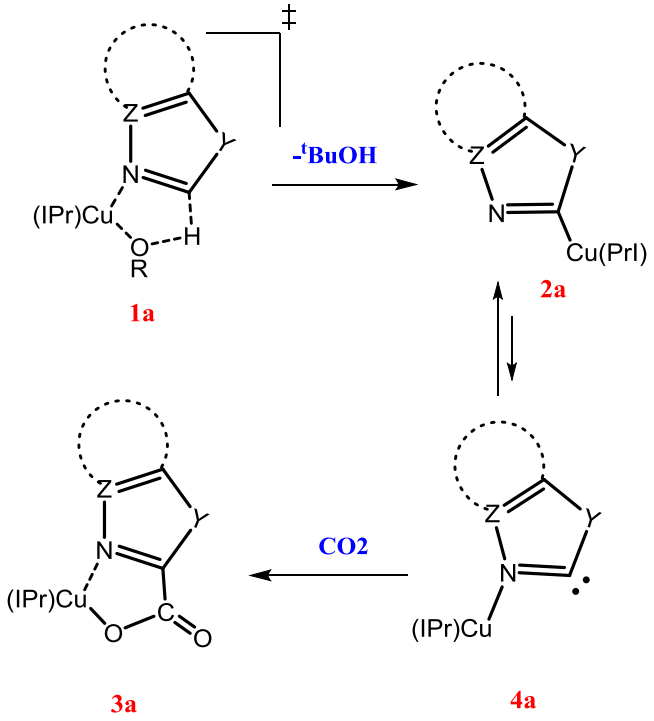

Figure 1.3. Mechanism emerging from the DFT study by Yates and co-workers for the copper-catalyzed formation of carboxylate compounds from heteroarenes

formation of a free carbene which in turn could attack carbon dioxide (29).

DFT studies carried out by Lin and co-workers on the NHC-Cu catalyzed carboxylation reactions of arylboronate esters suggest that insertion of CO_2 into the Cu–Ar bond is the rate-determining step in which nucleophilic attack of the aryl moiety on CO_2 affords the new C–C bond (30). The cycloaddition reaction of CO_2 with epoxides catalyzed by Zn(salphen)/NBu4 X(X= Br, I) affording cyclic carbonates was studied by Bo and coworkers. The importance of using a binary catalytic system in this reaction was

explained by the mechanism presented in Figure 1.4 (31). In a recent study in our group, it was shown that silver and gold complexes with phosphine or carbene ligands make good catalysts for the carboxylation of terminal alkynes which usually carried out by copper complexes (32).

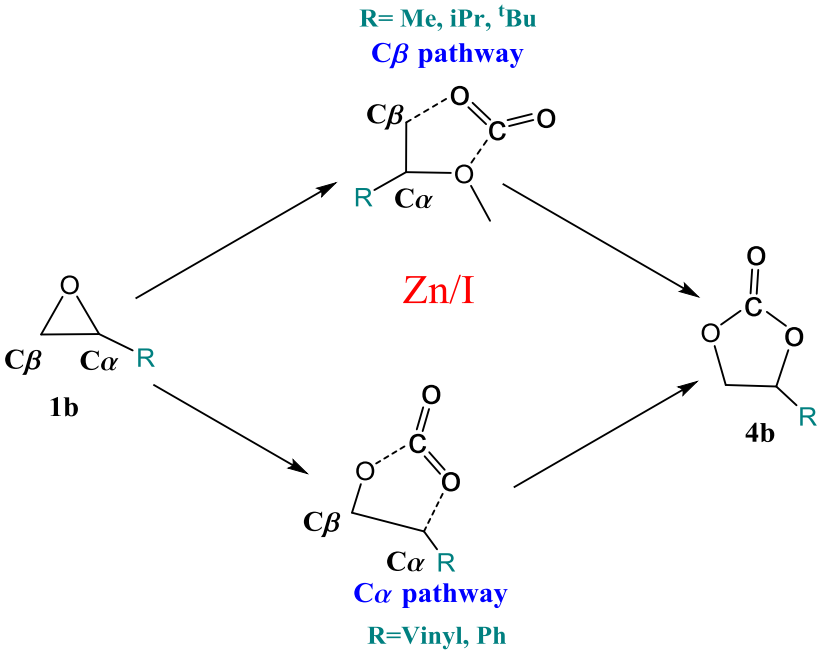

Figure 1.4. Mechanism obtained from DFT calculation by Bo and co-workers for the cycloaddition reaction of CO_2 with epoxides catalyzed by Zn(salphen)/NBu4 X(X= Br, I)

Leitner and coworkers reported a detailed study on the ruthenium-catalyzed reduction of CO_2 to methanol. The calculations shows that a sequential series of hydride transfer and protonolysis steps can account for the transformation of CO_2 via formate/formic acid to hydroxymethanolate/formaldehyde and finally methanolate/ methanol as shown in Figure 1.5 (31).

.

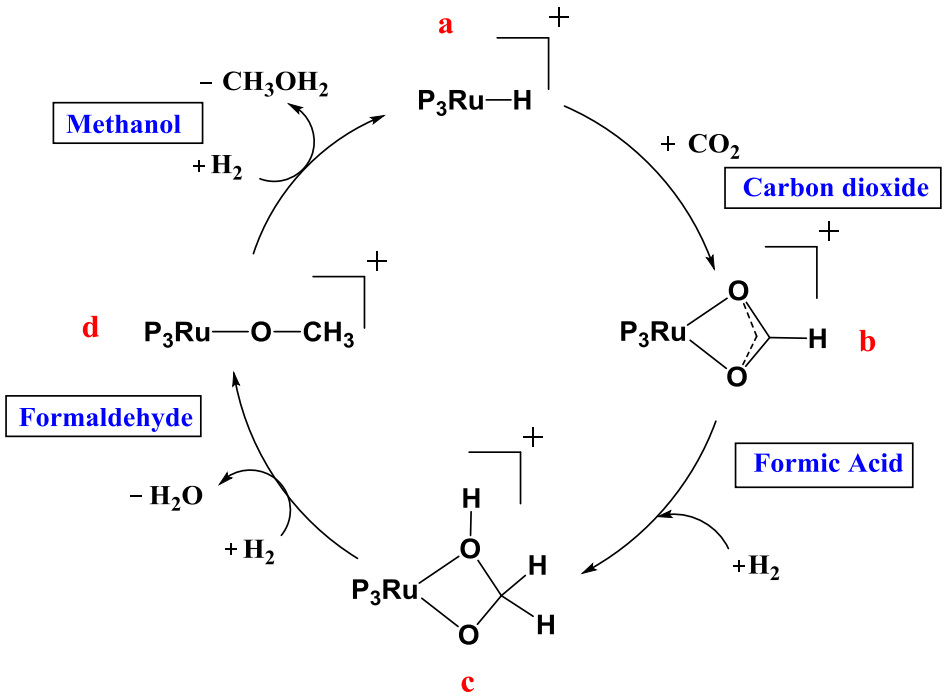

Figure 1.5. Mechanism emerging from DFT calculations by Leitner and co-workers on the ruthenium-catalyzed reduction of CO_2 to methanol

1.6 Objectives

A plethora of methods have been reported over the years for the activation and utilization of CO_2. Transition metal catalysis makes possible a number of selective and atom-economical transformations of CO_2. The basic ideas of several of the transformations have been long known. But detailed mechanistic understanding is still scarce. In this thesis we set out to study computationally the complete mechanistic details of the selected reactions in the area of transition metal catalyzed activation of CO_2.

We will study the mechanism of three different processes which we consider representative of modern carbon dioxide chemistry.

- The carboxylation of allenes by carbon dioxide and tri(ethyl)aluminum under catalysis by palladium complexes has been studied experimentally by Hazari and co-workers, who have carried out a systematic analysis of related stoichiometric processes. There are therefore a lot of experimental data, but a mechanism able to explain all of them is still missing. In particular, we intend to clarify the role of the aluminum salt, which is critical, and the requirements for excess amounts of some of the reactants.

- The stoichiometric conversion of the α-siloxy silanes to α-hydroxy acids reported by Sato and co-workers constitutes an interesting example of fluoride-induced reactivity. Both carboxylation and fluoride reactivity are interesting topics, so we aim to clarify the mechanism of the reaction. The fact that the reaction seems to require the specific presence of the CsF salt as fluoride source is particularly intriguing.

- The mechanisms for carbon dioxide extrusion from cyclic carbonates are also relevant, and we have analyzed them in collaboration with the group of Kleij, in our same institute. We are in particular interested in the microscopic origin for the high selectivity of these palladium-catalyzed processes.

We expect that our computational studies will contribute to the understanding of important details of these reactions, and also to the design of more efficient strategies for attaining a more sustainable chemistry based on the activation of carbon dioxide.

1.7 References

(1) (a) Aresta, M. *Carbon Dioxide as a Chemical Feedstock*, Wiley-VHC Weinheim, **2010** (b) Sakakura, T.; Kohon, K. *Chem. Commun.* **2009**, *11*, 1312 (c) Sakakura, T.; Choi, J. C.; Yasuda, H. *Chem. Rev.* **2007**, *107*, 2365 (d) Marks, T. J. et al. *Chem. Rev.* **2001**,

101, 953 (e) Clément, C.; Cantat, T. *ACS Catal.* **2017**, *7*, 2071 (f) Olah, G. A. *Angew. Chem., Int. Ed.* **2005**, *44*, 2636 (g) Cokoja, M.; Bruckmeier, C.; Rieger, B.; Herrmann, W. E.; Kuhn, F. E. *Angew. Chem., Int. Ed.* **2011**, *50*, 8510 (h) Kielland, N.; Whiteoak, C. J.; Kleij, A. W. *Adv. Synth. Catal.* **2013**, *355*, 2115 (i) Tsuji, Y.; Fujihara, T. *Chem. Commun.* **2012**, *48*, 9956 (j) Saptal, V. B.; Bhanage, B. M. *ChemSusChem* **2016**, *9*, 1980

(2) (a) Mikkelsen, M.; Jorgensen, M.; Krebs, F. C. *Energy Environ. Sci.* **2010**, *3*, 43 (b) Maeda, C.; Miyazaki, Y.; Ema, T. *Catal. Sci. Technol.* **2014**, *4*, 148 (c) Yang, L.; Wang, H. *ChemSusChem* **2014**, *7*, 962 (d) Aresta, M.; Dibenedetto, A.; Quaranta, E. *J. catal.*, **2016**, *343*, 2 (e) Lu, X. B.; Darensbourg, D. J. *Chem. Soc. Rev.* **2012**, *4*, 1462 (f) Liu, Q.; Wu, L.; Jackstell, R.; Beller, M. *Nat. Commun.* **2015**, *6*, 593 (g) Desens, W.; Werner, T. *Adv. Synth. Catal.* **2016**, *358*, 622 (h) Braunstein, P.; Matt, D.; Nobel, D. *Chem. Rev.* **1988**, *88*, 747 (i) Behr, A.; Henze, G. *Green Chem.* **2011**, *13*, 25 (j) Zhang, L.; Hou, Z. *Chem. Sci.* **2013,** *4*, 3395

(3) (a) Chang, X.; Wang, T.; Gong, J. *Energy Environ. Sci.* **2016**, *9*, 2177 (b) Lehn, J. M.; Ziessel, R. *Proc. Natl. Acad. Sci. USA*, **1982**, *79*, 70 (c) Sato, S.; Morikawa, T.; Kajino, T.; Ishitani, O. *Angew. Chem., Int. Ed.* **2013**, *52*, 988 (d) Ettedgui, J.; Diskin-Posner, Y.; Weiner, L.; Neumann, R. *J. Am. Chem. Soc.* **2011**, *133*, 188 (e) Wang, W-H.; Himeda.; Muckerman, J. T.; Manbeck, G. F.; Fujita, E. *Chem. Rev.* **2015**, *115*, 12936 (f) Maeda, C.; Miyazaki, Y.; Ema, T. *Catal. Sci. Technol.* **2014**, *4*, 1482

(4) (a) Angamuthu, R.; Byers, P.; Lutz, M.; Spek, A. L.; Bouwman, E. L. *Science* **2010**, *327*, 313 (b) Qiao, J.; Liu, Y.; Hong, F.; Zhang, J. C*hem. Soc. Rev.*, **2014**, *43*, 631 (c) Lu, Qi. et. al. *Nat. commun.* **2014**, *5*, 3242 (d) Finn, C.; Schnittger, S.; Yellowlees, L. J.; Love, J. B. *Chem. Commun.* **2012**, *48*, 1392

(5) Wittcoff, H. A.; Reuben, B. G. *Industrial organic chemicals*, Wiley New York, **1996**

(6) Song, C. *Catal. Today* **2006**, *115*, 2

(7) Lindsey, A. S.; Jeskey, H. *Chem. Rev.* **1957**, *57*, 583

(8) (a) Porosoff, M. D.; Yan, B.; Chen, J. G. *Energy Environ. Sci.* **2016**, *9*, 62 (b) Fernández Alvarez, F. J.; Aitani, A. M.; Oro, L. A.; *Catal. Sci. Technol.* **2014**, *4*, 611 (c) Wang, W.; Wang, S.; Ma. X.; Gong, J. *Chem. Soc. Rev.* **2011**, *40*, 3703

(9) (a) Behr, A. *Angew. Chem.* **1988**, *100*, 681 (b) Huang, K.; Sun, C. L.; Shi, Z. J. *Chem. Soc. Rev.* **2011**, *40*, 2435

(10) Aresta, M.; Nobile, C. F.; Albano, V. G.; Forni, E.; Manassero, M. *J. Chem. Soc. Chem. Commun.* **1975**, *0*, 636

(11) (a) Patai, S. *The Chemistry of Acid Derivatives*, Wiley New York, **1992** (b) Gooßen, L. J.; Rodríguez, N.; Gooßen, K. *Angew. Chem., Int. Ed.* **2008**, *47*, 3100 (c) Maag, H. *Prodrugs of Carboxylic acids*, Springer US, **2007**

(12) (a) Bew, S. P. *In comprehensive organic functional groups transformation II*, Elsevier Oxford, **2007** (b) Franklin, A. S. *J. Chem. Soc. Perkin. Trans.* **1998**, *1*, 2451

(13) (a) Huang, K.; Sun, C. L.; Shi, Z. L. *Chem. Soc. Rev.* **2011**, *40*, 2435 (b) Riduan, S. N.; Zhang,Y. *Dalton Trans.* **2010**, *39*, 3347 (c) Boogaerts, I. I. F.; Nolan, S. P. *Chem. Commun.* **2011**,*47*, 3021

(14) (a) Hay, A. S. *J. Org. Chem*. **1962**, *27*, 3320 (b) Fukue, Y.; Inoue, Y. *Chem. Commun*. **1994**, *18*, 2091 (c) Zhang, W. Z.; Li, W. J.; Zhang, X.; Zhou, H.; Lu, X. B. *Org. Lett.* **2010**, *12*, 4748 (d) Inamoto, K.; Asano, N.; Kobayashi, K.; Yonemoto, M.; Kondo, Y. *Org. Biomol. Chem.* **2012**, *10*, 1514 (e) Yu, B.; Diao, Z.; Guo, C.;

Zhong, C.; He, L.; Zhao, Y.; Song, Q.; Liu, A.; Wang, J. *Green Chem*. **2013**, *15*, 2401 (f) Gooßen, L. J.; Rodrıíguez, N.; Manjolinho, F.; Lange, P. P. *Adv. Synth. Catal*. **2010**, 352, 2913 (g) Yu, D.; Zhang, Y. *Proc. Natl. Acad. Sci. USA*, **2010**, *107*, 20184 (h) Riduan, S. N.; Ying, J. Y.; Zhang, Y. G. *Org. Lett*. **2012,** *14*, 1780 (i) Riduan, S. N.; Ying, J. Y.; Zhang, Y. G. *ChemCatChem* **2013**, *5*, 1490 (j) Zhang, X.; Zhang, W. Z.; Ren, X.; Zhang, L. L.; Lu, X. B. *Org. Lett*. **2011,** *13*, 2402 (k) Arndt, M.; Risto, E.; Krause, T.; Gooben, L. J. *ChemCatChem* **2012**, *4*, 484 (l) Yu, D.; Zhang, Y.; *Green Chem*. **2011**, *13*, 1275 (m) Gaillard, S.; Cazin, C. S. J.; Nolan, S. P. *Acc. Chem. Res.* **2012**, *45*, 778 (n) Boogaerts, I. I. F.; Fortman, G. C.; Furst, M. R. L.; Cazin, C. S. J.; Nolan, S. P. *Angew. Chem., Int. Ed.* **2010**, *49*, 8674 (o) Inomata, H.; Ogata, K.; Fukuzawa, S.; Hou, Z. *Org. Lett*. **2012,** *14*, 3986

(15) (a) Correa, A.; Martin, R. *J. Am. Chem. Soc*. **2009**, *131*, 15974 (b) Fujihara, T.; Nogi, K.; Xu, T.; Terao, J.; Tsuji, Y. *J. Am. Chem. Soc.* **2012**, *134*, 9106 (c) Leon, T.; Correa, A.; Martin, R. *J. Am. Chem. Soc*. **2013**, *135*, 1221 (d) Liu, Y.; Cornella, J.; Martin, R. *J. Am. Chem. Soc.* **2014**, *136*, 11212 (e) Tran-Vu, H.; Daugulis, O. *ACS Catal*. **2013**, *3*, 2417 (f) Miaoa, B.; Ma, S. *Chem. Commun.* **2014**, *50*, 3285 (g) Börjesson, M.; Moragas, T.; Gallego, D.; Martin, R. *ACS Catal.* **2016**, 6, 6739 (h) Juliá-Hernández, F.; Moragas, T.; Cornella, J.; Martin. R. *Nature* **2017**, *545*, 84 (i) Gemmeren, M. V.; Börjesson, M.; Tortajada, A.; Sun, S. Z.; Okura, K.; Martín, R. *Angew. Chem., Int. Ed.* **2017**, *56*, 6558 (j) Fu, M. C.; Shang, R.; Cheng, W. M.; Fu, Y. *Chem. Eur. J.* **2017**, *23*, 8818

(16) (a) Shi, M.; Nicholas, K. M. *J. Am. Chem. Soc*. **1997**, *119*, 5057 (b) Johansson, R.; Wendt, O. F. *Dalton Trans*. **2007**, *4*, 488 (c) Takaya, J.; Tadami, S.; Ukai, K.; Iwasawa, N. *Org. Lett.* **2008**, 10, 2697 (d) Ochiai, H.; Jang, M.; Hirano, K.; Yorimitsu, H.; Oshima, K. *Org. Lett.* **2008**, *10*, 2681 (e) Yeung, C. C.; Dong, M. *J. Am.*

Chem. Soc. **2008**, *130*, 7826 (f) Ukai, K.; Aoki, M.; Takaya, J.; Iwasawa, N. *J. Am. Chem. Soc.* **2006**, *128*, 8706 (g) Ohishi, T.; Nishiura, M.; Hou, Z. *Angew. Chem., Int. Ed.* **2008**, *47*, 5792 (h) Ohmiya, H.; Tanabe, M.; Sawamura, M. *Org. Lett.* **2011,** *13*, 1086

(17) (a) Sugimoto, H.; Kawata, I.; Aniguchi, H. T.; Fujiwara, Y. *J. Organomet. Chem*. **1984**, *266*, C44 (b) Li, S.; Yuan, W.; Ma, S. *Angew. Chem., Int. Ed.* **2011**, *50*, 2578 (c) Zhang, Y. G.; Riduan, S. N. *Angew. Chem., Int. Ed.* **2011**, *50*, 6210 (d) Fujihara, T.; Xu, T.; Semba, K.; Terao, J.; Tsuji, Y. *Angew. Chem., Int. Ed.* ***2011***, *50*, *6210* (e) Takimoto, M.; Mori, M. *J. Am. Chem. Soc.* **2002**, *124*, 10008 (f) Greenhalgh, M. D.; Thomas, S. P. *J. Am. Chem. Soc.* **2012**, *134*, 11900 (g) Williams, C. M.; Johnson, J. B.; Rovis, T. *J. Am. Chem. Soc.* **2008**, *130*, 14936 (h) Cao, T.; Yang, Z.; Ma, S. *ACS Catal.* **2017**, *7*, 4504 (i) Doi, R.; Abdullah, I.; Taniguchi, T.; Saito, N.; Sato, Y. *Chem. Commun*. **2017**, *53*, 7720 (j) Simon, M. J.; Laursen, L. R.; Huang, Y.; Nielsen, D. U.; Daasbjerg, K.; Skrydstrup, T. *ACS Catal.* **2017**, *7*,1392 (k) Chen, Y. G.; Shuai, B.; Ma, C.; Zhang, X. J.; Fang, P.; Mei, T. S. *Org. Lett.* **2017,** *19*, 2969

(18) (a) Sakakura, T.; Kohno, K. K. *Chem. Commun.* **2009**, *11*, 1312 (b) Fukuoka, S.; Kawamura, M.; Komiya, M.; Tojo, M.; Hachiya, H.; Hasegawa, K.; Aminaka, M.; Okamoto, H.; Fukawa, I.; Konno, S. *Green Chem*. **2003**, *5*, 497

(19) Paddock, R. L.; Nguyen, S. T. *J. Am. Chem. Soc.* **2001**, *123*, 11498 (b) Decortes, A.; Kleij, A. W. *ChemCatChem* **2011**, *3*, 831 (c) North, M.; Pasquale, R. *Angew. Chem., Int. Ed.* **2009**, *48*, 2946 (d) Whiteoak, C. J. et. al. *J. Am. Chem. Soc.* **2013**, *135*, 1228

(20) (a) Jin, L. et al. *J. Mol. Catal. A. chem.* **2007**, *261*, 262 (b) Ema, T.; Miyazaki, Y.; Koyama, S.; Yano, Y.; Sakai, T. *Chem. Commun.* **2012**, *48*, 4489 (c) Paddock, R. L.; Nguyen, S. T. *J. Am. Chem. Soc.* **2001**, *123*, 11498 (d) Decortes, A.; Kleij, A. W.

ChemCatChem **2011,** *17,* 3831 (e) Whiteoak, C. J. et al. *J. Am. Chem. Soc.* **2013**, *135*, 1228 (f) Nakano, K.; Kobayashi, K.; Ohkawara, T.; Imoto, H.; Nozaki, K. J. *Am. Chem. Soc*. **2013**, *135*, 8456 (g) North, M.; Riccardo P.; Young, C. *Green Chem.* **2010**, *12*, 1514 (h) Xiao, W.; North, M. *ChemSusChem* **2017**, *10,* 74 (i) Rintjema, J.; Kleij. A. W. *ChemSusChem* **2017**, *10*, 1274 (j) Castro-Osma, J. A.; North, M.; Wu. X. *Chem. Euro. J.* **2016**, *22*, 2100 (k) Rintjema, J. et al. *Angew. Chem., Int. Ed.* **2016**, *55*, 3972

(21) (a) Adhikari, D. et al. *Chem. Sci.* **2015**, *6,* 1293 (b) Fontana, F.; Chen, C. C.; Aggarwal, V. K. *Org. Lett.* **2011**, *13*, 3454 (c) Aaron W. M.; Nguyen. S. T. *Org. Lett.* **2004**, *6*, 2301

(22) (a) Sasano, K.; Takaya, J.; Iwasawa, N. *J. Am. Chem. Soc*. **2013**, *135*, 10954 (b) Arndt, M.; Risto, E.; Krause, T.; Gooben, L. J. *ChemCatChem* **2012**, *4*, 484 (c) Kim, S. H.; Kim, K. H.; Hong, S. H. *Angew. Chem., Int. Ed*. **2014**, *53*, 771 (d) Cheng, J.; Ohishi, T.; Zang, L.; Hou, Z. *Angew. Chem., Int. Ed.* **2010**, *49*, 8670 (e) Inomata, H.; Ogata, O.; Fukuzawa, S.; Hou, Z. *Org. Lett.* **2012**, *14*, 3986 (f) Boogaerts, I. I. F.; Nolan, S. P. *J. Am. Chem. Soc.* **2010**, *132*, 8858 (g) Johnson, M. T.; Rensburg, V.; Axelsson, M.; Ahlquist, M. S. G.; Wendt, O. F. *Chem. Sci.* **2011**, *2*, 2373 (h) Louie, J.; Gibby J. E.; Farnworth, V. M.; Tekavec, T. N. *J. Am. Chem. Soc.* **2002**, *124*, 15188

(23) (a) Shaikh, A. G.; Sivaram, S.; *Chem. Rev*. **1996**, *96*, 951 (b) Omae, I. *Catal. Today* **2006**, *115*, 33 (c) Haworth, W. N.; Machemer, H. *J. Chem. Soc*. **1932**, *12*, 2270 (d) Reetz, M. T.; Lohmer, G.; *Chem. Commun*. **1996**, 1921 (e) Behr, A.; Naendrup, F.; Obst, D. *Adv. Synth. Catal*. **2002**, *344*, 1142 (f) Behr, A.; Naendrup, F.; Obst, D. *Eur. J. Lipid Sci. Technol*. **2002**, *104*, 161 (g) Bayardon, J.; Holz, J.; Schaffner, B.; Andrushko, V.; Verevkin, S.; Preetz, A.; Borner, A. *Angew. Chem., Int. Ed.* **2007**, *46*, 5971 (h) Schaffner, B.; Holz, J.; Verevkinand, S. P.; Borner, A.

ChemSusChem **2008**, *1*, 249 (i) North, M.; Pizzato, F.; Villuendas, P. *ChemSusChem* **2009**, *2*, 862 (j) North, M.; Villuendas, P. *Org. Lett.* **2010**, *12*, 2378 (k) Kowalewicz, A.; Wojtyniak, W. *J. Automobile Eng.* **2005**, *219*, 103 (b) Zevenhoven, R.; Eloneva, S.; Teir, S. *Catal. Today* **2006**, *115*, 73

(24) (a) Yoshino, T.; Inaba, S.; Komura, H.; Ishido, Y. *J. Chem. Soc. Perkin Trans. 1*, 1**977**, *0*, 1266 (b) Apicella, B.; Serio, M.; Fiocca, L.; Po, R.; Santacesaria, E. *J. Appl. Polym. Sci.* **1998**, 69, 2423 (c) Ohno, M.; Yamagiwa, S. Process for Producing Cyclic Carbonic Esters. U.S. Patent 6,054,596, 2000 (d) Angeles, E.; Santillan, A.; Martinez, I.; Ramirez, A.; Moreno, E. *Synth. Commun.* **1994**, *24*, 2441 (e) Doya, M.; Kimizuka, K.; Kanbara, Y. Process for the production of Dialkyl Carbonate. European Patent 638,541, 1995 (f) Swarup, S.; Singer, D.; McCollum, G.; Olson, K. Aqueous Aminoplast Curable Film-Forming Compositions Providing Films Having Resistance to Acid Etching. U.S. Patent 6,103,816, 2000

(25) (a) Guo, W.; Martínez-Rodríguez, L.; Kuniyil, R.; Martin, E.; Escudero-Adán, E. C.; Maseras, F.; Kleij, A. W. *J. Am. Chem. Soc.* **2016**, *138*, 11970 (b) Khan, A.; Zheng, R.; Kan, Z.; Ye, J.; Xing, J.; Zhang, Y, J. *Angew. Chem., Int. Ed.* **2014**, *53*, 6439 (c) Khan, A.; Xing, J.; Zhao, J.; Kan, Y.; Zhang, W.; Zhang, Y. J. *Chem. Eur. J.* **2015**, *21*, 120 (d) Yang, L.; Khan, K.; Zheng, R.; Jin, L. Y.; Zhang, Y. J. *Org. Lett.* **2015**, *17*, 6230 (e) Khan, A.; Yang, L.; Xu, J.; Jin, L. Y.; Zhang, Y. J. *Angew. Chem., Int. Ed.* **2014**, *53*, 11257 (e) Cai, A.; Guo, W.; Martínez-Rodríguez, L.; Kleij, A. W. *J. Am. Chem. Soc.* **2016**, *138*, 14194 (f) Guo, W.; Martínez-Rodríguez, L.; Martin, E.; Escudero-Adán, E. C.; Kleij, A. W. *Angew. Chem., Int. Ed.* **2016**, *55*, 11037 c) Ohmatsu, K.; Imagawa, N.; Ooi, T.; *Nat. Chem.* **2014**, *6*, 47

(26) (a) Jessop, P. G.; Ikariya, T.; Noyori, R. *Chem. Rev.* **1995**, *95*, 259 (b) Leitner,W. *Angew. Chem., Int. Ed.* **1995**, *34*, 2207 (c)

Jessop, P. G.; Jo, F.; Tai, C. C. *Coord. Chem. Rev.* **2004**, *248*, 2425 (d) Wang, W.; Wang, S.; Ma, X.; Gong, J. *Chem. Soc. Rev.* **2011**, *40*, 3703 (e) Yeung, C. S.; Dong, V. M. *J. Am. Chem. Soc*. **2008**, *130*, 7826 (f) Ochiai, H.; Jang, M.; Hirano, K.; Yorimitsu, H.; Oshima, K. *Org. Lett*. **2008**, *10*, 2681 (g) Kobayashi, K.; Kondo, Y. *Org. Lett*. **2009**, *11*, 2035 (h) Onishi, T.; Nishiura, M.; Hou, Z. *Angew. Chem., Int. Ed*. **2008**, *47*, 5792 (i) Takaya, J.; Tadami, S.; Ukai, K.; Iwasawa, N. *Org. Lett*. **2008**, *10*, 2697 (j) Ukai, K.; Aoki, M.; Takaya, J.; Iwasawa, N. *J. Am. Chem. Soc*. **2006**, *128*, 8706 (k) Duong, H. A.; Huleatt, P. B.; Tan, Q.-W.; Shuying, E. L. *Org. Lett.* **2013**, *15*, 4034 (l) Ohishi, T.; Zhang, L.; Nishiura, M.; Hou, Z. *Angew. Chem., Int. Ed.* **2011**, *50*, 8114 (m) Ohmiya, H.; Tanabe, M.; Sawamura, M. *Org. Lett*. **2011**, *13*, 1086

(27) (a) Whiteoak, C. J.; Nova, A.; Maseras, F.; Kleij, A. W. *ChemSusChem* **2012**, *5*, 2032 (b) Sameera, W. M. C.; Maseras, F. *WIREs Comput. Mol. Sci.* **2012**, *2*, 375 (c) García-Melchor, M.; Braga, A. A. C.; Lledós, A.; Ujaque, G.; Maseras, F. *Acc. Chem. Res.* **2013**, *46*, 2626 (d) Vikse, K.; Naka, T.; McIndoe, J. S.; Besora, M.; Maseras, F. *ChemCatChem* **2013**, *5*, 3604 (e) Ortuño, M. A.; Lledós, A.; Maseras, F.; Ujaque, G. *ChemCatChem* **2014**, *6*, 3132 (f) Goehry, C.; Besora, M.; Maseras, F. *ACS Catal*. **2015**, *5*, 2445 (g) Fernández-Álvarez, V. M.; Nappi, M.; Melchiorre, P.; F. Maseras. *Org. Lett.* **2015**, *17*, 2676 (h) Funes-Ardoiz, I.; Maseras, F. *Angew. Chem., Int. Ed.* **2016**, *55*, 2764 (i) Liu, C.; Besora, M.; Maseras, F. *Chem. Asian J.* **2016**, *11*, 411 (j) Funes-Ardoiz, I.; Garrido-Barros, P. G.; Llobet, A.; Maseras, F. A*CS Catal.* **2017**, *7*, 1712 (k) Kuniyil, R.; Maseras, F. *Theor. Chem. Acc.* **2017**, *136*, 65

(28) (a)Ting, F.; Sheong, F. K.; Lin, Z. *Organometallics* **2013**, *32*, 5224 (b) Lafage, M.; Pujol, A.; Saffon-Merceron, N.; Mézailles, N. *ACS Catal.* **2016,** *6*, 3030 (c) Qinghua, R.; Wu, N.; Cai, Y.; Fang, J. *Organometallics* **2016,** *35*, 3932 (c) Liu, C.; Luo,Y.; Zhang, W.;

Qu, J.; Lu, W. *Organometallics* **2014,** *33*, 2984 (d) Zhao, Y.; Liu, Y.; Bi, S.; Liu, Y. *J. Organomet. Chem*. **2013**, *166*, 745 (e) Das Neves Gomes, C.; Blondiaux, E.; Thuéry, P.; Cantat, T. *Chem. Eur. J.* **2014**, *20*, 7098 (f) Musashi, Y.; Sakaki, S. *J. Am. Chem. Soc.* ***2002***, *124*, 7588 (g) Ohnishi, Y. -Y.; Nakao, Y.; Sato, H.; Sakaki, S. *Organometallics* **2006**, *25*, 3352 (h) Ostapowicz, T. G.; Hölscher, M.; Leitner, W. *Eur. J. Inorg. Chem.* ***2012***, *34*, 5632 (i) Aresta, M.; Dibenedetto, A.; Fracchiolla, E.; Giannoccaro, P.; Pastore, C.; Pápai, I.; Schubert, G. *J. Org. Chem*. **2005,** *70*, 6177

(29) Ariafard, A.; Zarkoob, F.; Batebi, H.; Stranger, R.; Yates, B. F. *Organometallics* **2011**, *30*, 6218

(30) Dang, L.; Lin, Z.; Marder, T. B. *Organometallics* **2010,** *29*, 917

(31) Castro-Gómez, F.; Salassa, G.; Kleij, A. W.; Bo, C. *Chem. Eur. J.* **2013**, *19*, 6289

(32) Jover, J.; Maseras, F. *J. Org. Chem*. **2014,** *79*, 11981

(33) Wesselbaum, S.; Moha, V.; Meuresch, M.; Brosinski, S.; Thenert, K. M.; Kothe, J.; Stein, T. V.; Englert, U.; Hölscher, M.; Klankermayer, J.; Leitner, W. *Chem. Sci*. **2015**, *6*, 693

Chapter 2

Computational Methods

2.1 General Overview

Computational chemistry is the study of chemical problems using computers (1). The choice of the computational method depends on various factors which include the type of problem being studied, the accuracy required and the availability of computational resources. While large systems of biological interest as well as polymers are studied using molecular mechanics (MM), high accuracy for smaller systems can be achieved with quantum mechanical (QM) methods. MM methods rely on the use of force fields which are developed on the basis of certain parameters and are specific for particular kind of molecules. These methods, implemented in programs such as GROMACS, AMBER, CHARMM etc., have been extremely useful in enzymatic reactions and drug design. Semi-empirical, *ab initio* and density functional theory (DFT) methods fall in the category of quantum mechanical methods and are based on the Schrödinger equation. While semi-empirical methods are parameterized against experiments, the *ab initio* methods are mostly based on calculations. DFT methods are not based on the wave function although they use similar mathematical algorithms. DFT methods have emerged are the option of choice for the study of reactivity in medium-sized systems like those studied in this thesis.

2.2 The Schrödinger equation

Quantum mechanics is the fundamental branch of science that studies the behaviour of matter and its interaction with energy at the atomic and sub-atomic level. Quantum chemistry, the application of quantum mechanics to chemistry gives the complete description of a molecule which in turn is given by its wave function. The wave function is obtained as a solution of the Schrödinger equation; the prime equation is quantum chemistry. The time independent Schrödinger equation is the one that is most widely used in

computational chemistry and depends on the spatial coordinates. The wave functions obtained from such an equation are called stationary-state wave functions. However, the more general time-dependent Schrödinger equation is important in studying the interaction of light with molecules and thus is an integral part of molecular spectroscopy. Just as the Lagrangian or Hamilton treatments are key to classical mechanics, the Schrödinger equation is fundamental to quantum mechanics.

The time independent Schrödinger equation is:

$$\hat{\mathrm{H}}\,\psi = \mathrm{E}\psi \qquad (1)$$

For a molecule consisting of *N* number of nuclei with position *R* and *n* number of electrons with position *r*, the Schrödinger equation is:

$$\hat{\mathrm{H}}\,\psi(R_1,\ R_2,\ldots.R_{N,}\ r_1,\ r_2,\ldots.\ r_n) = E\,\psi\ (R_1,\ R_2,\ldots\ldots.R_{N,}\ r_1,\ r_2,\ldots.\ r_n) \qquad (2)$$

The Hamiltonian in atomic units can be written as:

$$\hat{\mathrm{H}} = -\frac{1}{2}\sum_I^N \frac{\nabla^2 I}{M_I} - \frac{1}{2}\sum_i^n \nabla^2 i - \sum_i^n \sum_I^N \frac{\mathrm{Z}_I}{r_{Ii}} + \sum_{I>J}^N \frac{Z_I Z_J}{R_{IJ}} + \sum_{i<j}^N \frac{1}{r_{ij}} \qquad (3)$$

where M_I = mass of the nucleus *I*, Z_I = atomic number of nucleus *I*.

$$\hat{\mathrm{H}} = \hat{T}_N + \hat{T}_e + \hat{V}_{Ne} + \hat{V}_{NN} + \hat{V}_{ee} \qquad (4)$$

where $\hat{T}_N$ = operator for the kinetic energy of the nuclei, $\hat{T}e$ = operator for the kinetic energy of the electrons, $\hat{V}_{Ne}$ = operator for the Coulomb attraction between the electrons and nuclei, $\hat{V}_{\mathrm{NN}}$ = operator for the repulsion between the nuclei, and $\hat{V}_{ee}$ = operator for the repulsion between the electrons. It should be noted that the exact solution for systems containing more than one electron is unknown and therefore we require approximations to solve the

Schrödinger equation for multielectron systems.

2.3 The Born-Oppenheimer Approximation

Due to the presence of the term $\hat{V}_{Ne}$, the electronic and nuclear parts of the wave function cannot be separated in principle. Since the nuclei are much heavier than the electrons, the nuclei can be considered to be moving much more slowly than the electrons. We can thus assume that the electrons will adapt instantaneously to any movement by the nuclei, and the equations can be separated in two parts. When solving the electronic part, this means neglecting $\hat{T}_N$ and assuming $\hat{V}_{NN}$ to be a constant in equation (4). This is the Born-Oppenheimer approximation.

Thus the wave function can now be written as a product of electronic wave function and a nuclear wave function:

$$\psi = \psi_e\,(r,R)\;\psi_N\,(R) \qquad (5)$$

The electronic wave function (ψ_e) parametrically depends on the nuclear coordinates. In other words, a different electronic wave function is obtained for every different position of the nuclei. Thus, the electronic energy is not a constant and depends on the nuclear coordinates (geometry of the molecule). The total energy of a molecule can now be calculated by solving the electronic Schrödinger equation and adding to it the internuclear repulsion. The total electronic energy (and the other properties) is therefore a function of the electronic coordinates alone, but parametrically depends on the nuclear coordinates. The variation of the total electronic energy with the nuclear coordinates gives rise to what is known as the potential energy surface (PES). A PES is a Born-Oppenheimer surface, on which different points represent different geometries and their corresponding energies.

2.4 Density Functional Theory

Hartree-Fock-based methods are usually very time consuming for systems of the size considered in this thesis. An appealing alternative is the Density Functional Theory (DFT) method. This is based on the electron density (ρ) which is the probability of finding an electron in a volume element *dxdydz* (2). The electron density is an observable which depends on the three spatial coordinates and one spin coordinate (3). Current DFT methods are based on the formulation given by Kohn and Sham, which is based on two theorems given by Hohenberg and Kohn (4). According to the first theorem all the properties of a molecule in a ground electronic state are determined by the ground state density function. If we can determine the electron density function in the ground state we can calculate the energy or any other property of a molecule in the ground state.

DFT is relatively faster than HF-based methods and is considered to be a good method for solving chemical problems described in the current thesis. The main inconvenient for DFT is the lack of a clear hierarchy of methods; it is not always clear which functional is better for a given problem.

The electron density for a multi-electron system can be given as:

$$\rho = \sum_{i=1}^{n} n_i \left|\psi_i\right|^2 \qquad (6)$$

The energy of a molecule is given as:

$$E_o = F[\rho_o] = E[\rho_o] \qquad (7)$$

where F is a functional which in turn is a rule that transforms a function into a number. The exact functional is unknown, and therefore approximate functionals are used in DFT.

The energy value can be calculated by the Kohn-Sham (KS) equations. In the KS approach, the energy is expressed as a sum of terms, of which only one contains the unknown functional. An initial guess of the electron density is used to generate initial orbitals which then undergo iterative procedure until the convergence is obtained. The ground state electronic energy of a molecule can be expressed as:

$$E_o[\rho_o] = T[\rho_o] + V_{ee}[\rho_o] + V_{Ne}[\rho_o] \qquad (8)$$

where, T is the sum of electron kinetic energies, V_{ee} is the potential energy due to electron-electron repulsion and V_{Ne} is the nucleus electron potential energy. The individual energy terms are functionals of the electronic density. In this equation only V_{Ne} is known and can be represented as:

$$V_{Ne} = \int \rho_o(r)\, \nu(r) dr \qquad (9)$$

where, $\nu(r)$ is the external potential representing the attraction of an electron to the nuclei. However, due to the unknown functionals in $T[\rho_o]$ and $V_{ee}[\rho_o]$, the exact solution is not known.

To solve equation (8), Kohn and Sham considered a reference system in which the electrons do not interact with each other. A quantity $\Delta T[\rho_o]$ is defined, which is the deviation of the real kinetic energy from the kinetic energy of the reference system. Similarly, $\Delta V_{ee}[\rho_o]$ is defined; which is the deviation of the real electron-electron repulsion energy from the classical coulomb repulsion energy.

The two quantities; $\Delta T[\rho_o]$ and $\Delta V_{ee}[\rho_o]$ can be represented as:

$$\Delta T[\rho_o] = T[\rho_o] - T_r[\rho_o] \qquad (10)$$

$$\Delta V_{ee}[\rho_o] = V_{ee}[\rho_o] - \frac{1}{2} \iint \frac{\rho_o(r_1)(r_2)}{r_{12}} dr_1 r_2 \qquad (11)$$

Using equations (10) and (11), the ground state electronic energy can now be written as:

$$\mathrm{E}_o = \int \rho_o(r)\, \nu(r) dr + T_r[\rho_o] + \frac{1}{2}\iint \frac{\rho_o(r_1)(r_2)}{r_{12}} dr_1 r_2 + \Delta \mathrm{T}[\rho_o] + \Delta V_{ee}[\rho_o] \qquad (12)$$

The exchange-correlation energy (EXC) which includes the difference between classical and quantum-mechanical electron-electron repulsion and difference between the kinetic energy of non-interacting system with the real system can now be defined as:

$$E_{XC}[\rho_o] = \Delta \mathrm{T}[\rho_o] + \Delta V_{ee}[\rho_o] \qquad (13)$$

Thus,

$$\mathrm{E}_o = \int \rho_o(r)\, \nu(r) dr + T_r[\rho_o] + \frac{1}{2}\iint \frac{\rho_o(r_1)(r_2)}{r_{12}} dr_1 r_2 + E_{XC}[\rho_o] \qquad (14)$$

The ground state electronic energy can be written in an elaborate way as follows:

$$\mathrm{E}_o = -\sum_A Z_A \int \frac{\rho_o(r_1)}{r_{1A}} dr_1 - \frac{1}{2}\sum_{i=1}^{2n} \langle \psi_i{}^{KS}(1) | \nabla^2{}_i | \psi_i{}^{KS}(1) \rangle + \frac{1}{2}\iint \frac{\rho_o(r_1)\rho_o(r_2)}{r_{1A}} dr_1 r_2 + E_{XC}[\rho_o] \qquad (15)$$

where, $\psi_i{}^{KS}$ are the KS spatial orbitals.

The electron density of a real system which is equal to that of the reference system can be given as:

$$\rho_r = \sum_{i=1}^{2n} \left| \psi_i{}^{KS}(1) \right|^2 \qquad (16)$$

Substituting the above equation 16 in equation 15, will yield the KS equations:

$$\left[-\frac{1}{2}\nabla^2{}_i - \sum_A \frac{Z_A}{r_{1A}} + \int \frac{\rho(r_2)}{r_{12}} dr_2 + \nu_{XC}(1)\right] \psi_i{}^{KS}(1) = \varepsilon_i{}^{KS}\psi_i{}^{KS}(1) \qquad (17)$$

where $\varepsilon_i{}^{KS}$ are the KS energy levels and $\nu_{XC}(1)$ is the exchange correlation potential for a particular electron.

The KS equation can be further written as:

$$\hat{h}^{KS}(1)\psi_i{}^{KS}(1) = \varepsilon_i{}^{KS}\psi_i{}^{KS}(1) \qquad (18)$$

where $\hat{h}^{KS}$ is the KS operator. This equation can now be solved in a way that an initial guess of orbitals is made to first calculate the KS operator, which is then used to calculate the coefficients. These coefficients are further used to calculate a better density function and the process is continued till convergence is obtained.

The major problem in DFT is to devise approximations to the exchange-correlation functionals. Several methods have been devised to calculate the exchange-correlation term. One of the simplest approximations is the local density approximation, LDA; which is based solely on the electron density of a uniform electron gas. Assigning different spatial orbitals to the electrons of different spins is done in an improved method; local spin density approximation (LSDA) (5). A further improvement over the LSDA method are the gradient corrected functionals (GGA) (6). In this method, both the electron density and its gradient are utilized. In the exchange-correlation energy functional, the exchange functional is more important and has a much higher contribution to the total exchange-correlation energy. GGA functionals are further improved by considering the second derivative (Laplacian) of electron density in meta-GGA functionals (7). One of the most important pure functional which is self-contained and are not combined with any other functional keyword components is B97D (8). This is

Grimme's functional including dispersion (9). Most of the studies presented in the current thesis, molecular systems are of larger size and hence dispersion effects are expected to play a key role. Hence B97D is a perfect choice as functional which incorporate the dispersion effect.

2.5 Basis Set

A basis set is a set of mathematical functions, linear combinations of which can be linearly combined to produce the monoelectronic functions called molecular orbitals. The mathematical functions are basis functions. Most usually they are atom-based, and can be related to atomic orbitals. Using the linear combination of atomic orbitals (LCAO) approach, the molecular orbital can be represented as:

$$\psi_i = \sum C_{si}\, \phi_s \qquad (19)$$

where, ϕ_s is an atomic orbital type function. There are different mathematical forms for the basis set functions: (a) hydrogen-like wave function, (b) polynomial functions, (c) Slater functions, and (d) gaussian functions. Slater and gaussian functions are the most common choices. The atomic orbitals are better described using a Slater function, as they decay exponentially and have the maximum value at the zero. In this respect, they resemble hydrogen type atomic orbitals. However, the use of Slater functions results in two-electron integrals which are time-consuming to evaluate. An alternative is to use gaussian functions. In Cartesian coordinates, a Slater type orbital (STO) (10) and a Gaussian type orbital (GTO) (11) can be represented as:

$$\chi_{abc}^{STO}(x,y,z) = Nx^a y^b z^c e^{-\zeta \mathrm{r}} \qquad (20)$$

$$\chi_{abc}^{GTO}(x,y,z) = Nx^a y^b z^c e^{-\zeta \mathrm{r}^2} \qquad (21)$$

where *a*, *b* and *c* control the angular momentum, i.e., $L = a + b + c$ and ζ (zeta) is the orbital exponent and controls the space reach of the orbital. The computation of two-electron integrals using gaussian type functions is easier because the product of two gaussians centered on two atoms is a gaussian centered on a point along the axis connecting them. However, gaussian functions represent less accurately the atomic wave function. Unlike the Slater functions, Gaussian functions do not form a cusp at $r = 0$ and decay much faster at larger values of *r*. Thus, the regions closest to and farthest from the nucleus are not treated properly using the Gaussian functions. To circumvent this problem, Boys proposed the use of several Gaussian functions instead of one is used to approximate the atomic wave function (12). STO-3G is the minimal basis function wherein three contracted GTOs are used to approximate an STO (13). Contracted GTOs are constructed from primitive Gaussians using a fixed linear combination.

STO-3G is a minimal basis function in which each atomic orbital in an atom is represented by one basis function alone. In a double zeta basis set, each atomic orbital is approximated using two basis functions. This can be extended to triple-zeta, quadruple-zeta, etc. In a split-valence basis set, the core electrons are described using one basis function for each atomic orbital and the valence electrons which are more important in chemical processes are represented using larger number of basis functions (14). A well-known family of basis sets is that proposed by Pople and co-workers. In a typical 6-31G basis set, the core electrons are represented using one basis function composed of six primitive GTOs (hence the 3), and the valence electrons are represented using two basis functions. The first basis function (inner shell) is approximated using three primitive Gaussians (hence the 3), while the second basis function (outer shell) is composed of one primitive Gaussian (hence the 1). Thus, for a carbon atom, total of 9 basis

functions are used with a split-valence double-zeta basis set.

Increasing the number of contracted GTOs (CGTOs) may not be sufficient to describe the electron distribution. Other different types of Gaussians need to be added to approximate the density in the molecule. As two atoms approach each other, the atomic orbitals can be polarized. For instance, an *s* orbital can be polarized in one direction when it is mixed with a *p* orbital. Similarly, *p* orbitals can polarize when mixed with *d* orbitals. Adding CGTOs of angular momentum higher than those of valence orbitals on an atom helps to increase the flexibility of atoms to form chemical bonds. These gaussian functions are known as polarization shells. In Pople's family of basis sets, they were represented initially using an asterisk '*' for heavy atoms. Adding *p* functions to hydrogen was represented by '**'. This labeling has however been discouraged and replaced by a (d) instead of '*', and (d,p) instead of '**'. In the basis set 6-31G(d), six *d* functions are added per second period atom, resulting in a total of 15 (9+6) basis functions. Another type of function is the diffuse functions which are recommended for anionic systems (15). Heteroatoms, anions and excited state molecules are better described with the addition of diffuse functions. In Pople's family of basis sets, these functions are represented by a '+' for addition to each valence orbital of heavy atoms and by a '++' for addition to hydrogen and helium as well. Most of the calculation in the current thesis involves the optimization with lower basis set 6-31G(d) (16) and the single point calculations with higher basis set 6-311++G(d,p) (17).

As the size of atom increases, the calculations become more expensive due to the large number of two-electron integrals. An approximation which is based on the fact that the properties of most molecules depend on the valence electrons to a greater extent than that of core electrons can be used to speed up calculations. The core

electrons and the nuclear potential are replaced by an effective core potential (ECP). They have the additional advantage of including relativistic effects. The LANL2DZ (Los Alamos NL ECP) (18) and SDD basis set (Stuttgart/Dresden ECPs) (19) are applied in different chapters in this thesis.

2.6 Geometry Optimization

A potential energy surface (PES) expresses the energy of a system as a function of its nuclear coordinates. This concept is a consequence of the Born-Oppenheimer approximation according to which the electronic and nuclear motion can be separated. Different points represent in the PES represent different geometries of a molecule. Points on the surface where the gradient is zero are known as stationary points. In other words, at a stationary point, the first derivative of the potential energy with respect to each geometric parameter is zero. In a one dimensional PES, energy is a function of only one parameter; *i.e.*, bond length. In a PES, where the number of parameters to be varied are equal to or more than three, results in a hypersurface. In studying a reaction mechanism, a key task is the determination of the structure and energy of a molecule. Useful stationary points located on a PES correspond to a minimum, maximum or a saddle point. A transition state or a first order saddle point is a point on the PES, which is a maximum in one direction and minimum in all other directions, thereby resembling a saddle shaped surface. A transition state connects two minima along the minimum energy pathway known as the *intrinsic reaction coordinates* (IRC).

A stationary point is a point on the PES, where the first derivative of energy with respect to each geometric parameter is zero, i.e.,

$$\frac{\partial E}{\partial q_i} = 0 \qquad (22)$$

To characterize this stationary point as a minimum or maximum, the second derivative is evaluated.

For a minimum,

$$\frac{\partial^2 E}{\partial {q_i}^2} > 0 \qquad (23)$$

In the case of a transition state, equation holds for all values by one, where the second derivative is negative, and corresponds to the reaction coordinate. For all other *q*, the second derivative is greater than zero. Geometry optimization of a molecule begins by creating an initial guess and calculating the first and second derivatives of energy with respect to the geometric parameters. The gradient matrix is written as:

$$\begin{bmatrix} \partial E/\partial q_1 \\ \partial E/\partial q_2 \\ \vdots \\ \partial E/\partial q_i \end{bmatrix} \qquad (24)$$

and the second derivative (also known as force matrix or Hessian) is:

$$\boldsymbol{H} = \begin{bmatrix} \partial^2 E/\partial q_1\,\partial q_1 & \partial^2 E/\partial q_1\,\partial q_2 & \partial^2 E/\partial q_1\,\partial q_i \\ \partial^2 E/\partial q_2\,\partial q_1 & \partial^2 E/\partial q_2 \partial q_2 & \partial^2 E/\partial q_2\,\partial q_i \\ \vdots & \vdots & \vdots \\ \partial^2 E/\partial q_i\,\partial q_1 & \partial^2 E/\partial q_i\,\partial q_2 & \partial^2 E/\partial q_i\,\partial q_i \end{bmatrix} \qquad (25)$$

The diagonalization of the Hessian matrix at a stationary point yields eigenvectors and eigenvalues. For a minimum, all eigenvalues are positive, and a transition state has a single negative eigenvalue. The eigenvector associated with this eigenvalue is downhill and a steepest descent from the transition state using mass weighted coordinates gives the minimum energy pathway (IRC). It should be noted that in the most commonly used optimization

algorithms, the Hessian is not calculated for every optimization steps, but only updated. The algorithm used in the optimization of intermediates and transition states in the present thesis is the Berny algorithm which is based on the rational function optimization (RFO) method.

Diagonalization of the Hessian matrix gives the force constants for the normal modes of vibration of a molecule. These force constants can be used to determine the frequencies by including the effect of mass. Since, the frequency calculation involves taking the square root of the force constant (equation (26)), the transition state has one imaginary frequency.

$$S = \frac{1}{2\pi c}\sqrt{\frac{k}{\mu}} \qquad (26)$$

2.7 Solvation Models

The chemical processes investigated in the current thesis are all carried out in a solvent (20). Thus, to represent the energetics of a reaction in a more accurate manner, it is important to consider the effect of solvent on the reaction. The effect of a solvent can be evaluated using two different models: implicit solvation (21) and explicit solvation. As the name suggests, in the explicit solvation model, the solvent molecules are explicitly included in the reaction. The number of solvent molecules may vary depending upon the computational methodology used. While molecular mechanics (MM) and combined quantum and molecular mechanics (QM/MM) methods can be used to treat large number of solvent molecules, the QM methods alone are capable of handling only a few molecules. The use of explicit solvation allows the treatment of various interactions between a solute and the solvent. The implicit solvation model is used for most of the reactions in the thesis which are

carried out in solvents such as benzene and DMF. These solvents are not likely to interact with the substrate via strong interactions and hence can be treated by using a continuum. The solute is placed in a pre-generated cavity of certain size and shape within the solvent reaction field. Two different models are commonly used for the introduction of solvent effects. They are the Polarizable Continuum Model (PCM) (22) and the Solvation Model based on Density (SMD) (23), which differs in minor technical aspects. The SMD method is employed in the current thesis.

2.8 Boltzmann Distribution and Enantioselectivity

The Arrhenius and Eyring equations are two extremely important equations in transition state theory that correlate rate and temperature (24). The higher the temperature, the larger is the kinetic energy associated with the molecules which consequently helps in crossing activation barriers at a faster rate. According to transition state theory the rate of the reaction as given by Eyring can be expressed as:

$$k_{rate} = \left(\frac{k_B T}{h}\right) e^{(-\Delta G^{\ddagger}/RT)} \qquad (27)$$

where k_B, T, h and $\Delta G^{\ddagger}$ are the transmission coefficient, Boltzmann constant, temperature, Planck constant, and free energy of activation, respectively. According to the Boltzmann distribution, population of an energy state is related to the temperature as follows:

$$\frac{N_i}{N_j} = e^{[-[E_i - E_j]/RT]} \qquad (28)$$

The potential energy is assumed to be populated according to the Boltzmann distribution. However it should be noted that in the derivation of the Eyring equation, statistical mechanics is used to

make a substitution for the equilibrium constant. A transition state is not in equilibrium with the reactants, as it would lead to the transition state being sufficiently populated.

For the problems investigated in the current thesis, no accurate measurement of the kinetics has been performed using experiments and hence it is difficult to compare the calculated activation barriers. However, the success of asymmetric reactions which is reported in terms of the enantiomeric excess (*ee*) can be readily evaluated using computational methods. Enantiomeric excess is the difference in the mole fractions of enantiomers *R* and *S*, and can be represented as: $X_R - X_S$. If the amount of the two enantiomeric products is [R] and [S], the % *ee* can be further expressed as:

$$\%ee = \frac{[R] - [S]}{[R] + [S]} \times 100 \qquad (29)$$

According to the Curtin-Hammett principle, the formation of two products from preceding interconvertible intermediates depends on the relative energies of the transition states and is not influenced by the relative energies of the intermediates. Thus, using the Boltzmann distribution, the enantiomeric ratio can be calculated using the following equation:

$$\frac{R}{S} = e^{(-\Delta G^{\ddagger}/RT)} \qquad (30)$$

where, $\Delta G^{\ddagger}$ represents the difference in Gibbs free energies of the diastereomeric transition states leading to the *R* and *S* enantiomers. The % *ee* can now be calculated as follows:

$$\%ee = \frac{1 - e^{(-\Delta G^{\ddagger}/RT)}}{1 + e^{(-\Delta G^{\ddagger}/RT)}} \times 100 \qquad (31)$$

2.9 Kinetic Models

It is easy to get an idea of the kinetics involved in the reaction by comparing energy barriers. However, for mechanisms involving non-straightforward kinetics, containing loops, ramifications, or large differences in initial concentrations, the use of kinetic models may be crucial to understand experimental results (25). In the framework of the work presented in this thesis, the rate constants for all elementary steps were calculated using the Eyring equation (Equation 27). Here the activation energies were determined as the difference in free energy between the transition state corresponding to a particular state, and the previous intermediate connected to it. To illustrate how the simulation is carried out, consider the following reaction mechanism for the conversion of **A** to **D**. Figure 2.1 shows the energy profile corresponding to this hypothetical reaction

$$\mathbf{A} \rightleftharpoons \mathbf{B} + \mathbf{C} \rightarrow \mathbf{D}$$

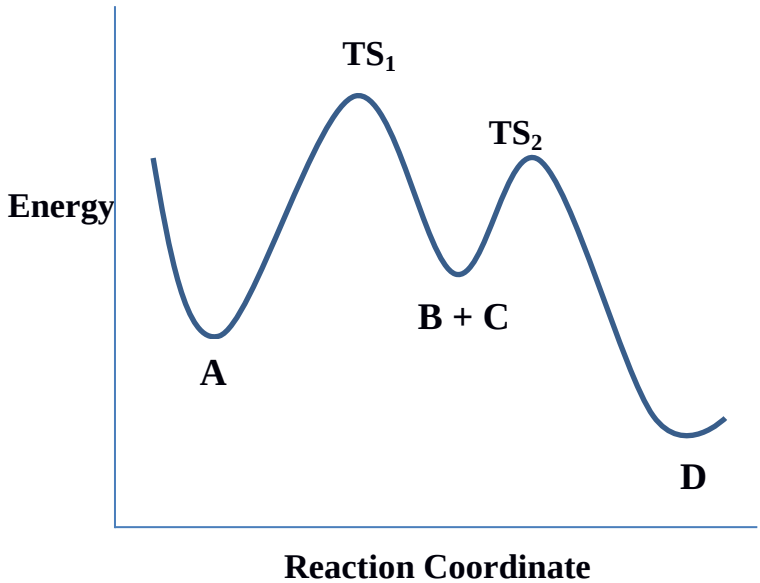

Figure 2.1. Free energy profile of the A → D reaction

The reaction step from **A** to **B + C** is marked as equilibrium since the energies of both states are comparable. This is not the case for the generation of **D,** as the reverse barrier is too high to return in the intermediate state. In this simple case there are three rate equations to consider: (1) the dissociation of **A** into **B** and **C**, (2) the addition of **B** and **C** to restore **A**, and (3) the formation of **D** from **C** and **B**. Each of these equations has a rate constant associated which can be calculated using the energy barrier for each step (*e.g.* k_{-1} is calculated using the energy difference between $\mathbf{TS_1}$ and **C + B**)

1. $\mathbf{A} \underset{k_1}{\rightarrow} \mathbf{B} + \mathbf{C}$
2. $\mathbf{B} + \mathbf{C} \underset{k_{-1}}{\longrightarrow} \mathbf{A}$
3. $\mathbf{B} + \mathbf{C} \underset{k_2}{\rightarrow} \mathbf{D}$

With the elementary step equations, it is simply a problem of solving the differential rate equations for all the species involved to obtain the profile of their concentrations in time. Normally these equations are solved using algorithms. In the work presented in this thesis, concentrations profiles were computed using the Acuchem software (26). Kinetic simulations were carried out to obtain information on reaction mechanisms that do not follow a simple kinetic behavior

2.10 Reference States

Electronic structure programs calculate thermodynamic properties (Enthalpy, Gibbs free energy, entropy, etc.) at some default standard state concentration (pressure) and temperature. In the case of Gaussian09 this is 1 atm and 298K. According to ideal gas law the concentration at these conditions is 0.040874M. The usual reference state however is 1 M, so free energy calculations need to account for the cost of converting from one concentration to the other. Equation (32) shows the straight forward conversion from

ideal gas to 1M.

$$\Delta G_{1M} = -nRTln\left(\frac{0.040874M}{1M}\right) \qquad (32)$$

This results in 1.893 kcal/mol. If the number of mols in the process (n) is conserved, the conversions cancel out since the free energy process id calculated by subtracting the energy of both states involved. For any other process however, the correct free energy needs to be corrected. This conversion is often neglected in computational works as the aim is to obtain qualitative information and large entropic errors are expected in addition/dissociation process. However when quantitative agreement is expected, the conversion becomes necessary.

2.11 Multilayer Methods

Sometimes the size of a system becomes too computationally demanding for a full DFT calculation. However, computationally cheaper methods like force field may be insufficient for the description if complex systems are unable to describe the formation or breakup of bonds, making the inadequate for simulating chemical reactions. Fortunately, for such cases there are methods that allow the computation of a system at two or more different levels of theory. The region that requires a high level description can be calculated at a higher level than the rest of the system. This approach is more accurate than using a model system that sacrifices all interactions from the surroundings (27). To this end, many quantum mechanics/molecular mechanics (QM/MM) strategies have been developed (28).

In a nutshell, in QM/MM approaches a portion of the molecule is described using molecular mechanics, while the rest is assigned to a more demanding method. Among these strategies, there is the ONIOM method (29, 30), which is the QM/MM strategy used in

this thesis. In the ONIOM approach the real system is partitioned into two regions. The first region consists of atoms composing the most important part of the system under study and this part is described at the QM level. The rest of the system is described at the MM level. Equation 33 shows the scheme of the partition between high and low level within the ONIOM approach:

$$E_{tot}\left(\frac{QM}{MM}\right) = E_{MM}(Real) + E_{QM}(Model) - E_{MM}(Model) \qquad (33)$$

Where the subscripts refer to the level of theory applied, and the parenthesis refer to the region of the system being described. Figure 2.2 shows the ONIOM partition scheme represented as spheres.

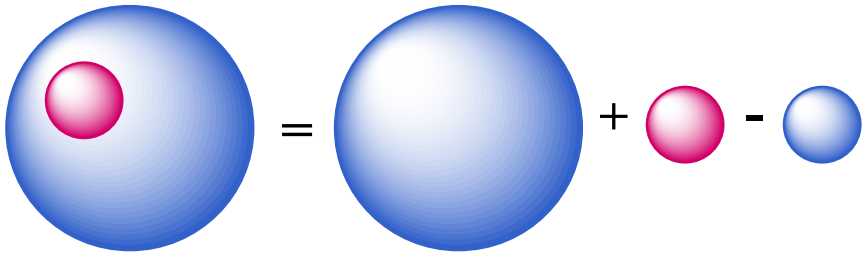

Figure 2.2. Representation of the ONIOM partition scheme

The ONIOM scheme indicates that the entire system is calculated exclusively at the MM level, and only the model system is calculated at the computationally expensive level. One consequence of this is that all interactions that involve the outside system (inner and outside part) are described at the MM level, which is particularly important for non-covalent interactions such as Van der Waals forces. Once the partition is defined, any fragment in the outer layer that is bonded to the model system is replaced by hydrogen in the QM calculation. Therefore, the layers are often divided across a single bond to avoid large errors in the partition.

2.12 Methods Used in this Thesis

The specific methods will be discussed in each section/chapter, but a general comment is pertinent here. The approach adopted in the current thesis involves the use of solvent phase calculations (using continuum solvent model) to establish the reaction profile by identifying various intermediates and the interconnecting transition states for catalytic reactions. Once important stationary points on the potential energy surface are identified, structural and electronic factors are examined in detail. Valuable stereoelectronic features are obtained through such analysis. Since the energetics is computed for different steps of a multi-step reaction, the most likely pathway is established on the basis of the energies. Furthermore, the thermodynamic and kinetic features of such reactions are established on the basis of the knowledge of the potential energy surface. After studying the mechanism in detail, the stereocontrolling transition state is examined for the required projects. A thorough conformation sampling is carried out for the selectivity determining transition state.

2.13 References

(1) (a) Levine, I. N. *Quantum Chemistry 4th edition*, Prentice-Hall Englewood Cliffs, NJ, **1991** (b) Lewars, E. G. *Computational Chemistry: Introduction to the Theory and Application of Molecular and Quantum Mechanics*, Springer, **2006** (c) Szabo, A.; Ostlund, N. S. *Modern Quantum Chemistry: Introduction to Advanced Electronic Structure Theory*, McGraw-Hill, Dover, **1996** (d) Bachrach, S. M. *Computational Organic Chemistry*, John Wiley & Sons Inc., Hoboken, New Jersey, **2007**

(2) (a) Parr, R. G.; Yang, W. *Density Functional Theory of Atoms and Molecules*, Oxford Univiversity Press, New York, **1989** (b)

Kohn, W.; Becke, A. D.; Parr, R. G. *J. Phys. Chem*. **1996**, *100*, 12974

(3) Koch, W.; Holthausen, M. C. *A Chemist's Guide to Density Functional Theory*, Willey VCH, **2001**

(4) Hohenberg, P.; Kohn, W. *Phys. Rev.* **1964**, *136*, B864

(5) (a) Kohn, W.; Sham, L. *J. Phys. Rev. A* **1965**, *140*, 1133 (b) Kohn, W. *Rev. Mod. Phys.* **1999**, *71*, 1253

(6) (a) Perdew, J. P. *Phys. Rev. Lett*. **1985**, *55*, 1665 (b) Perdew, J. P.; Wang, Y. *Phys. Rev. B* **1986**, *33*, 8800 (c) Perdew, J. P.; Schmidt, K. *AIP Conf. Proc.* **2001**, *577*, 1

(7) (a) Proynov, E. L.; Sirois, S.; Salahub, D. R. Int. *J. Quantum Chem.* **1998**, *64*, 427 (b) Van Voorhis, T.; Scuseria, G. E. *J. Chem. Phys.* **1998**, *109*, 400 (c) Perdew, J. P.; Kurth, S.; Zupan, A.; Blaha, P. *Phys. Rev. Lett.* **1999**, *82*, 2544

(8) Ref.2, Appendix

(9) Grimme, S. *J. Comput. Chem*. **2006**, *27*, 1787

(10) Slater, J. C. *Phys. Rev.* **1930**, *36*, 57

(11) Gill, P. M. W. *Advances in Quantum Chemistry* **1994**, *25*, 141

(12) Boys, S. F. *Proc. R. Soc. London Ser. A* **1950**, *200*, 542

(13) Hehre, W. J.; R. F. Stewart; J. A. Pople *J. Chem. Phys*. **1969**, *51*, 2657

(14) (a) Ditchfield, R.; Hehre, W. J.; Pople, J. A. *J. Chem. Phys.* **1971**, *54*, 724 (b) Hehre, W. J.; Ditchfield, R.; Pople, J. A. *J. Chem. Phys*. **1972**, *56*, 2257 (c) Hariharan, P. C.; Pople, J. A. *Theoret. Chim. Acta* **1973**, *28*, 213

(15) Spitznagel, G. W.; Clark, T.; Chandrasekhar, J.; Schleyer, P. V. R. *J. Comput. Chem.* **1982**, *3*, 363

(16) Ref.6, Appendix

(17) Ref.7, Appendix

(18) Ref.8, Appendix

(19) Ref.5, Appendix

(20) (a) Schlegel, H. B. *J. Comput. Chem*. **1982**, *3*, 214 (b) Pulay, P.; Fogarasi, G. *J. Chem. Phys*. **1992**, *96*, 2856 (c) Baker, J. *J. Comp. Chem.* **1993**, *14*, 1085 (c) Peng, C.; Ayala, P. Y.; Schlegel, H. B.; Frisch, M. J. *J. Comp. Chem*. **1996,** *17*, 49

(21) Cramer, C. J.; Truhlar, D. G. *Chem. Rev*. **1999**, *99*, 2161

(22) (a) Miertuš, S.; Scrocco, E.; Tomasi, *J. Chem. Phys.* **1981**, *55*, 117 (b) Miertuš, S.; Tomasi, *J. Chem. Phys.* **1982,** *65*, 239 (c) Pascual-Ahuir, J. L.; Silla, E.; Tuñón, I. *J. Comp. Chem*. **1994**, *15*, 1127 (d) Cossi, M.; Barone, V.; Cammi, R.; Tomasi, J. Chem. Phys. Lett. **1996**, *255*, 327 (e) Tomasi, J.; Mennucci, B.; Cancés, E. *J. Mol. Struct. (THEOCHEM)* **1999**, *464*, 21 (f) Tomasi, J.; Mennucci, B.; Cammi, R. *Chem. Rev.* **2005**, *105*, 2999

(23) Ref.4, Appendix

(24) Anslyn, E. V.; Dougherty, D. A. *Modern Physical Organic Chemistry*, University Science Books, **2005**

(25) Goehry, C.; Besora, M.; Maseras, F. *ACS Catal.* **2015**, *5*, 2445

(26) Braun, W.; Herron, J. T.; Kahaner, D. K. *J. Chem. Kinet*. **1988**, *20*, 51

(27) (a) Maseras, F.; Morokuma, K. J. *Comp. Chem.* **1995**, *16*, 1170 (b) Field, M. J.; Bash, P. A.; Warshel, A. *J. Comp. Chem*. **1990**, *11*,

700

(28) Ref.9, Appendix

(29) Svensson, M.; Humbel, S. Froese, R. D. J.; Matsubara, T.; Sieber, S.; Morokuma, K. *J. Phys. Chem.* **1996**, *100*, 19357

(30) (a) Bo. C.; Maseras, F. *Dalton Trans*. **2008**, 2911 (b) Carbo, J. J.; Maseras, F.; Bo, C.; Van Leeuwen, P. W. N. M. *J. Am. Chem. Soc*. **2001**, *123*, 7630

Chapter 3

Palladium Catalyzed Allene Carboxylation

3.1 Introduction

The catalytic reaction of carbon dioxide with unsaturated compounds was first reported by Inoue and co-workers in 1970's (1). Good yields were obtained for the lactone formation from the reaction of cyclopropane derivatives with carbon dioxide using $Pd(dba)_2$ as the catalyst. Inspired by cross-coupling reactions, a series of methods were further developed which involve the reaction of CO_2 with highly reactive unsaturated small molecules such as ethylene (2) and related π-systems (3). In a seminal report in 2001, Mori and co-workers reported the hydrocarboxylation of polyenes such as allenes (4). They obtained the 1,4-double carboxylation intermediates in good yield by treating 1,3-dienes and allenes with carbon dioxide, one equivalent of $Ni(cod)_2$ and two equivalents of DBU(1,8-Diazabicyclo[5.4.0]undec-7-ene). The final product was then obtained upon reduction with five equivalents of dimethyl zinc.

The reaction of carbon dioxide with allenes was further developed by Takaya and Iwasawa, who reported the regioselective hydrocarboxylation of terminal allenes, in the reaction shown in Scheme 3.1 (5).

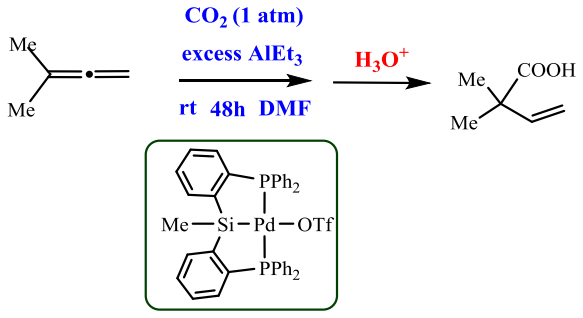

Scheme 3.1. Allene carboxylation reaction reported by Iwasawa and coworkers

The reaction uses tri(ethyl)aluminum as reducing agent, and a tridendate silyl pincer-type palladium complex as catalyst. This process leads to a facile and regioselective synthesis of β,γ-unsaturated carboxylic acids. Remarkably, CO_2 does not insert into the α position of Pd-allyl bond but exclusively into the most substituted γ-carbon. The same methodology was later applied on the carboxylation of 1,3-dienes by the same group (6).

The mechanism proposed by this experimental group is shown in Scheme 3.2. They suggested the presence of a hydride complex (^{Ph}PSiP)Pd-H (C), that could be formed from the precatalyst (^{Ph}PSiP)Pd(OTf) (A) by transmetallation with $AlEt_3$ followed by β–hydride elimination. Then, the allene substrate could undergo hydropalladation to generate an allyl palladium intermediate (D). This allyl complex would be attacked by carbon dioxide at the γ-position regioselectively (E). Finally the transmetallation of the palladium carboxylate complex with $AlEt_3$

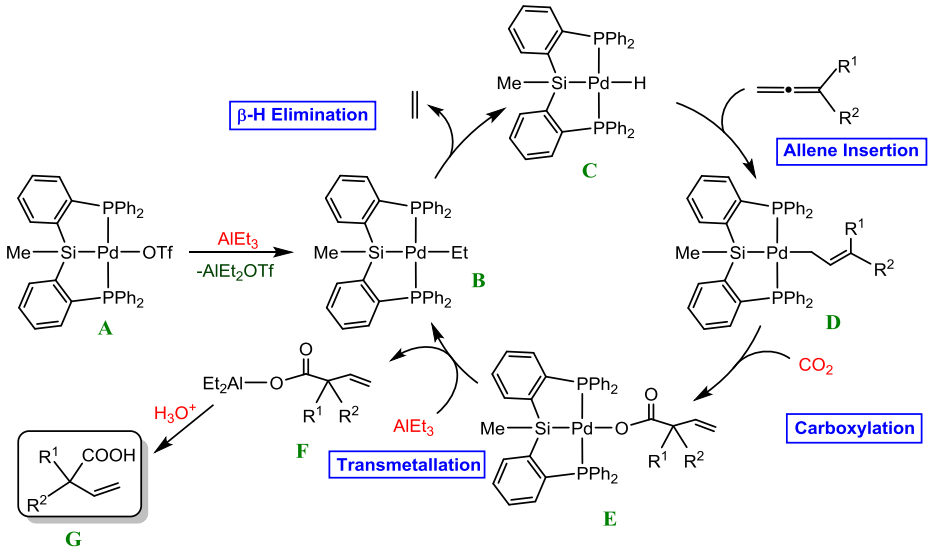

Scheme 3.2. Mechanism of the allene carboxylation reaction suggested by Iwasawa and coworkers

would generate the (^{Ph}PSiP)Pd(Et) (B) species and an aluminum carboxylate salt (F). This ethyl complex is the initial species of the catalytic cycle, which could then be restarted. The final carboxylic acid (G) could then be obtained outside the catalytic cycle by the treatment with acid of the aluminum carboxylate (F). The main drawback of this suggested method is that none of the intermediates including the key Pd-hydride has been isolated and there is no explanation for the observed regioselectivity (7).

A similar process, shown in Scheme 3.3, has been reported more recently by Hazari and co-workers (8). There are minor differences in the system, as the precursor is directly (^{cy}PSiP)Pd-H (Instead of Ph, here the cyclohexyl group (cy) is bound to phosphorus), and the solvent is also different, but the mechanism should be similar. The big contribution from Hazari's work is the performance of a number of stoichiometric reactions that allow isolation of many intermediates and lead to the proposal of an alternative mechanism.

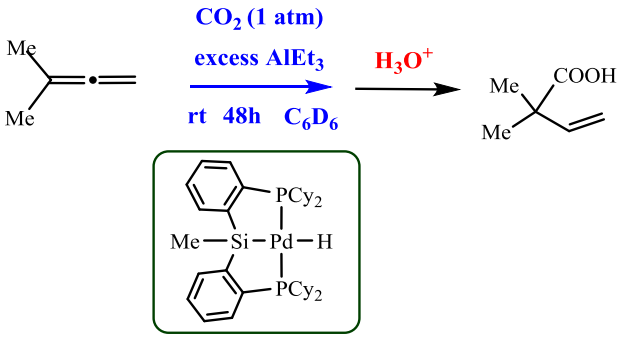

Scheme 3.3. Allene carboxylation reaction reported by Hazari and coworkers

The mechanism proposed by Hazari and co-workers is shown in Scheme 3.4. This mechanism consists of two linked cycles. The one in the right-hand of the Scheme is similar to that proposed by Iwasawa and co-workers. The one on the left-hand is necessary to

account for the observations in the additional stoichiometric experiments. The idea is that the hydride intermediate **1** may react either with the allene or with carbon dioxide.

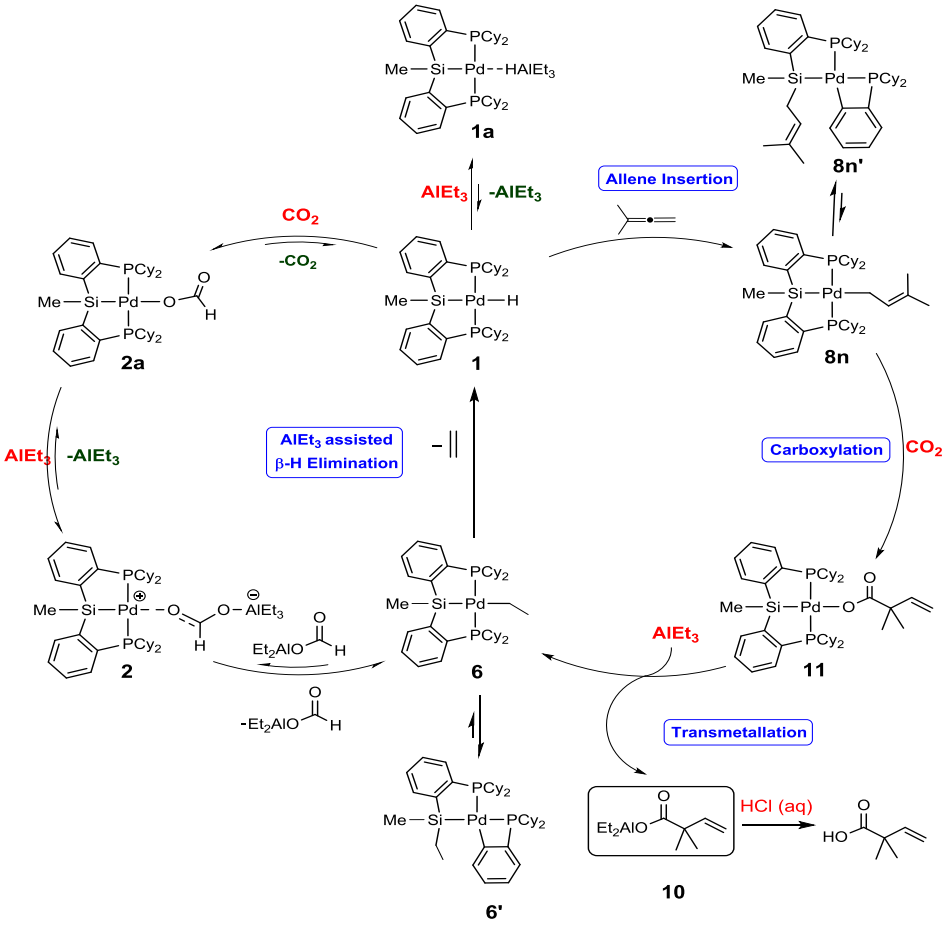

Scheme 3.4. Mechanism of the allene carboxylation reaction suggested by Hazari and co-workers

We found quite puzzling that the reaction requires specifically tri(ethyl)aluminum, as other reducing agents are not efficient. There are also other aspects in this complex catalytic cycle that are not clear. Because of this, we decided to analyze the system with DFT calculations that have been used in our group for

other reactions involving carbon dioxide (9).

3.2 Computational Details

The geometries of all the intermediates and transition states were optimized by using a hybrid QM/MM ONIOM method (10) employing the Gaussian 09 suite of programs (11). Molecular mechanics were used for all the cyclo hexyl group in the catalyst (Pd-pincer complex) and quantum mechanics were used for rest of the system which involves the chemical process. For the quantum mechanical part, we employed the B97D functional (12). The SDD basis set (13) with the effective core potential was applied for Pd and the 6-31G(d) basis set (14) was used for all other atoms. The UFF force field was used for the molecular mechanics part (15). Frequency calculations were carried out at the same level of theory to identify stationary points as transition or as minima and obtain free energy corrections at 298.15 K and 1 atm. Geometry optimization of all the stationary points was carried out in the gas phase. Transition states were characterized by a unique imaginary frequency, which was verified to represent the desired reaction coordinate in each case. Connectivity between intermediates and transitions states by manual displacement of geometries in case of doubt. Potential energies were refined with a higher basis set and solvation effects through full QM single point calculations. These were done with SDD for Pd and 6-311++g(d,p) for all other atoms (16). Implicit solvation (benzene, ε= 2.2706) was introduced with SMD (17). All the reported energies are free energies in kcal/mol calculated with respect to the separated reactants.

3.4 Results and Discussions

The computational study used the mechanism proposed by Hazari and co-workers as the starting point, but some significant nuances were added by the calculation.

Our computed mechanism is shown in Scheme 3.5. It is composed of two linked cycles. That on the left, labeled as cycle 1, yields a formate metal complex from the reaction between the catalyst, carbon dioxide and tri(ethyl)aluminium. This formate complex **7** will then interact with allene in the cycle in the right, cycle 2, resulting in the carboxylate compound **10**. The ligand system, ^{cy}PSiP is denoted as L_n throughout the chapter. The detailed free energy profile diagram corresponds to the first cycle is given in Figure 3.1 and that of second cycle is given in the Figure 3.2.

The reaction in cycle 1 can be envisaged as beginning with the L_n-Pd-H complex **1**. This complex is in equilibrium with **1a**, an adduct with $AlEt_3$. The $AlEt_3$ species present in the system as additive will readily coordinate to **1**, where the hydride is bridging between Pd and Al. This complex is quite stable (-15.2 kcal/mol with respect to **1**), and we will use it as origin of energies. However, **1a** is not able to advance the reaction, and must revert to **1**. The hydride complex **1** is indeed able to insert CO_2 (18).

The most efficient mechanism for the insertion of CO_2 occurs with the assistance of $AlEt_3$. This occurs via two steps. In the first step, nucleophilic attack of hydride to the carbon atom of CO_2 and coordination of $AlEt_3$ into one of the oxygen atoms of CO_2 occur in a concerted fashion to form intermediate **1b**, which has an energy 2.3 kcal/mol above **1a**. This complex isomerizes to complex **2** containing a Pd-O bond through a low barrier transition state **t(1b-2)** (19). The highest energy in the path from **1** to **2** belongs to transition state **t(1-1b)**, corresponding to the formation of intermediate **1b**, which is 4.0 kcal/mol above reactants. One could envisage a direct reaction between carbon dioxide and **1** without participation of tri(ethyl)aluminum. This path is shown in Figure 3.3, and has a highest energy point **t(1-1d)** 7.8 kcal/mol above reactants. This is far above **t(1-1b)**, which confirms a role for $AlEt_3$

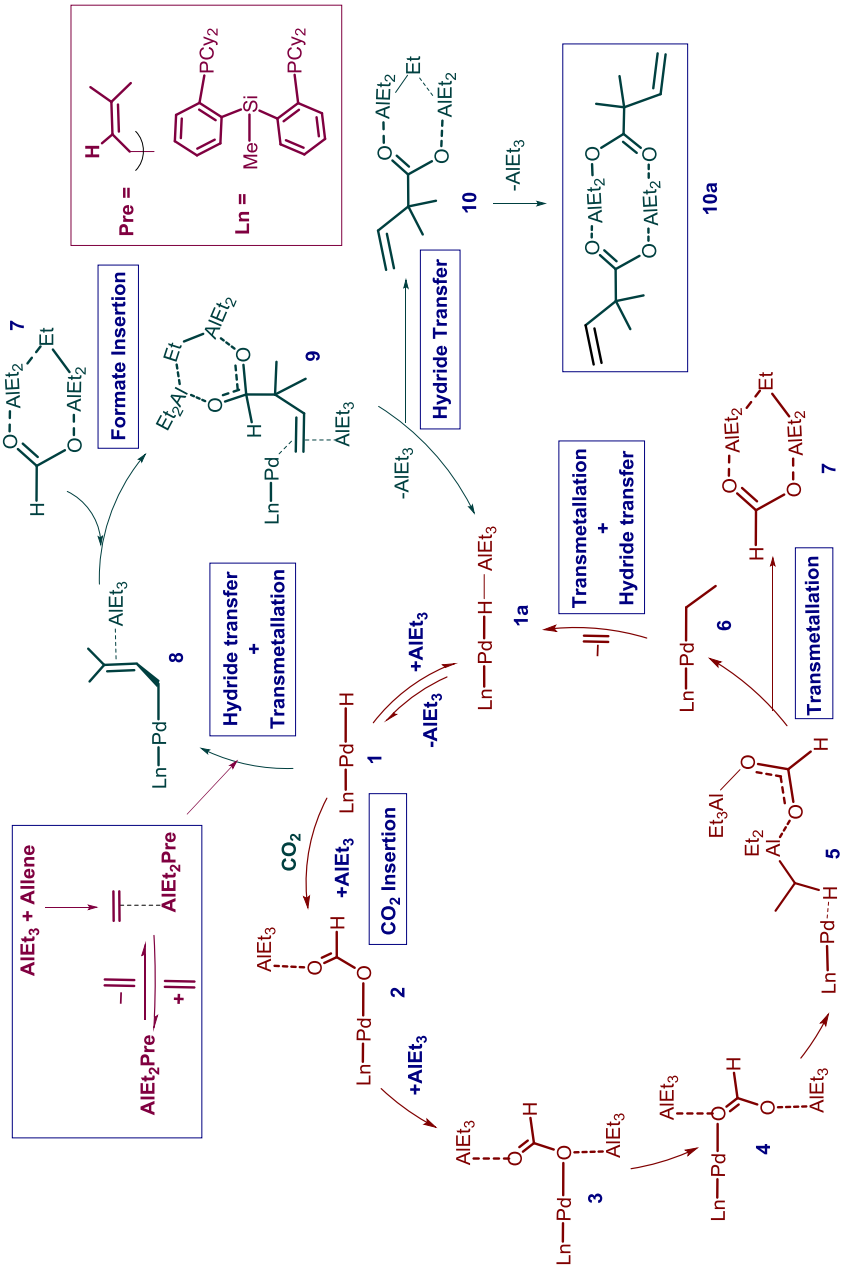

Scheme 3.5. Computed overall mechanism for the allene carboxylation reaction

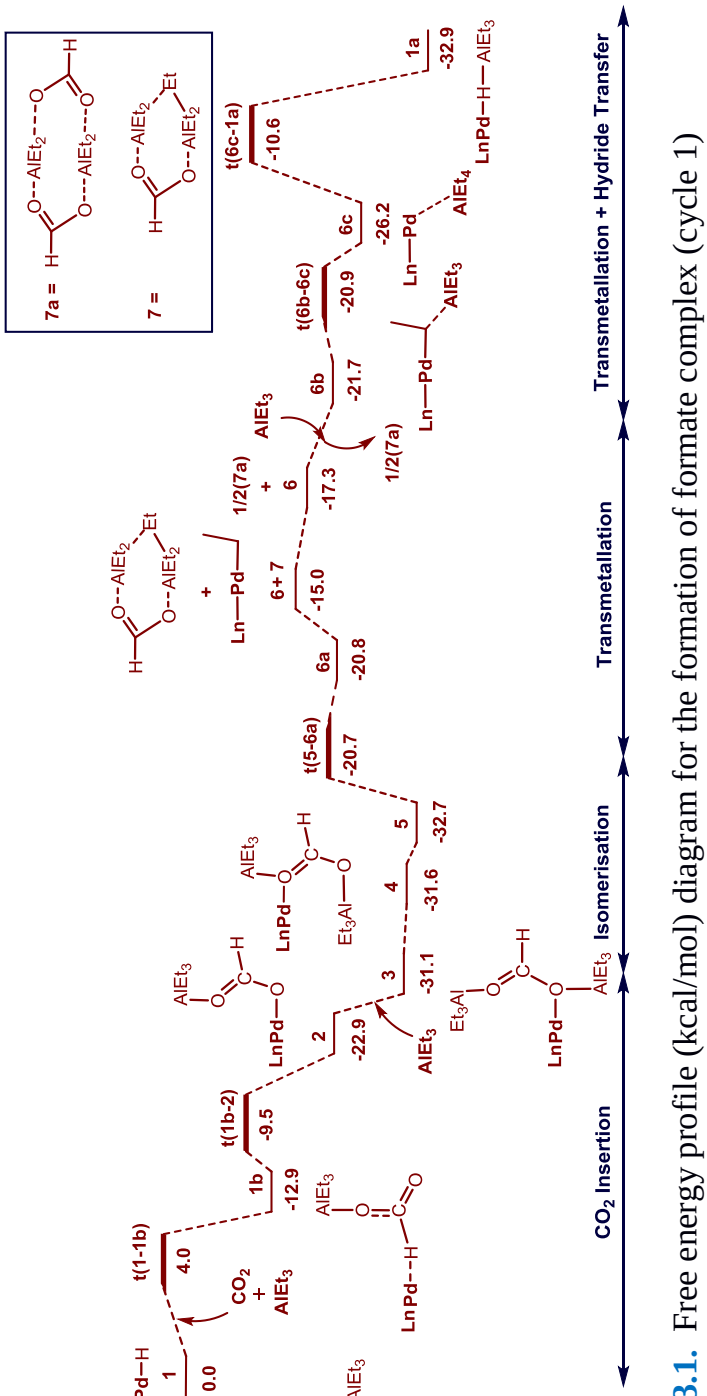

Figure 3.1. Free energy profile (kcal/mol) diagram for the formation of formate complex (cycle 1)

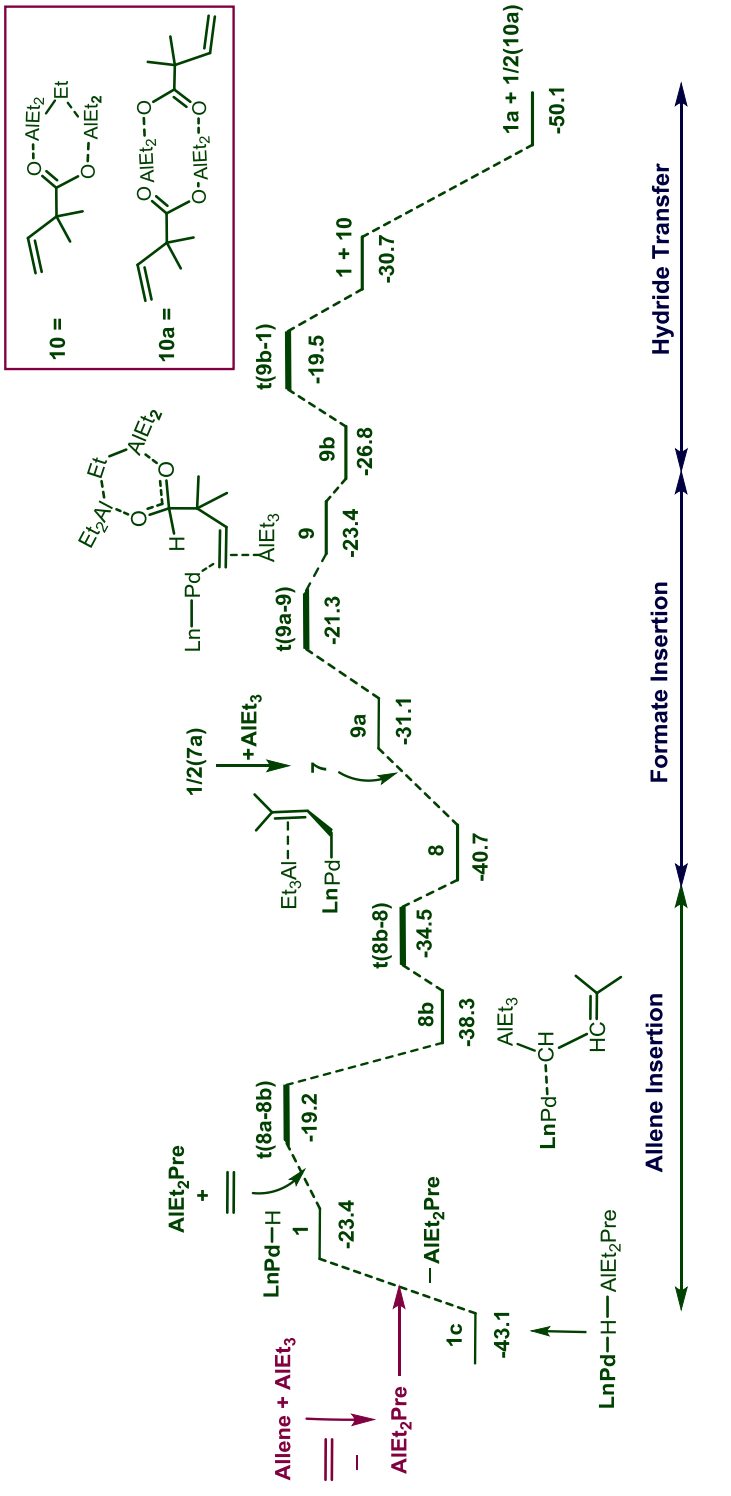

Figure 3.2. Free energy profile (kcal/mol) diagram for cycle 2 in the allene carboxylation

$AlEt_3$ in lowering the barrier for the fixation of CO_2 by the complex.

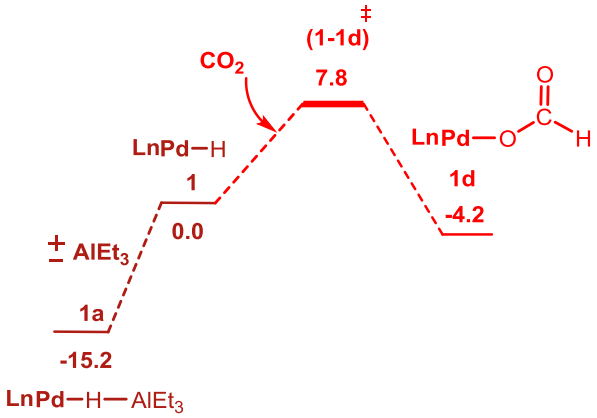

Figure 3.3. Free energy profile (kcal/mol) diagram for the direct CO_2 insertion to Pd-H species

Complex **2** continues the reaction by forming an adduct **3**, with an additional molecule of $AlEt_3$. Intermediate **3** is quite stable at 31.1 kcal/mol, and the backward reaction from **3** to **1** that had been postulated in the experimental proposal has to be discarded because forward paths have lower barriers.

Complex **3** contains a peculiar $(HCO_2^-)(AlEt_3)_2$ in the palladium coordination sphere that changes its coordination to palladium in complexes **4** and **5**, all of them with similar energies. Complex **5** is interesting because coordination to palladium is not through the oxygen atoms of the formate subunit, but through one of the ethyl substituents. This ethyl group is transferred to the palladium center to form Pd-ethyl species **6** plus the remarkable formate complex **7,** containing two aluminum centers and five ethyl substituents. The transition state **t(5-6a)** for this step is only 12.0 kcal/mol above **5**. Complex **6** will continue cycle 1, while species **7** will be used in cycle 2, discussed below. From the ethyl complex **6**, the regeneration of catalyst **1a** occurs. This is assisted by $AlEt_3$ via two steps. The first step is the abstraction of ethyl group by $AlEt_3$ in

an S_N2 fashion from intermediate **6b,** resulting in intermediate **6c.** In **6c**, Pd is stabilized by the hydrogen in the sp^3 carbon of one of the ethyl group in the $AlEt_4$ complex. The second step involves the hydride transfer to Pd from the sp^3 carbon of one of the ethyl group

In cycle 2, the allene insertion occurs. Prior to its entrance in the catalytic cycle, the allene molecule is activated by the $AlEt_3$ present in the system to form the $AlEt_2Pre$ species (pre = prenyl, which is the name of the substituent obtained from allene by hydride addition to its central carbon atom. This label will be used throughout this section because of the ubiquitous presence of these species) (**IM2,** Scheme 3.6). This activation has a free energy barrier of 22.3 kcal/mol, and an energy gain of 7.7 kcal/mol. This off cycle step is important, as it contains a species such as **IM1**

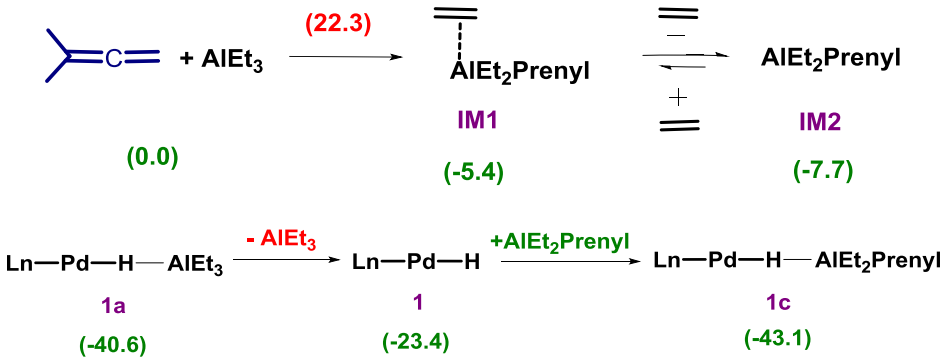

Scheme 3.6. Activation of the allene by $AlEt_3$

where aluminum is coordinated by two ethyls, one prenyl and one ethylene group. The prenyl group is in particular activated for further reaction.

The free energy profile for cycle 2 is shown in Figure 3.2. Similar to the formation of **1a** from **1**, the $AlEt_2Pre$ fragment can form an adduct with **1** to form **1c**. This **1c** species acts as a thermodynamic sink, as it must revert to **1** before the reaction proceeds forward. Next follows a complicated step where **1**

interacts with the **IM1** adduct (from Scheme 3.6), resulting in species **8b**, containing a Pd-$AlEt_3$Pre unit. The ligand involving prenyl and aluminum is rearranged in the next step resulting in intermediate **8**.

The formate complex **7** which was generated in cycle 1 will insert to the Pd-prenyl complex (**8**) in the next step. Here either $AlEt_3$ or $AlEt_2$Pre can assist the further reaction pathway depending upon the rate of formation of $AlEt_2$Pre (which was generated from allene and $AlEt_3$). The profile in Figure 3.2 shows the reaction with $AlEt_3$ although a similar one could be reported with $AlEt_2$Pre. C-C bond formation by the insertion of formate complex into the most substituted carbon of prenyl group in complex **8** produce intermediate **9**. Subsequent transfer of hydride occurs from the ligand to Pd leads to release of product **10** and regeneration of catalyst **1**. The geometry of the key transition states involved in Scheme 3.5 is given in Figure 3.4

The generation of the prenyl-substituted $AlEt_2$Pre along the reaction path prompted us to investigate if it could play an extended role replacing $AlEt_3$. The resulting reaction cycle is shown in Scheme 3.7, with the corresponding free energy profiles provided in Figures 3.5 and 3.6. The geometry of the key transition states involved in Scheme 3.7 is given in Figure 3.7. The reaction is not substantially different from the initial proposal. First, the generated $AlEt_2$Pre readily coordinates with **1** to form **1c**. The CO_2 insertion occurs after the decoordination of $AlEt_2$Pre from **1c** to form **1**. The CO_2 insertion occurs in two steps which are similar as discussed in the previous pathway to form **2p**. The advantage in this alternative cycle is that the prenyl group is naturally incorporated in the catalytic cycle. A close examination of the free energy profile diagram (Figure 3.5) which corresponds to the green cycle in Scheme 3.7 explains that the energy of all the steps involved in the

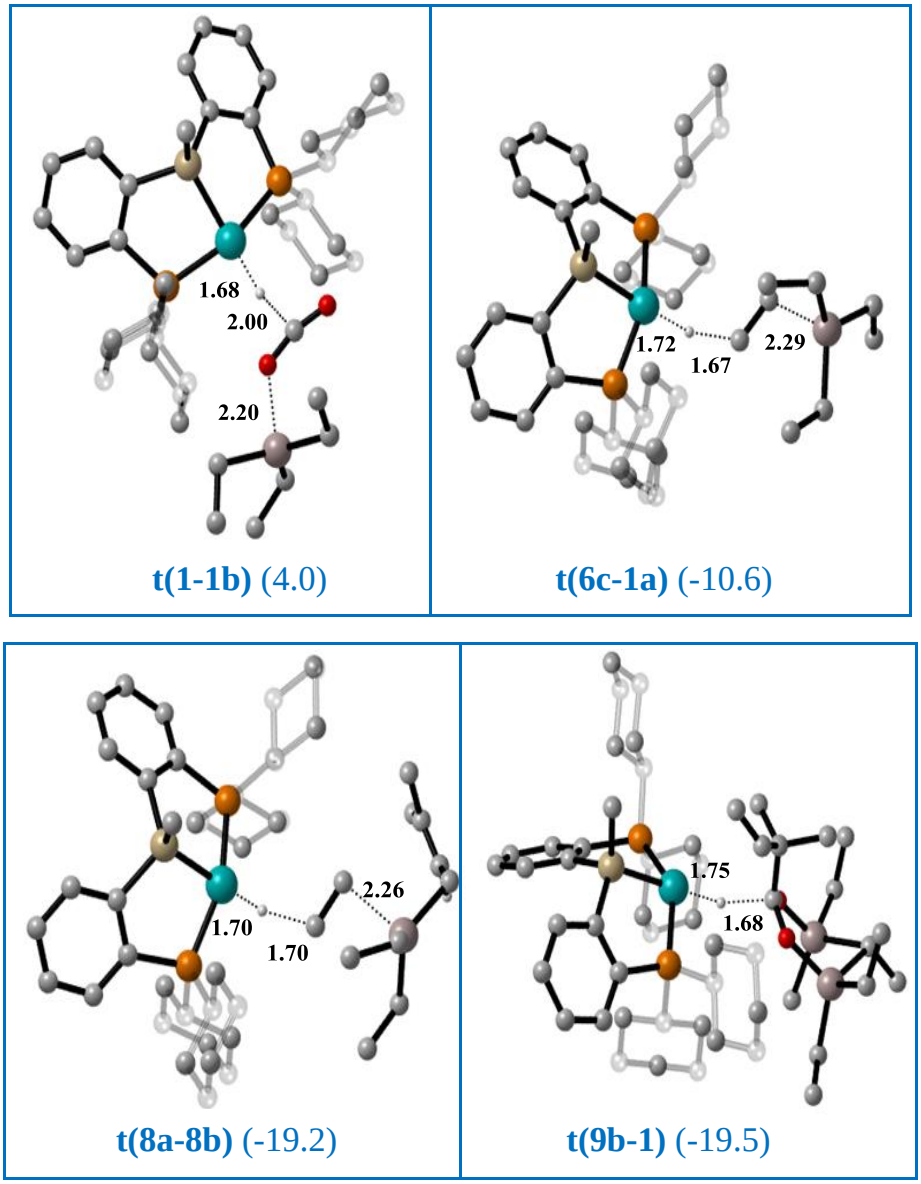

Figure 3.4. Optimized geometries of the key transition states involved in the catalytic cycle shown in Scheme 3.5. The relative free energies (kcal/mol) are given in parentheses. All distances are in Å

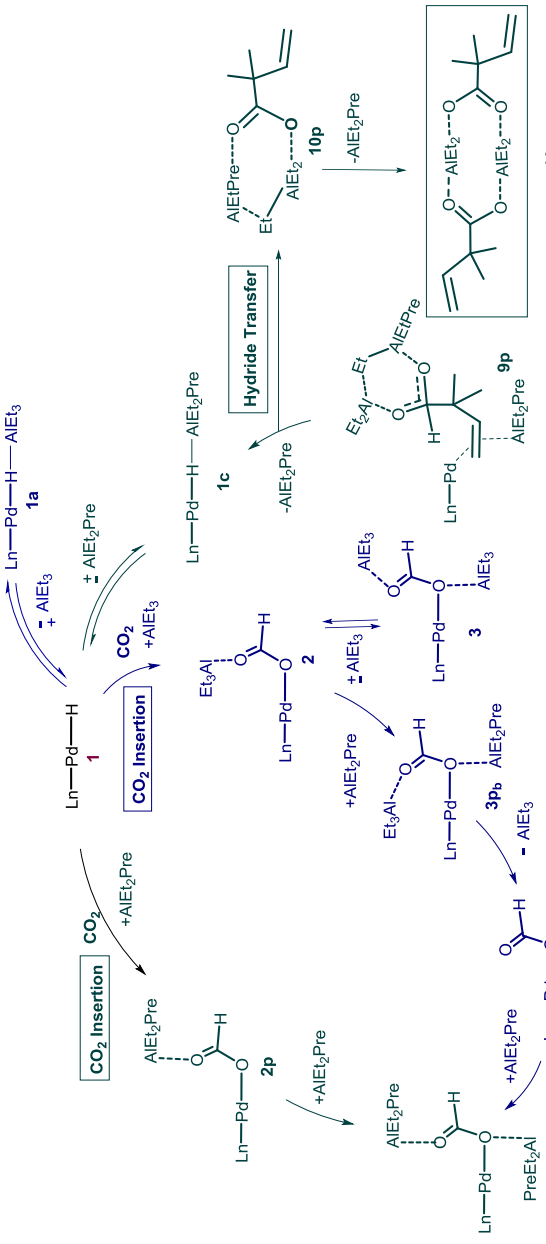

Scheme 3.7. Alternative mechanism for the allene carboxylation reaction

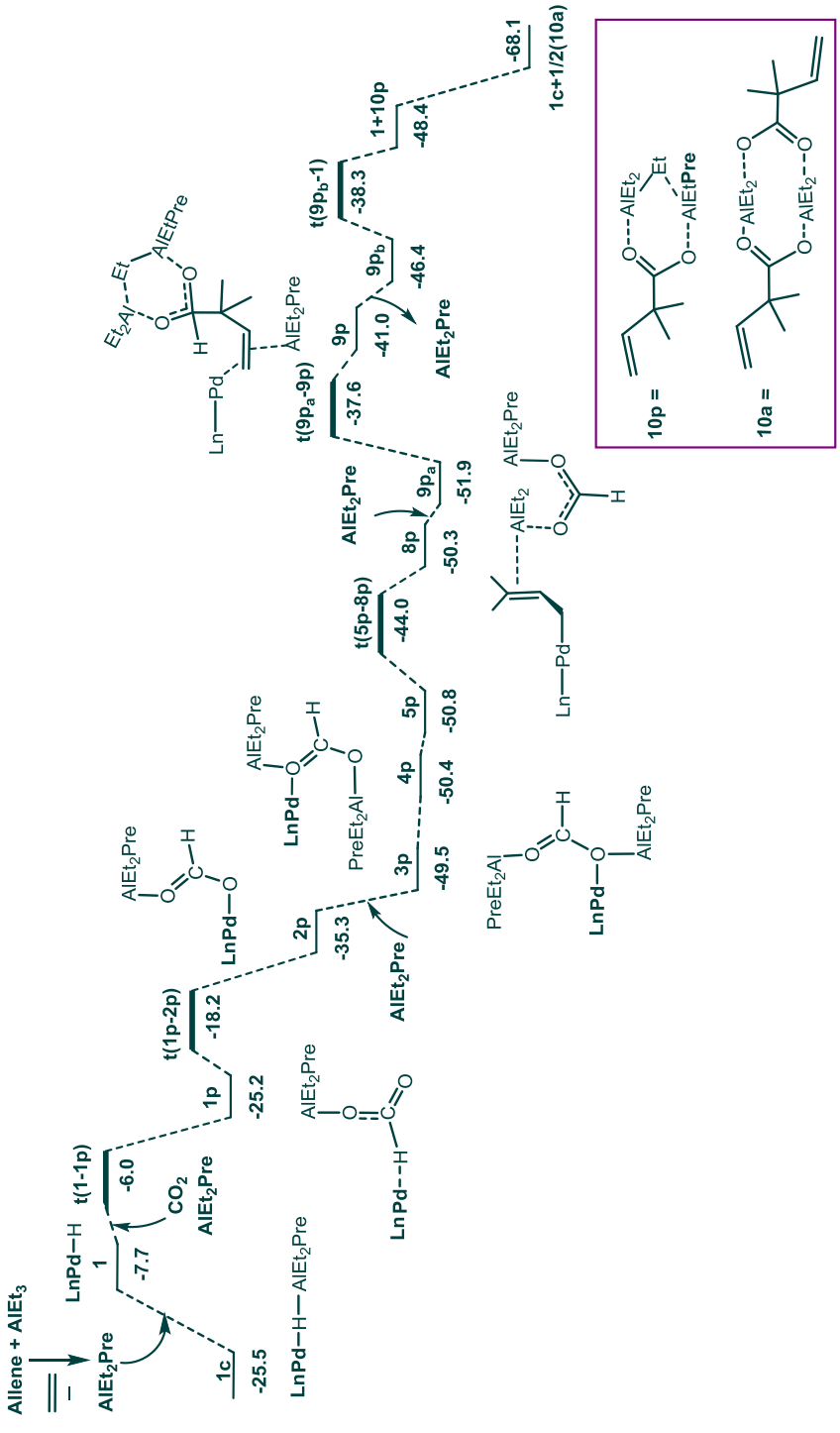

Figure 3.5. Free energy profile (kcal/mol) diagram for the green cycle in scheme 3.7

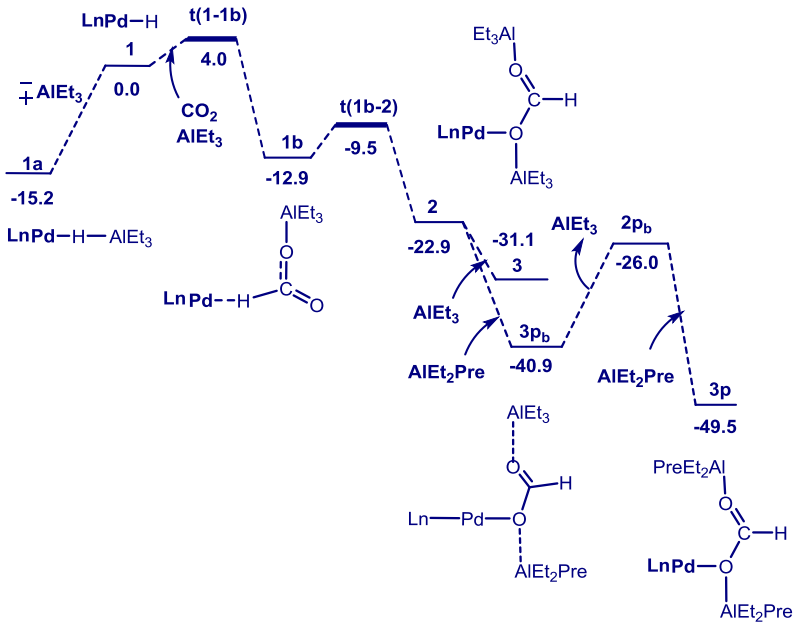

Figure 3.6. Free energy profile (kcal/mol) diagram for the blue cycle in scheme 3.7

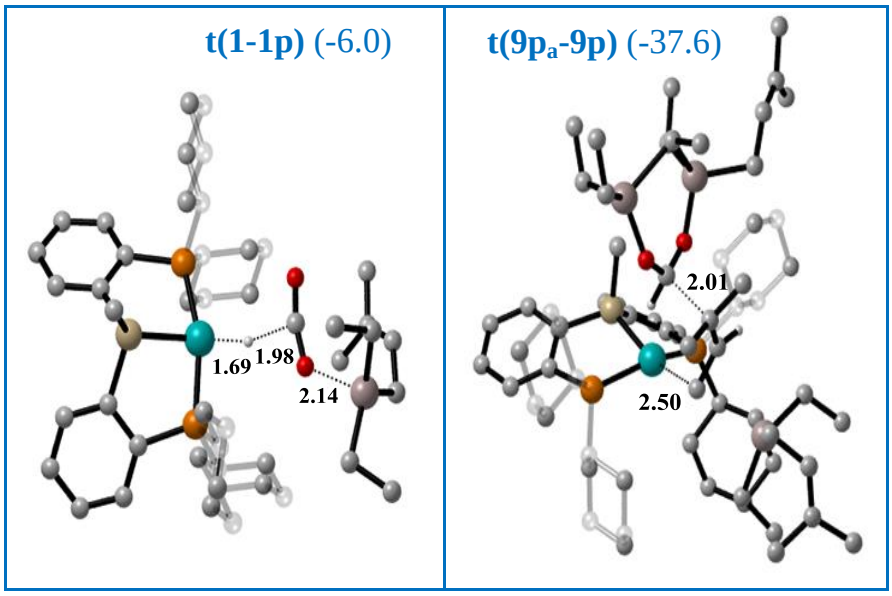

Figure 3.7. Optimized geometries of the key transition states involved in the catalytic cycle shown in Scheme 3.7. The relative free energies (kcal/mol) are given in parentheses. All distances are in Å

mechanism is below 20 kcal/mol. The only required step with a high barrier is the formation of $AlEt_2Pre$ from $AlEt_3$ and allene. This means that once the allene is activated into $AlEt_2Pre$, the reaction proceeds faster with its assistance. There are of course other possibilities combining the two proposed catalytic cycles. $AlEt_3$ may participate in the reaction in the beginning and later merge to the stable intermediate **3p** by the exchange of $AlEt_3$ with $AlEt_2Pre$. We have also considered the possible insertion of allene prior to the CO_2 and it is found that CO_2 insertion is energetically favorable over allene insertion. In summary, there are a lot of possible variations of the same mechanism with similar affordable barriers.

3.5 Conclusion

A detailed study on the mechanism of the allene carboxylation was carried out. The overall reaction barrier is 22.3 kcal/mol, which is in agreement with the experimental conditions. Carbon dioxide does not seem to insert into the Pd-prenyl complex, as was originally proposed. Instead, the aluminum additive has an important effect throughout the mechanism, both in carbon dioxide activation and in allene activation. The role of the aluminum-based Lewis acid goes much beyond the original suggestion as an assistant for the transmetallation step through β-hydride elimination. It may act either in its original $AlEt_3$ form or in $AlEt_2Pre$, with different paths possible coexisting in solution. The widespread role of this additive in the reaction points to a difficult replacement by seemingly similar Lewis acids.

3.6 References

(1) (a) Sasaki, Y.; Inoue, Y.; Hashimoto, H. *J. Chem. Soc. Chem. Commun.* **1976**, *15*, 605 (b) Inoue, Y.; Ito, Y.; Hashimoto, H. *Chem. Lett.* **1977**, *8*, 855 (c) Inoue, Y.; Ito, Y.; Hashimoto, H. *Chem. Lett.*

1978, *9*, 633 (d) Inoue, Y.; Hibi, T.; Satake, M.; Hashimoto, H. *J. Chem. Soc. Chem. Commun.* **1979**, *18*, 982

(2) (a) Hoberg, H.; Peres, Y.; Krüger, C.; Tsay, Y.-H. *Angew. Chem., Int. Ed.* **1987**, *26*, 771 (b) Bernskoetter, W. H.; Tyler, B. T. *Organometallics* **2011**, *30*, 520 (c) Wolfe, J. M.; Bernskoetter, W. H. *Dalton Trans.* **2012**, *41*, 10763 (d) Jin, D.; Schmeier, T. J.; Williard, P. G.; Hazari, N.; Bernskoetter, W. H. *Organometallics* **2013**, *32*, 2152 (e) Jin, D.; Williard, P. G.; Hazari, N.; Bernskoetter, W. H. *Chem. Eur. J.* **2014**, *20*, 3205 (f) Lejkowski, M. L.; Lindner, R.; Kageyama, T.; Bodizs, G. E.; Plessow, P. N.; Mueller, I. B.; Schaefer, A.; Rominger, F.; Hofmann, P.; Futter, C.; Schunk, S. A.; Limbach, M. *Chem. Eur. J.* **2012**, *18*, 14017 (g) Plessow, P. N.; Weigel, L.; Lindner, R.; Schaefer, A.; Rominger, F.; Limbach, M.; Hofmann, P. *Organometallics* **2013**, *32*, 3327

(3) (a) Williams, C. M.; Johnson, J. B.; Rovis, T. *J. Am. Chem. Soc.* **2008**, *130*, 14936 (b) Fujihara, T.; Xu, T.; Semba, K.; Terao, J.; Tsuji, Y. *Angew. Chem., Int. Ed.* **2011**, *50*, 523 (c) Li, S.; Yuan, W.; Ma, S. *Angew. Chem., Int. Ed.* **2011**, *50*, 2578 (d) Zhang, Y.; Riduan, S. N. *Angew. Chem., Int. Ed.* **2011**, *50*, 6210 (e) Greenhalgh, M. D.; Thomas, S. P. *J. Am. Chem. Soc.* **2012**, *134*, 11900

(4) (a) Takimoto, M.; Mori, M. *J. Am. Chem. Soc.* **2001**, *123*, 2895 (b) Takimoto, M.; Mori, M. *J. Am. Chem. Soc.* **2002**, *124*, 10008 (c) Takimoto, M.; Nakamura, Y.; Kimura, K.; Mori, M. *J. Am. Chem. Soc.* **2004**, *126*, 5956 (d) Takimoto, M.; Kawamura, M.; Mori, M.; Sato, Y. *Synlett,* **2005**, 2019 (e) Takimoto, M.; Kawamura, M.; Mori, M.; Sato, Y. *Synlett* **2011**, 1423

(5) Takaya, J.; Iwasawa, N. *J. Am. Chem. Soc.* **2008**, *130*, 15254

(6) Takaya, J.; Sasano, K.; Iwasawa, N. *Org. Lett.* **2011**, *13*, 1698

(7) (a) Johansson, R.; Wendt, O. F. *Organometallics* **2007**, *26*, 2426 (b) Chakraborty, S.; Zhang, J.; Krause, J. A.; Guan, H. *J. Am. Chem. Soc.* **2010**, *132*, 8872 (c) Schmeier, T. J.; Hazari, N.; Incarvito, C. D.; Raskatov, J. R. *Chem. Commun.* **2011**, *47*, 1824 (d) Chakraborty, S.; Patel, Y. J.; Krause, J. A.; Guan, H. *Polyhedron* **2012**, *32*, 30 (e) Suh, H.-W.; Schmeier, T. J.; Hazari, N.; Kemp, R. A.; Takase, M. K. *Organometallics* **2012**, *31*, 8225; (f) Mitton, S. J.; Turculet, L. *Chem. Eur. J.* **2012**, *18*, 15258 (g) Venkanna, G. T.; Tammineni, S.; Arman, H. D.; Tonzetich, Z. J. *Organometallics* **2013**, *32*, 4656 (h) Yoo, C.; Kim, J.; Lee, Y. *Organometallics* **2013**, *32*, 7195 (i) Takaya, J.; Iwasawa, N. *Organometallics* **2009**, *28*, 6636 (j) Takaya, J.; Iwasawa, N. *Dalton Trans.* **2011**, *40*, 8814

(8) Suh, H. W.; Guard, L. M.; Hazari, N. *Chem. Sci.* **2014**, *5*, 3859

(9) (a) Guo, W.; Martínez-Rodríguez, L.; Kuniyil, R.; Martin, E.; Escudero-Adán, E. C.; Maseras, F.; Kleij, A. W. *J. Am. Chem. Soc.* **2016**, *138*, 11970 (b) Whiteoak, C. J.; Nova, A.; Maseras, F.; Kleij, A. W. *ChemSusChem*, **2012**, *5*, 2032 (c) Kuniyil, R.; Maseras, F. *Theor. Chem. Acc.* **2017**, *136*, 65

(10) Ref.9 Appendix

(11) Ref.3 Appendix

(12) Ref.2 Appendix

(13) Ref.5 Appendix

(14) Ref.6 Appendix

(15) Ref.10 Appendix

(16) Ref.7 Appendix

(17) Ref.4 Appendix

(18) (a) Santi, R.; Marchi, M. *J. Organomet. Chem.* **1979**, *182*, 117 (b) Hung, T.; Jolly, P. W.; Wilke, G. *J. Organomet. Chem.* **1980**, *190*, C5 (c) Behr, A.; Von Ilsemann, G. *J. Organomet. Chem.* **1984**, *276*, C77 (d) Jolly, P. W. *Angew. Chem., Int. Ed.* **1985**, *24*, 283 (e) Johansson, R.; Wendt, O. F. *Dalton Trans.* **2007**, 488 (f) Johnson, M. T.; Johansson, R.; Kondrashov, M. V.; Steyl, G.; Ahlquist, M. S. G.; Roodt, A.; Wendt, O. F. *Organometallics* **2010**, *29*, 3521 (g) Wu, J.; Hazari, N.; Incarvito, C. D. *Organometallics* **2011**, *30*, 3142 (h) Braunstein, P.; Matt, D.; Nobel, D. *J. Am. Chem. Soc.* **1988**, *110*, 3207 (i) Pitter, S.; Dinjus, E. *J. Mol. Catal. A: Chem.* **1997**, *125*, 39 (j) Aresta, M.; Quaranta, E.; Tommasi, I. *New J. Chem.* **1994**, *18*, 133 (k) Shi, M.; Nicholas, K. M. *J. Am. Chem. Soc.* **1997**, *119*, 5057 (l) Franks, R. J.; Nicholas, K. M. *Organometallics* **2000**, *19*, 1458

(19) Bondi, A. *J. Phys. Chem.* **1964**, *68*, 441

(20) (a) Evans, W. J.; Meadows, J. H.; Wayda, A. L.; Hunter, W. E.; Atwood, J. L. *J. Am. Chem. Soc.* **1982**, *104*, 2015 (b) Evans, W. J.; Forrestal, K. J.; Ansari, M. A.; Ziller, J. W. *J. Am. Chem. Soc.* **1998**, *120*, 2180 (c) Yan, K.; Duchimaza Heredia, J. J.; Ellern, A.; Gordon, M. S.; Sadow, A. D. *J. Am. Chem. Soc.* **2013**, *135*, 15225 (d) Yan, K.; Schoendorff, G.; Upton, B. M.; Ellern, A.; Windus, T. L.; Sadow, A. D. *Organometallics* **2013**, *32*, 1300

(21) (a) Deeming, A. J.; Johnson, B. F. G.; Lewis, J. *J. Chem. Soc., Chem. Commun.* **1970**, 598 (b) Deeming, A. J.; Johnson, B. F. G.; Lewis, J. *J. Chem. Soc., Dalton Trans.* **1973**, 1848 (c) Ros, R.; Michelin, R. A.; Bataillard, R.; Roulet, R. *J. Organomet. Chem.* **1979**, *165*, 107 (d) Bercaw, J. E.; Moss, J. R. *Organometallics* **1992**, *11*, 639 (e) Hogarth, G.; Lavender, M. H. *J. Chem. Soc., Dalton Trans.* **1992**, 2759 (f) Delis, J. G. P.; Groen, J. H.; Vrieze,

K.; van Leeuwen, P. W. N. M.; Veldman, N.; Spek, A. L. *Organometallics* **1997**, *16*, 551 (g) Choi, J.-c.; Osakada, K.; Yamamoto, T. *Organometallics* **1998**, *17*, 3044 (h) Osakada, K.; Kimura, M.; Choi, J. C. *J. Organomet. Chem.* **2000**, *602*, 144 (i) Nakanishi, S.; Sasabe, H.; Takata, T. *Chem. Lett.* **2000**, 1058 (j) Zhao, C.-Q.; Han, L.-B.; Tanaka, M. *Organometallics* **2000**, *19*, 4196 (k) Xue, P.; Zhu, J.; Hung, H. S. Y.; Williams, I. D.; Lin, Z.; Jia, G. *Organometallics* **2005**, *24*, 4896 (l) Bai, T.; Zhu, J.; Xue, P.; Sung, H. H.-Y.; Williams, I. D.; Ma, S.; Lin, Z.; Jia, G. *Organometallics* **2007**, *26*, 5581 (m) Cabeza, J. A.; del Rio, I.; Fernandez-Colinas, J. M.; Perez-Carreno, E.; Vazquez-Garcia, D. *Organometallics* **2010**, *29*, 4818 (n) Hossain, M. I.; Ghosh, S.; Hogarth, G.; Golzar, H. G. M.; Kabir, S. E. *J. Organomet. Chem.* **2011**, *696*, 3036 (o) Bai, T.; Ma, S.; Jia, G. *Coord. Chem. Rev.* **2009**, *253*, 423 (p) Collado, A.; Esteruelas, M. A.; Lopez, F.; Mascarenas, J. L.; Onate, E.; Trillo, B. *Organometallics* **2010**, *29*, 4966 (q) Kuehnel, M. F.; Lentz, D. *Dalton Trans.* **2009**, 4747

Chapter 4

The Reaction of Carbon Dioxide with Siloxy Silanes

4.1 Introduction

Organosilanes have various uses in organic chemistry. They are among the most frequently employed protecting groups and they are usual intermediates in organic synthesis (1). Moreover they are appealing nucleophiles because they are less toxic, and with easier preparation and handling than tin or boron reagents. Yet, organosilanes display a nucleophilicity three to six orders of magnitude lower than other organometallic reagents such as organoboranes and organostannanes (2). Carboxylation with organosilanes has attracted some attention in the past few years. Several organosilanes have been used as nucleophiles for the synthesis of carboxylic acid derivatives such as propiolic acid (3), benzyl carboxylic acid (4), α-amino acid derivatives (5), cyclopropane carboxylic acids (6), α-hydroxy acid derivatives (7), etc. The C-Si bond has low polarity, and needs activation in order to be able to attack CO_2. One interesting aproach to activation is the use of a fluoride source which can generate a carbanion synthon. CsF has been a common fluoride source for the activation of the C-Si bond. Several reactions have been reported for the synthesis of α-hydroxy acid derivatives (8). We are particularly interested in the remarkable method for the synthesis of α-hydroxy acids and esters which was recently proposed by Sato and co-workers through fluoride-mediated CO_2 incorporation to α-siloxy silanes (Scheme 4.1) (7). One of the interesting features of this process is the use of of convenient reactants: the readily available, less toxic and easily handed organosilanes reacting with abundant, inexpensive and renewable carbon source CO_2. The α-hydroxy acid products are useful building blocks in organic synthesis (9). They are used in the synthesis of species such as glycolic and mandelic acids, which are of great commercial significance (10). They can also be used as precursors in the preparation of aldehydes via oxidative cleavage (11), and have a wide range of applications in the cosmetic industry

(12). The reaction mechanism proposed by Sato and co-workers is shown in Scheme 4.2. The mechanism assumes a key role for a carbanionic intermediate, labeled as im_2 in the scheme.

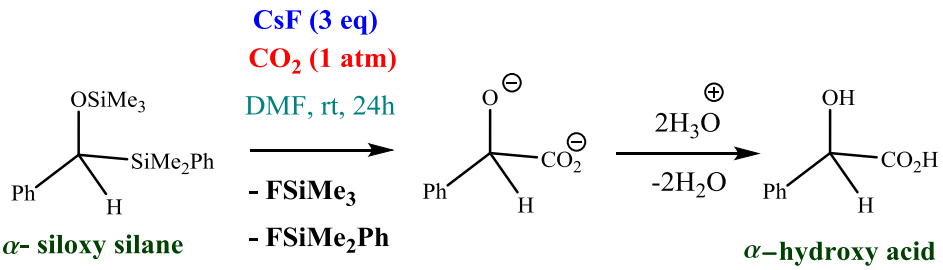

Scheme 4.1. Carboxylation reaction of α-siloxy silane proposed by Sato and coworkers

This intermediate is obtained from an anionic α-silyl alkoxy species (labeled as im_1) by Brook rearrangement. The Brook rearrangement is the intramolecular anionic migration of a silyl group from carbon to oxygen in an anionic fragment (Scheme 4.3) (13).

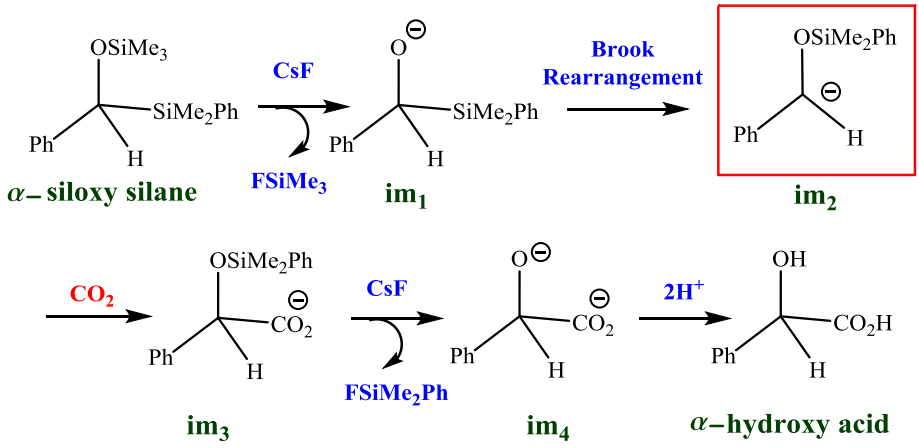

Scheme 4.2. General mechanism for the carboxylation of α-siloxy silane leading to the final product α-hydroxy acid. The key carbanionic intermediate im_2 is highlighted in a red box.

The larger strength of the oxygen-silicon bond compared to the carbon-silicon bond provides the driving force for the conversion of silyl carbinols (im_1, scheme 4.2) to the corresponding silyl ethers (im_2, Scheme 4.2). The resulting carbanionic intermediate is then

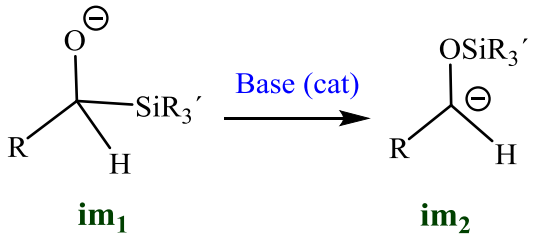

Scheme 4.3. Schematic representation of Brook rearrangement

able to carry out a nucleophilic attack on CO_2 to form the dianion (im_4, scheme 4.2). The final product, α-hydroxy acid, is then obtained by the reaction of dianion with two protons from the acidic medium (HCl/H_2O which is added during the workup process).

Although the main mechanistic trends seem clear, there are a number of intriguing features in the reaction which may be important for the extension of its scope. It would be relevant to confirm the existence of the anionic intermediates and to identify the rate limiting step. The exact role of the cesium fluoride which is in excess is moreover intriguing. The presence of a polar aprotic solvent, DMF along with the counterion Cs^+ has not been shown to have any role in the experimentally suggested mechanisms, but this issue deserves also exploration.

All these questions are addressed in this chapter by using DFT. Calculations have been previously used in our group in both fluoride (14) and carbon dioxide chemistry (15).

4.2 Computational Details

All the calculations were carried out through density functional theory (16) with the B97D (17) functional employing the Gaussian 09 suite of programs (18). Geometry optimization of all the stationary points was carried out with an implicit solvent phase (DMF, ε= 37.219) introduced with SMD (19). The LANL2DZ (20) basis set with the corresponding effective core potential was applied for Cs and the 6-31+g(d) (21) basis set was used for all other atoms. All intermediates were shown to be connected with the corresponding transition states by a manual displacement method. Transition states were characterized by a single imaginary frequency, which was verified to represent the desired reaction coordinate in each case. All the minimum energy structures such as the intermediates, reactants and products were confirmed to exhibit no imaginary frequency. Gibbs free energy corrections were computed at standard conditions of temperature (T= 298 K) and pressure (p= 1 atm).

4.3 Results and Discussions

A first set of calculations was carried out on the experimentally proposed mechanism, without explicit involvement of the Cs^+ counterion and solvent. The reaction follows the proposed mechanism shown in Scheme 4.4, with the energy profile shown in Figure 4.1. The reaction mainly involves 4 steps: $SiMe_3$ extrusion, Brook rearrangement, CO_2 insertion and $SiMe_2Ph$ extrusion.

The fluoride anion initially present attacks the α-siloxy silane reactant (**1**) resulting in the formation of adduct **1a**. The silyl group then coordinates to F through **t(1a-2a)**, which leads to species **2a**. Intermediate **2a** is characterized by the presence of an F-Si bond. It is worth noticing here that, according to our calculations, the O-$SiMe_3$ group is more easily activated by fluoride

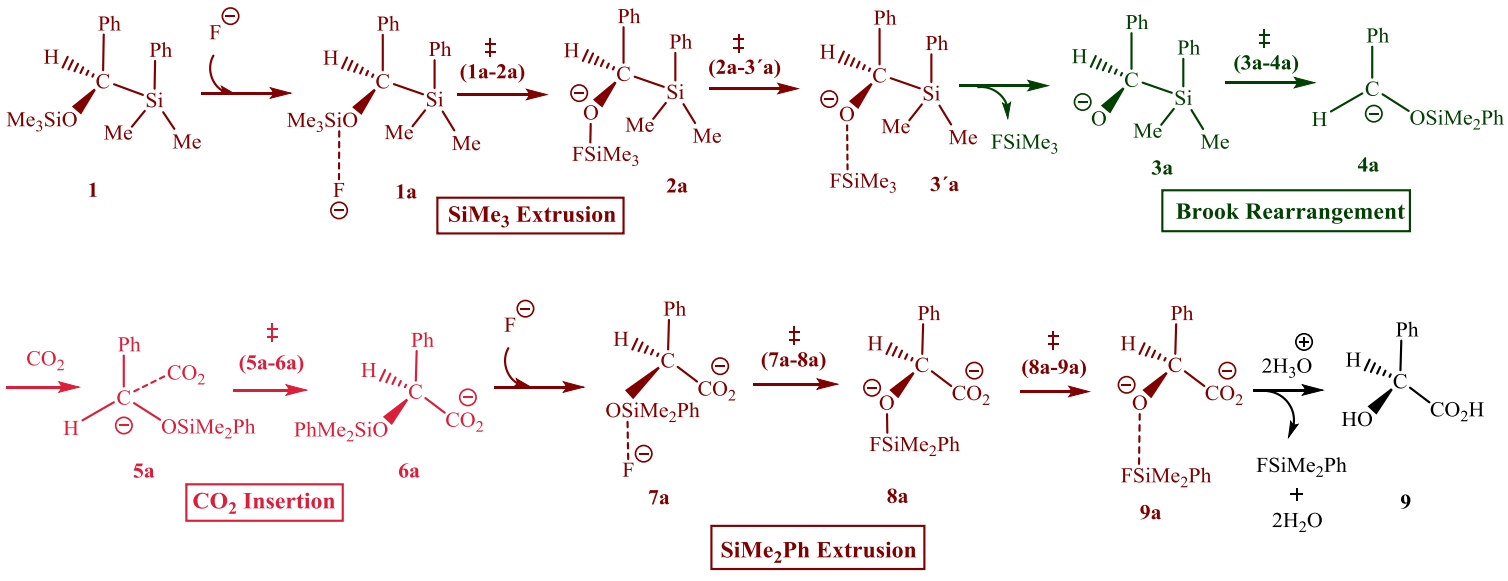

Scheme 4.4. Formation of α-hydroxy acid from α-siloxy silane without involvement of the counterion

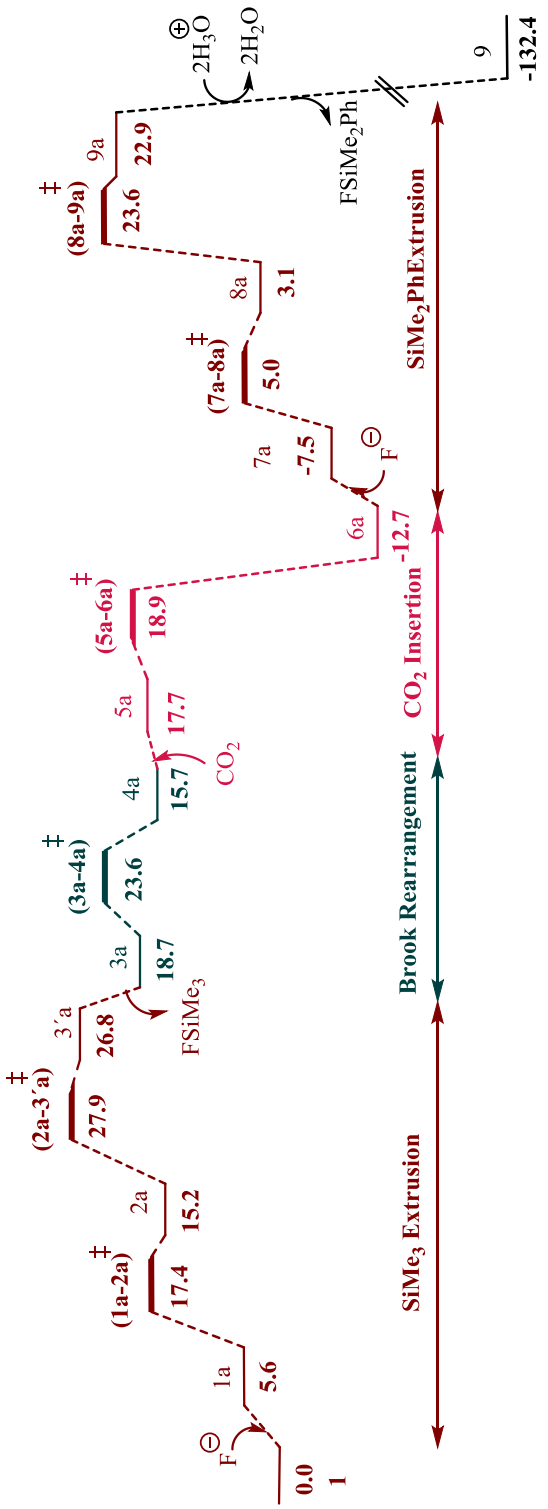

Figure 4.1. Free energy profile (kcal/mol) at the b97d/6-31+G(d) level of theory for the carboxylation of *α*-siloxy silane without involvement of the counterion

rather than the C-$SiMe_2Ph$ group. This is hardly surprising as the O-Si bond is expected to be more polar. The silyl group is then completely transferred from O to F through transition state (**2a-3´a**). The species **3´a** is an adduct between an alkoxy anion and the $FSiMe_3$ molecule. The release of the weakly bound $FSiMe_3$ molecule in **3´a** leads then to the α-silyl alkoxy anion **3a**. Thus the desilylation of $SiMe_3$ group occurs via two steps with transition states **t(1a-2a)** and **t(2a-3´a)**. The in situ formed α-silyl alkoxy anion **3a** is ready to undergo the Brook rearrangement. In the Brook rearrangement, the silyl group is transferred from carbon to oxygen, leading to carbanion **4a**.

The carbanion is then able to undertake a nucleophilic attack on the central atom of a carbon dioxide molecule through **t(5a-6a)**. The carboxylate anion **6a** still contains a silyl unit, which is again extruded from the system with the help of an external fluoride anion via two transition states in a way analogous to the first desilylation process. The attack of the second fluoride ion results in the formation of adduct **7a**. The silyl group is then coordinated to F via **t(7a-8a)** to form the dianion **8a**. **8a** rearranges through an O-to-F silyl transfer in **t(8a-9a).** The resulting dianion **9a** reacts with two protons from the acidic medium (HCl/H_2O which is added during the workup process is the proton source) to result into the desired product α-hydroxy acid **9**.

The close analysis of the free energy profile diagram in Figure 4.1 draws the conclusion that the qualitative features respond to expectations, but the quantitative ones do not. The computed kinetic barrier for the whole process is 36.3 kcal/mol, the difference between the free energies of reactant **6a** and **t(8a-9a)**, corresponding to the second desilylation step. This is too high for a reaction happening at room temperature. The barrier from the reactant **1** to the **t(2a-3´a)**, corresponding to the first desilylation

step is 27.9 kcal/mol, which is also in the limits of what could be deemed acceptable for a reaction at room temperature. It is difficult to attribute the discrepancies to the theoretical description of the system, as the reaction seems to be electronically rather simple. In order to improve the agreement between calculation and experiment we decided to reexamine the computational model.

Fluoride plays certainly a critical role in the process, its strong bond to silicon is a thermodynamic driving force for the whole process, and plays a key kinetic role favoring the individual silyl transfer steps. But fluoride is obviously not introduced as a free anion, but as part of a salt, cesium fluoride in the experimental case we are studying. We considered thus the role that the introduction of an explicit cesium cation in the computational model may have in the overall process (22). The introduction of a naked cesium cation would still be misleading, as it is likely coordinated by DMF solvent molecules (23).

4.3.1 Coordination of DMF to the Cs Cation

In order to evaluate how many solvent molecules are directly coordinated to Cs^+, we evaluated the free energy in DMF solution (ε=37.219) associated to reactions of the type:

$$Cs(DMF)_{n-1}^{+} + DMF \rightarrow Cs(DMF)_n^{+}$$

We carried this calculation for values of n between 1 and 6. It was found that the optimal value was 4. The ΔG value was negative for values of n between 1 and 4, but positive with n values of 5 and 6. This means that the addition of a fifth molecule to the solvation sphere is not favorable.

The favored structure corresponds thus to $Cs(DMF)_4^+$, with a tetrahedral arrangement around the metal, as shown in Figure 4.2.

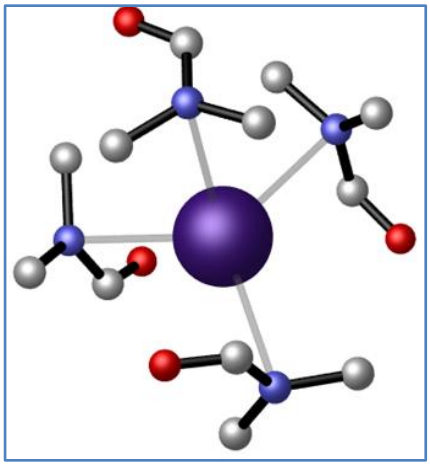

Figure 4.2. Optimized structure for the Cs^+ Cation Surrounded by 4 molecules of DMF at the B97d/6-31+G(d) level of theory.

The DMF molecules coordinate to the metal through the nitrogen atom. We repeated then the same treatment with the fluoride anion, and found that it is not coordinated by DMF.

4.3.2 Explicit Inclusion of $Cs(DMF)_4^+$ Complex into the Reaction Mechanism

We incorporated the $Cs(DMF)_4^+$ complex explicitly into our reaction system. We also needed to find out the number of solvent molecules that coordinate Cs^+ when bound to the system. We found that the favored number of coordinating solvent molecules in this case is two. That is, two molecules of DMF accompany Cs^+ when it coordinates to intermediate **1a** to form intermediate **1b**. This is because two of the phenyl groups in the substrate **1a** also coordinate with the Cs^+ center. The interaction between $Cs(DMF)_2^+$ and intermediate **1a**, resulting in adduct **1b**, is highlighted in Figure 4.3. The Cs^+ center has favourable cation-π interactions with the two phenyl groups in α-siloxy silane. We have applied the same strategy of involving counterion and solvent in all intermediates and the

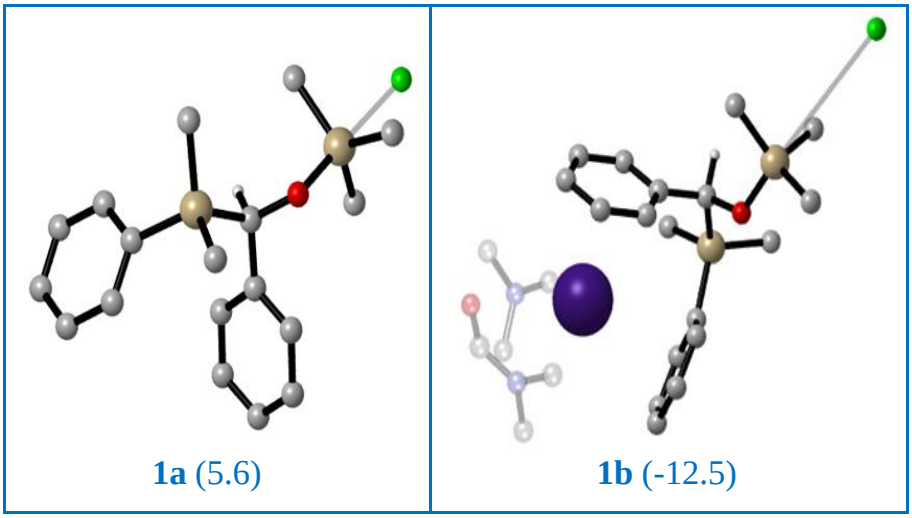

Figure 4.3. Optimized geometries of intermediates 1a and 1b at the B97d/6-31+G(d) level of theory. The relative free energies with respect to the separated reactants are provided in parentheses.

transition states along the entire reaction pathway. The mechanism computed when introducing the cesium species is summarized in Scheme 4.5 and Figure 4.4. The basic mechanistic steps are the same discussed above (in Scheme 4.4) for the reaction without cesium. But there are significant quantitative differences in the free energy profile.

It was clear from the observation of Figure 4.2 that the highest barriers corresponded to the first and second desilylation steps when considering the reaction without counterion. We focus thus our analysis of Figure 4.4, with the counterion, on these two energy barriers. For the first desilylation transition state, **t(2b-3´b)** the barrier is 21.7 kcal/mol (measured from **1b**), clearly below the 27.9 kcal/mol associated to transition state **t(2a-3´a)**. The structures of transition states **t(2a-3´a) and t(2b-3´b)** are given in Figure 4.5. The lowering of the barrier can be tracked down to the stability of adduct **1b**, which is 12.5 kcal/mol more stable than the separate

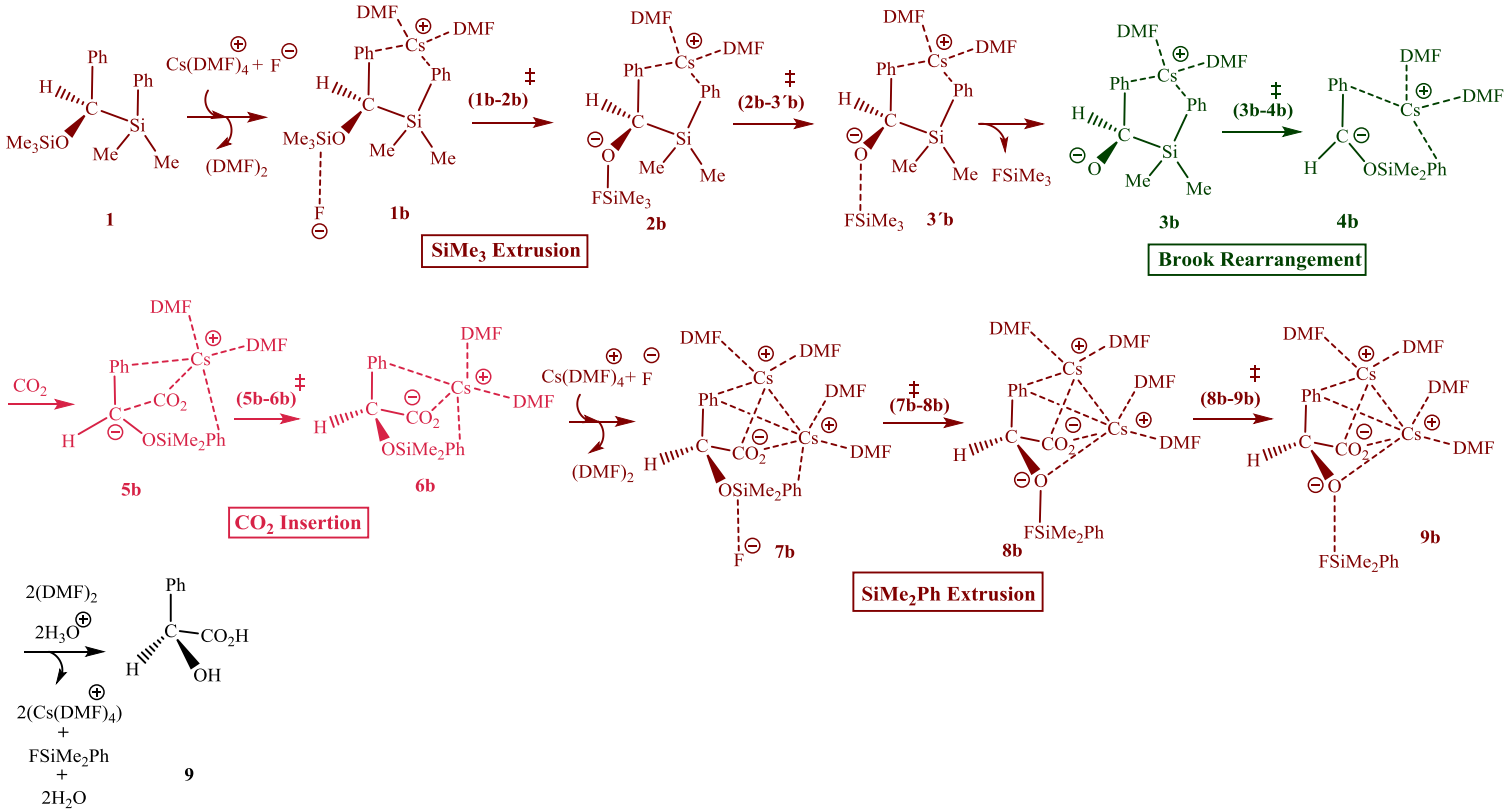

Scheme 4.5. Formation of α-hydroxy acid from α-siloxy silane with involvement of the counterion

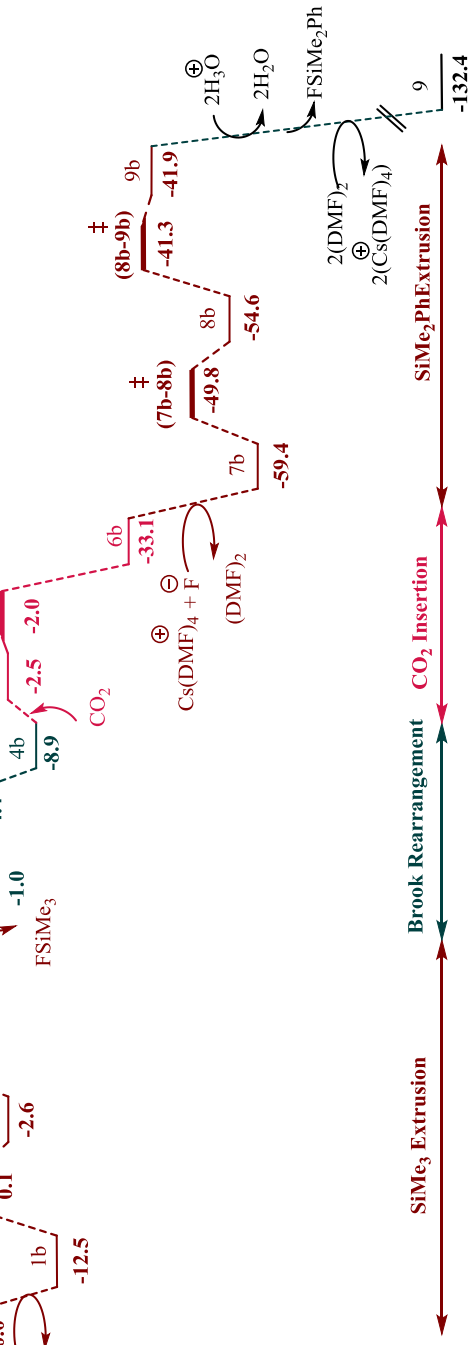

Figure 4.4. Free energy profile (kcal/mol) at the b97d/6-31+G(d) level of theory for the carboxylation of *α*-siloxy silane with involvement of the counterion

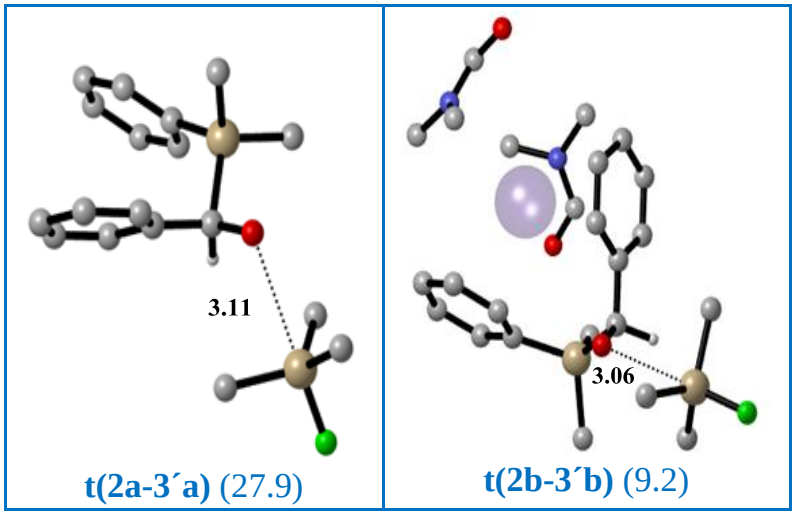

Figure 4.5. Optimized geometries of transition states t(2a-3´a) and t(2b-3´b) corresponding to first desilylation step at B97d/6-31+G(d) level of theory. The relative free energies with respect to the separated reactants (kcal/mol) are provided in parentheses.

reactants. This is in sharp contrast with **1a**, without Cs^+, which was 5.6 kcal/mol above reactants. This 5.6 kcal/mol penalty is no longer required when cesium is introduced in the system, which leads to a lower barrier for this step. The effect for the second desilylation is even more dramatic. A superior stabilization of the intermediates and transition state is observed after the introduction of second $Cs(DMF)_2^+$ and F^- into the system prior to the second desilylation step. In particular, **7a** which was 5.2 kcal/mol above **6a**, intermediate **7b** is 26.3 kcal/mol below **6b**. The strong cation-anion interaction between the two carboxylate oxygens and the two Cs^+ centers is the key factor explaining the stabilization of this intermediate, as can be seen in Figure 4.6. Even more critical is the improvement in the barrier associated to transition state **t(8b-9b)**, corresponding to the second desilylation. In this case, the barrier with cesium is 18.1 kcal/mol (measure from **7b**). This is a very substantial improvement from the 36.3 kcal/mol difference between **6a** and **t(8a-9a)** (Figure 4.7, Left). The key difference seems related to a specific

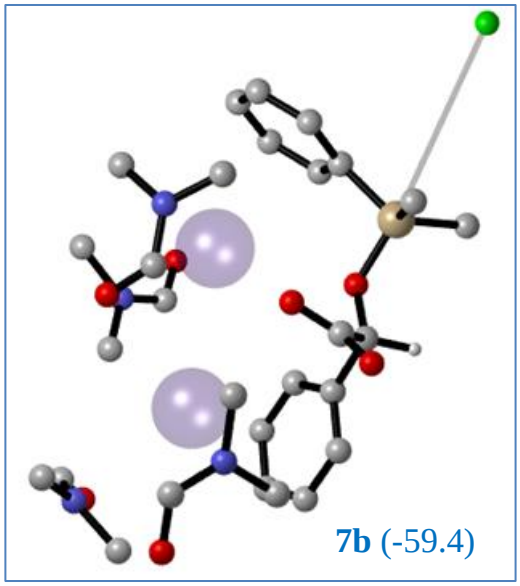

Figure 4.6. Optimized structure for the intermediate 7b, which is surrounded by 4 molecules of DMF and 2 Cs^+ at b97d/6-31+G(d) level of theory. The relative free energies with respect to the separated reactants are provided in parentheses.

stabilization of the transition state **t(8b-9b)** (Figure 4.7, Right) with respect to the preceding intermediate **8b**. The release of the $FSiMe_2Ph$

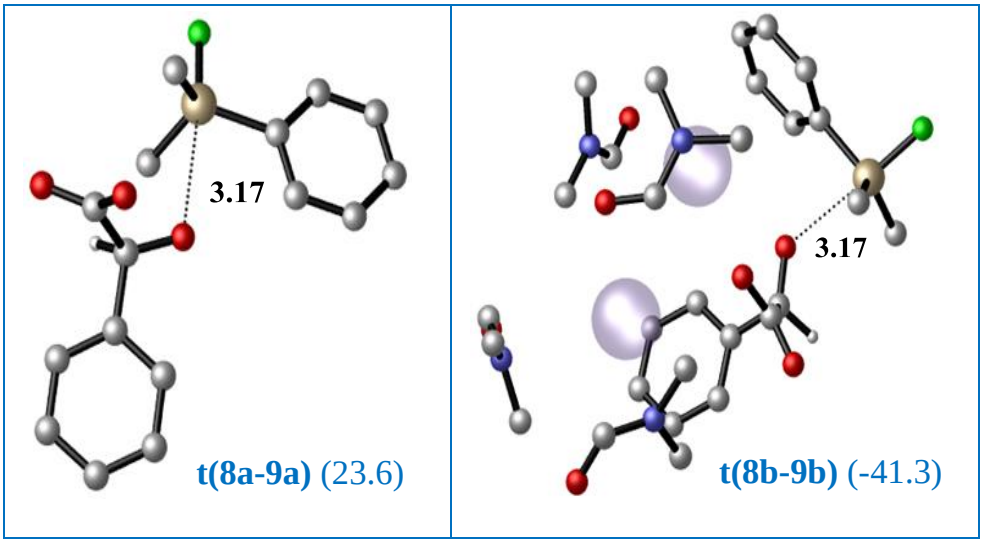

Figure 4.7. Optimized structure for the transition states t(8a-9a) and t(8b-9b) at the B97d/6-31+G(d) level of theory. The relative free energies (kcal/mol) with respect to the separated reactants are provided in parentheses.

molecule leaves a more anionic character on the oxygen center, which in turn strengthens its interaction with the positive charge at cesium. The remaining highest barrier in the catalytic cycle is then 21.7 kcal/mol corresponding to the first desilylation step, which is fully compatible with the experimental observation of a reaction taking place at room temperature. The presence of Cs^+ is thus critical for the reaction to take place. It stabilizes sufficiently the key transition state for the reaction to be complete. The importance of the presence of the seemingly innocent counterions in reaction mechanisms is in this way confirmed (24).

4.4 Conclusions

The mechanism of the fluoride-assisted carboxylation reaction between α-siloxy silanes and carbon dioxide to form α-hydroxy acids has been computationally characterized. Calculations confirm the fundamental role of a Brook rearrangement step, where a silyl group is transferred from carbon to oxygen, resulting in a carbanionic intermediate. This carbanionic center is responsible for the low barrier nucleophilic attack on the central atom of carbon dioxide. Calculations have also revealed the unexpected importance of the cesium cation in the reaction. In particular, the seemingly innocent counterion in the fluoride salt plays a critical role. The interaction of cationic counterion, Cs^+ with the polar aprotic solvent DMF is also studied. The counterion is introduced not as a naked cation, but as a complex with solvent system. The cesium cation that was used in experiment has to be explicitly considered in the calculation in order to reproduce the experimental result.

4.5 References

(1) (a) Greene, T.; Wuts, P. *Protecting Groups in Organic Synthesis*, 2nd Ed., Wiley New York, **1991** (b) Blau, K.; Halket, J. *Handbook of Derivatives for Chromatography*, 2nd Ed., J. Wiley and Sons, New York, **1993** (c) Chatgilialoglu, C. *Acc. Chem. Res.* **1992**, *25*, 188 (d) Coats, R. M.; Denmark, S. *Handbook of Reagents for Organic Synthesis. Reagents, Auxillaries and Catalysts for C-C Bond Formation*, J. Wiley and Sons, GB, **1999**

(2) (a) Corral-Bautista, F.; Klier, L.; Knochel, P.; Mayr, H. *Angew.*

Chem., Int. Ed. **2015**, *54*, 12497 (b) Hagen, G.; Mayr, H. *J. Am. Chem. Soc.* **1991**, *113*, 4954

(3) Kobayashi, Y. M.; Inamoto, K.; Tanaka, Y.; Kondo, Y. *Org. Biomol. Chem.* **2013**, *11*, 3773

(4) Mita, T.; Michigami, K.; Sato, Y. *Org. Lett.* **2012**, *143*, 3462

(5) Mita, T.; Sugawara, M.; Saito, K.; Sato, Y. *Org. Lett.* **2014**, *16*, 3028

(6) Ohno, M.; Tanaka, H.; Komatsu, M.; Ohshiro, Y. *Synlett* **1991**, *0*, 919

(7) Tsuyoshi, M.; Yuki, H.; Sato, Y. *Org. Lett.* **2014,** *16*, 14

(8) (a) Shinobu, I.; Keiko, M.; Genichi, T. *J. Am. Chem. Soc*. **1975,** *97*, 596 (b) Quanxuan, Z.; Hong, R.; Gregory, B. *Beilstein. J. Org. Chem.* **2014**, *10*, 1365 (c) Kai, C.; Xin, L.; Shuo-Qing, Z.; Bing-Feng, S. *Chem. Commun.* **2016**, *52*, 1915

(9) (a) Coppola, G. M.; Schuster, H. F. *α-Hydroxy Acids in Enantioselective Syntheses*, Wiley-VCH Weinheim, **1997** (b) Gröger, H. *Adv. Synth. Catal.* **2001**, *343*, 547

(10) Ritzer, E.; Sundermann, R. *Ullmann's Encyclopedia of Industrial Chemistry*, **2000**

(11) Stephen, O. N.; Philip, M. K. *Tetrahedron Lett.* **1982**, *23*, 3135 (b) Harumi, O. *Bull. Chem. Soc. Jpn.* **1934**, *9*, 8

(12) Effron, C.; Briden, M, E.; Green, B. A. *Cutis* **2007**, *79*, 4

(13) (a) Brook, A. G. *Acc. Chem. Res.* **1974**, *7*, 77 (b) Seiichiro, H.; Woo, J. C.; Dong, S. L.; William, C. N. H.; Paul, J. T.; John, T. W. *J. Org. Chem.* **2004**, *69*, 6323

(14) Jover, J.; Maseras, F. *Chem. Commun.* **2013**, *49*, 10486

(15) Guo, W.; Martínez-Rodríguez, L.; Kuniyil, R.; Martin, E.; Escudero-Adán, E. C.; Maseras, F.; Kleij, A. W. *J. Am. Chem. Soc*. **2016**, *138*, 11970

(16) Ref. 1, Appendix

(17) Ref. 2, Appendix

(18) Ref. 3, Appendix

(19) Ref. 4, Appendix

(20) Ref. 8, Appendix

(21) (a) Hariharan, P. C.; Pople, J. A. *Theoret. Chim. Acta.* **1978**, *28*, 213 (b) Francl, M. M.; Petro, W, J.; Hehre, W. J.; Binkley, J. S.; Gordon, M. S.; DeFrees, D. J.; Pople, J. A. *J. Chem. Phys.* **1982**, *77*, 3654 (c) Clark, T.; Chandrasekhar, J.; Schleyer, P. V. R. *J. Comp. Chem.* **1983**, *4*, 294 (c) Krishnam, R.; Binkley, J. S.; Seeger, R.; Pople, J. A. *J. Chem. Phys.* **1980**, *72*, 650 (d) Gill, P. M. W.; Johnson, B. G.; Pople, J. A.; Frisch, M. J. *Chem. Phys. Lett.* **1992**, *197*, 499

(22) Anand, M.; Sunoj, R. B.; Schaefer, H. F. *J. Am. Chem. Soc.* **2014**, *136*, 5535

(23) Dijkstra, G.; Kruizinga, W. H.; Kellog, R. M. *J. Org. Chem.* **1987**, *52*, 4230

(24) (a) Macchioni, A. *Chem. Rev.* **2005**, *105*, 2039 (b) Basallote, M. G.; Besora, M.; Castillo, C. E.; Fernandez-Trujillo, M. J.; Lledos, A.; Maseras, F.; Manez, M. A. *J. Am. Chem. Soc.* **2007**, *129*, 6608

Chapter 5

Conversion of Cyclic Carbonates into Allylic Amines and Allylic Aldehydes

5.1 Introduction

Highly stereoselective construction of multi-functionalized tri- and tetra-substituted olefin scaffolds continues to be a major challenging task (1). Recently, attention has been given to the use of cyclic carbonates as intermediates in various organic synthesis which include the construction of multi functionalized olefins (2). The transformation of cyclic organic carbonate into various valuable organic molecules is thus an important ongoing research in the organic chemistry community. Decarboxylative functionalization of cyclic carbonate with suitable electrophiles such as Michael acceptors (3) is reported to be feasible under mild reaction conditions giving access to furans (3a), tertiary vinylglycols (3b), and highly functional pyrrolidines (3c). A key to the success of this approach has been attributed to the postulated in situ formation of zwitterionic π-allyl-Pd species as an intermediate upon CO_2 extrusion (Scheme 5.1) (4).

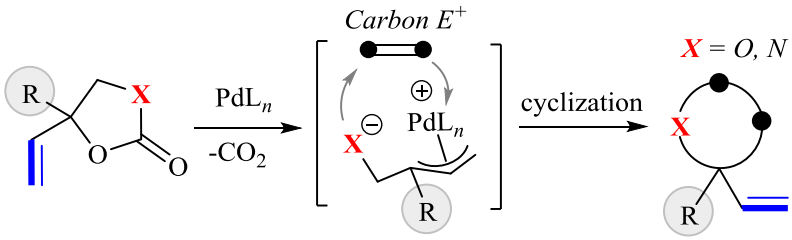

Scheme 5.1. Reaction of electrophile and vinyl cyclic carbonate/ carbamate including the postulated zwitterionic intermediate.

The charge-separated zwitterionic π-allyl-Pd should in principle possess ambivalent reactivity, with the Pd-allyl fragment being able to react in the central or terminal carbons. In fact, this fragment has been shown to be highly electrophilic and amenable to react with nucleophiles also such as water, amines, thiols etc (5), yielding diverse substituted olefins (Scheme 5.2). Nucleophilic attack of the allyl fragment into vinyl cyclic carbonates (6) and in to the internal carbon center of the allylic intermediate has also been proven as feasible (7).

Specifically, the attack of amine nucleophile to insitu generated allylic species selectively generates Z-allylic amine scaffolds as the product (Scheme 5.3, part 1) (4a). Even in the absence of any nucleophiles and

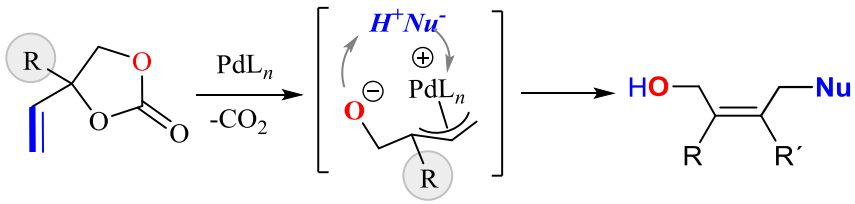

Scheme 5.2. Reaction of nucleophile and vinyl cyclic carbonate with indication of the postulated mechanism

electrophiles, cyclic vinyl carbonates are able to convert into Z-allylic aldehydes (Scheme 5.3, part 2). Since this area of research is currently in sharp growth, we believe that the mechanistic understanding of the origin of stereoselectivity in these reactions will open up new synthetic

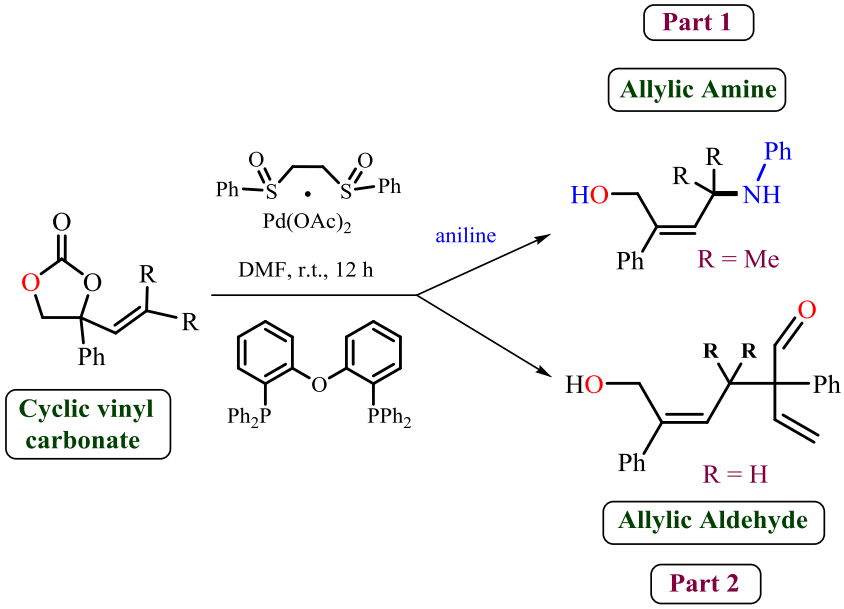

Scheme 5.3. Conversion of cyclic vinyl carbonates to allylic amines and allylic aldehydes

opportunities for the further construction of highly functionalized allylic amine and other olefin compounds. Computational approaches have been successful in mechanistic studies on palladium chemistry (8), selectivity (9) and in processes involving carbon dioxide (10). This chapter presents our computational studies on the mechanism of the palladium-catalyzed stereoselective formation of highly functionalized tri- and tetra-substituted

Z-allylic amines from cyclic vinyl carbonates (part1) and the decarboxylative construction of highly functionalized allylic aldehydes involving Csp^3-Csp^3 bond formation from cyclic vinyl carbonates (part2).

5.2 Computational Details

All the calculations were carried out by using density functional theory method (11) with the b97d functional (12) by employing the Gaussian 09 suite of quantum chemical program (13). Geometry optimization of all the stationary points was carried out with an implicit solvent phase (DMF, ε= 37.219) introduced with SMD (14). Two different basis sets were used. In basis set I, the SDD (15) basis set with the effective core potential was applied for Pd and the 6-31g(d) basis set was used for all other atoms (16). This basis set I was used for the geometry optimizations and frequency calculations. The transition states were characterized by a single imaginary frequency, which was verified to represent the desired reaction coordinate in each case. All the minimum energy structures such as the intermediates, reactants and products were confirmed to exhibit no imaginary frequency. Single point calculations of the potential energy were carried out, also in solution, with a more extended basis set II, consisting of the SDD basis set for Pd and the 6-311++g(d,p) basis set for all other atoms (17). Potential energies in solution computed with basis set II were then added to free energy corrections computed with basis set I to result in the free energies reported in the text. Conformational searches were carried out for most compounds, and only the most stable conformers are reported in most cases. Gibbs free energy corrections were computed in a first stage at ideal gas conditions of temperature (T= 298 K) and pressure (p= 1 atm). In part 2, where a microkinetic model was applied, the reference state was corrected to 1 M for all species. The kinetic simulation in part 2 was carried out with the Acuchem software (18).

Part 1

Palladium-Catalyzed Transformation of Cyclic Carbonates to Z-Allylic Amines

5.3 Pd Catalyzed Transformation of Cyclic Carbonates to Z-Allylic Amines

Allylic amines are fundamental building blocks in organic chemistry and their synthesis is an important industrial and synthetic goal (19). Significant progress has been observed in recent years in their synthesis. Metal-catalyzed conversion of allylic compounds has emerged as a powerful and practical methodology for the construction of E-selective, γ-mono-substituted allylic amine scaffolds (Scheme 5.4, route I). The most attractive routes towards such allylic amines include conventional allylic substitution reactions (20), hydroamination of dienes (19g, 21), and more recently developed C–H bond activation/functionalization strategies (22). Most of these processes are effective towards the preparation of E-allylic amines with limited potential to introduce three or four different substituents on the olefinic unit in a stereocontrolled fashion. Despite notable progress in this area, the development of a general methodology towards a stereoselective synthesis of highly functionalized tri- and tetra-substituted allylic amines based on metal catalyzed "allylic chemistry" (Scheme 5.4, route II) presents a fundamental and practical challenge yet unresolved (23). Various methodologies towards the formation of γ-disubstituted allylic amines have been developed (Scheme 5.2, route II; $R^3 = R^4$ = Me in most reported cases) (20m-o, 21a-d, 24) avoiding the formation of stereochemical mixtures and leaving rather limited potential for post-functionalization.

Limited methodologies other than those based on "allylic chemistry" have been developed towards the preparation of stereodefined, highly substituted allylic amines (25). These synthetic approaches generally require the use of sensitive metal reagents, (25a, 25c) stoichiometric amounts of additives (25a-d, 25f), or the use of synthetically challenging, stereodefined tri-substituted allylic surrogate precursors as starting materials (25e, 25f). These features adversely affect the accompanying waste profiles of such strategies and may limit their practical application and/or scale-up. Highly functionalized allylic amine and/or olefin scaffolds have been identified as useful building blocks/reaction partners

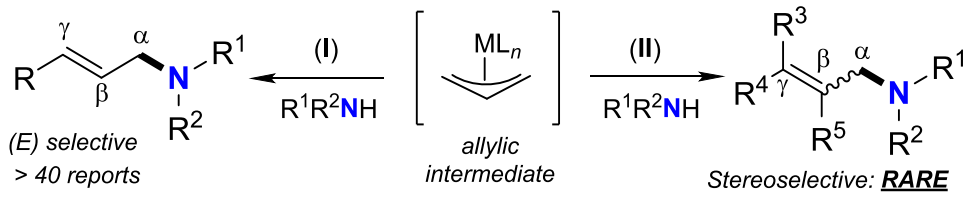

Scheme 5.4. Metal catalyzed transformations of allylic intermediates

(1, 26). Pd-catalyzed conversion of allyl surrogates readily obtained from cyclic vinyl carbonates is a promising method. Indeed, the reactions experimentally observed in the group of Kleij with species **r1** (Scheme 5.5) constitute the first general and practical methodology for the stereoselective synthesis of tri-and tetra-substituted allylic amines. Product **p1** is obtained by appropriately tuning the ligands $\mathbf{L_1}$, the metal precursor, and the reaction conditions (Scheme 5.5). The ligand derives from the so-called White catalyst and is also shown in the Scheme. Nucleophilic attack by amines on the hypothetic allylic fragment, **k1** (5, 6) is the key for the stereocontrolled formation of γ-disubstituted allylic amines. The product, **p1** is characterized by a high level of stereo-control towards the (Z) isomer. These rare conversions have excellent stereoselectivity, operational simplicity, mild reaction conditions, wide scope in reaction partners and provide access to a wide range of complex allylic amine scaffolds. Reactant **r1** may be replaced by H-substituted cyclic vinyl carbonates, while keeping excellent stereoselectivity. But the reaction of **r1** is especially appealing because of the exclusive formation of the Z-configured allylic amine. The (*Z*)-1,4-amino-alcohols **p1** are desirable precursors towards the synthesis of a wide variety of 1,4-diamines. Such compounds are of potential biological interest but are typically more difficult to prepare stereoselectively than vicinal diamines (27).

The mechanism reported in Scheme 5.5 provides a rationale for the formation of the products, but is a bad fit for the selectivity of the reaction. The allyl may be in principle obtained with either face pointing to the metal, and the attack of the nucleophile will take place from the opposite side. Intrigued by the high level of stereochemical control in the formation of the allylic amine products, we decided to rationalize the stereocontrol by performing mechanistic studies using computational methods.

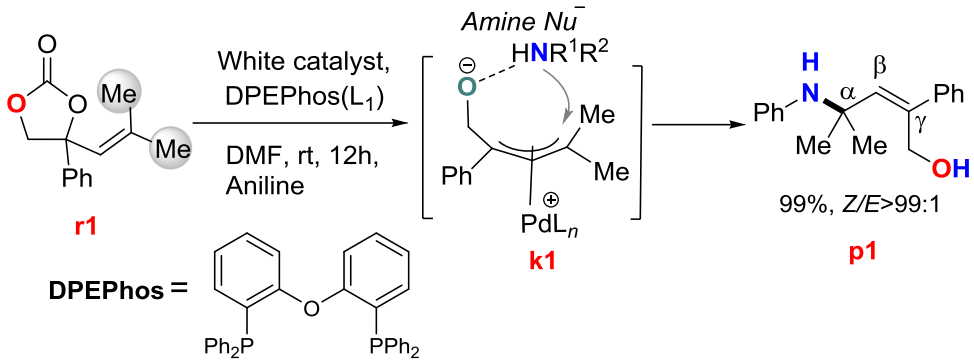

Scheme 5.5. Pd-catalyzed transformation of cyclic carbonates to Z-allylic amines. Reaction reported by Kleij and co-workers.

In this part **1** of chapter **5,** we have delineated the mechanistic details of palladium catalyzed transformation of cyclic carbonates to Z-allylic amines.

5.3.1 Results and Discussions

5.3.1.1 Pathway for the Formation of *Z*-Allylic Amines

The energetically preferred pathway for the formation of Z-allylic amines from cyclic carbonate is given in the simplified Scheme 5.6 and a detailed energy profile is shown in Figure 5.1. The reaction can be envisaged to begin with an active catalyst **t1**, which is derived from the White catalyst precursor and DPEPhos (**L_1**) ligand. The **t** label in **t1** makes reference to theoretical and we introduce it to represent our computed intermediates which are only seldom isolated experimentally. The initial steps of the reaction are as expected, *i.e.*, the reduced form of the White catalyst **t1** coordinates with the vinyl double bond to yield intermediate **t2**. Then an oxidative cleavage of the cyclic carbonate takes place via **t(2-3).** There is a formal transfer of two electrons from the Pd center to the organic substrate, and the resulting intermediate **t3** contains an η^3 allylic group attached to an open carbonate. Up to this intermediate **t3**, our calculations closely follow previous mechanistic postulations on related processes (3). Isomerization of **t3** through a $\pi-\sigma-\pi$ interconversion process leads to intermediate **t4**. The detailed free energy profile diagram for this isomerization is given in Figure 5.2. Initially, the anti-configured η^3 allylic group on **t3** will

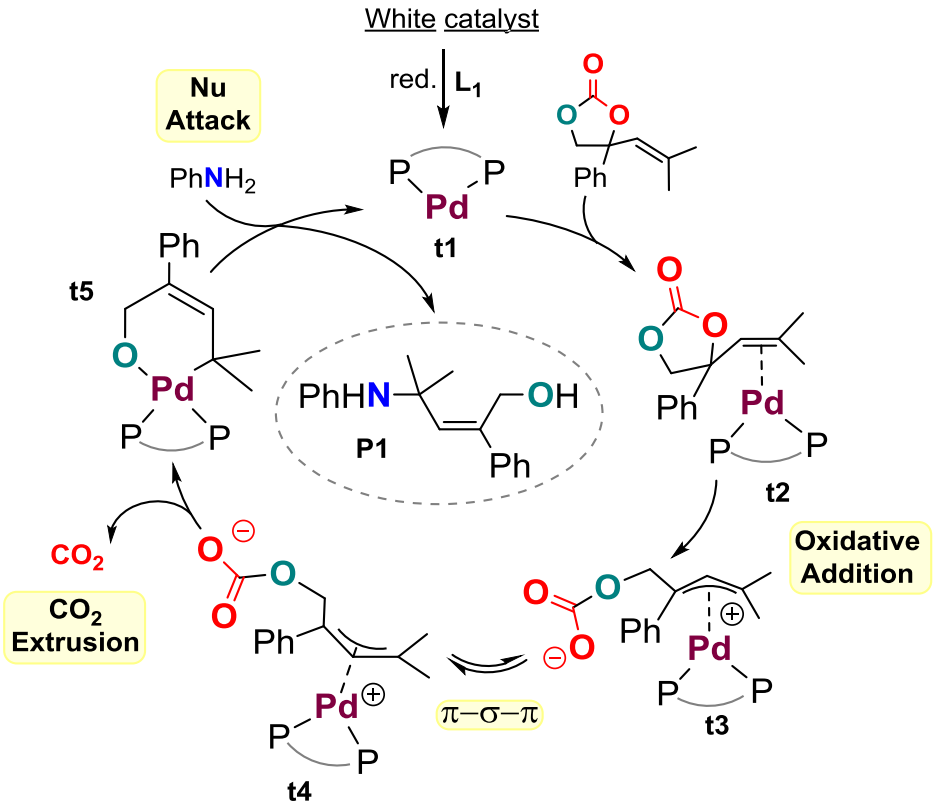

Scheme 5.6. Computed overall mechanism for the formation of Z-configured allylic amine p1

isomerize to the anti-configured η^1 allylic isomer **t15**. Intermediate **t15** is now capable of rotating its C_1-C_2 single bond via **t(15-16)** to form syn-configured η^1 allylic intermediate **t16** which can again isomerize to form more stable syn-configured η^3 allylic intermediate **t17**. The further rotation of C-O bond in **t17** will lead to **t4**. The arrangement of the substituents in allylic intermediate **t4** is in such a way that the product molecule **p1** produced will have a (Z) configuration. The extrusion of the carbon dioxide molecule from **t4** results in the formation of intermediate **t5** containing a six-membered palladacycle ring with a Pd-O chelation. The possibility of CO_2 extrusion from **t17**, which is a stable intermediate in the *syn*/*anti* isomerization process from **t3** to **t4,** has been also taken into consideration. The CO_2 extrusion from **t17** will lead to the cyclic epoxide ring shown in the Figure 5.3.

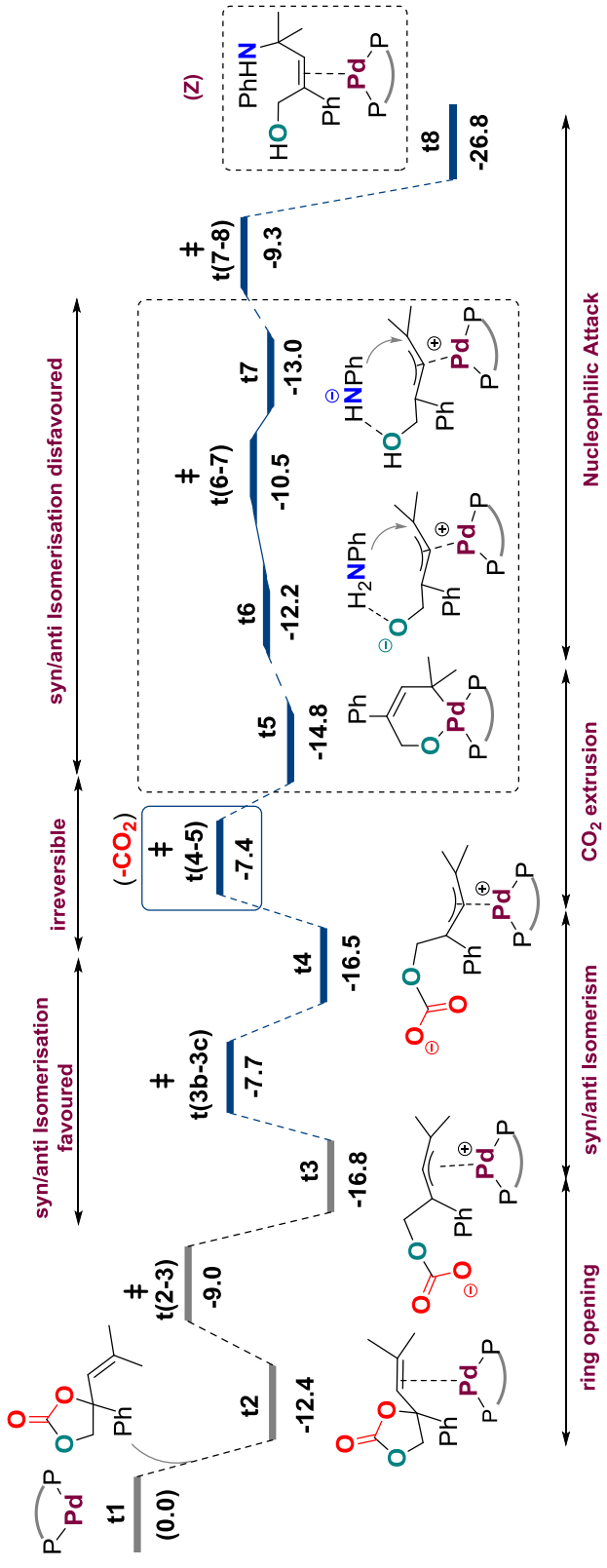

Figure 5.1. Free energy profile (kcal/mol) for the formation of Z-allylic amines p1

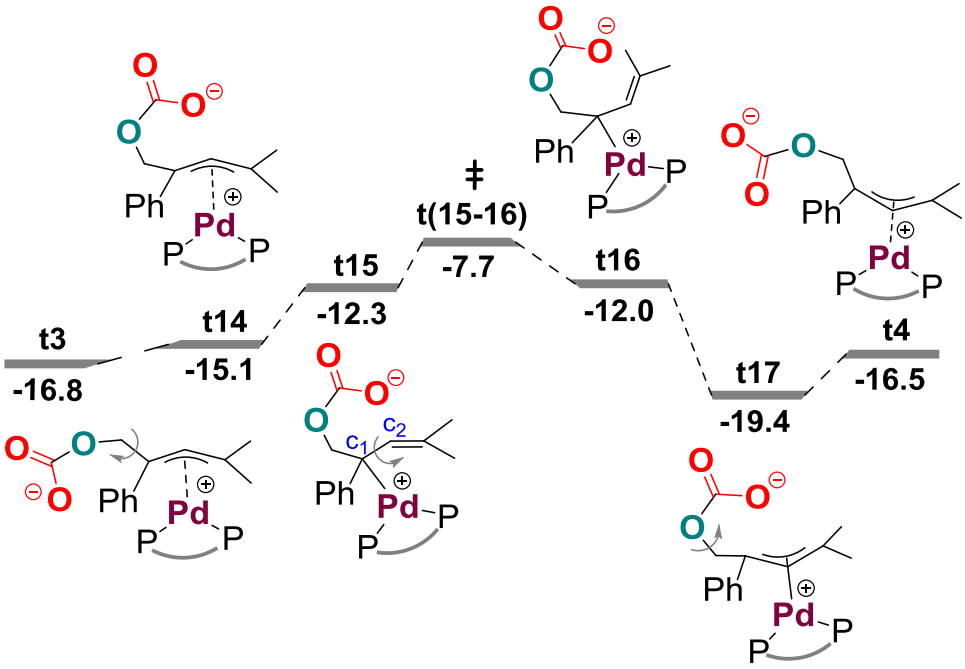

Figure 5.2. Free energy profile (kcal/mol) of *syn*/*anti* isomerization process t3→t4 through $\pi-\sigma-\pi$ interconversion

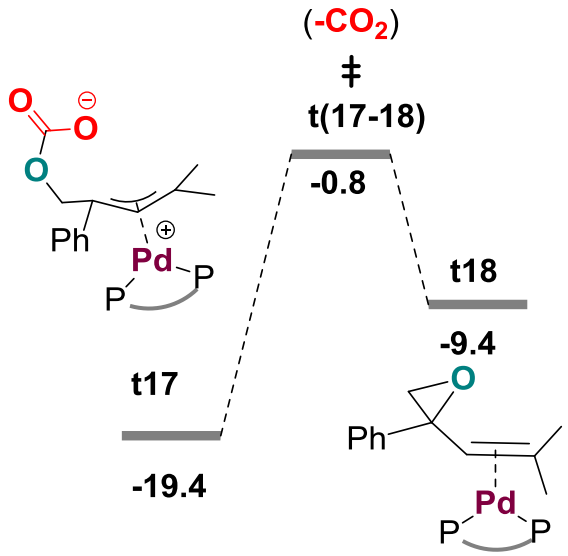

Figure 5.3. Free energy profile (kcal/mol) for the CO_2 expulsion from t17 to form epoxide intermediate t18

Comparing the free energy values of **t(4-5)** and **t(17-18)**, it is evident that

the CO_2 extrusion is more feasible from **t4** via transition state **t(4-5)** than from **t7** via **t(17-18)**. Subsequently the nucleophilic attack of the aniline occurs on the catalyst substrate complex **t5**. Initially aniline makes a hydrogen bond to the anionic oxygen center of **t5** resulting in intermediate **t6,** which rearranges through proton transfer to intermediate **t7**. From **t6** to the final product **t8** there are two possible routes. The preferred one is stepwise, with first formation of an O–H bond in intermediate **t7** followed by a nucleophilic attack of an amide nucleophile through **t(7-8)**. The concerted option (Figure 5.4) has a higher transition state, **t(6-8)** at –6.0 kcal/mol, and is 3.3 kcal/mol above **t(7-8)** and must thus be discarded.

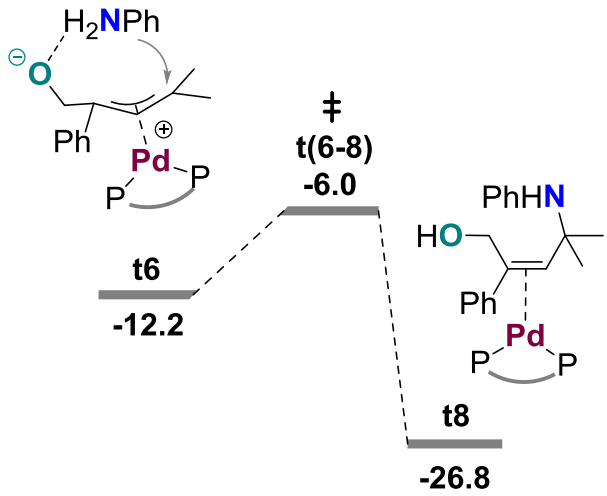

Figure 5.4. Free energy profile (kcal/mol) for the concerted nucleophilic attack

From intermediate **t5**, a pathway where the heterolytic N–H cleavage leads to an intermediate with a Pd–N bond as in **t14** (Scheme 5.7) could be envisaged. But intermediate **t14** has a free energy of +4.7 kcal/mol. This is already 13.5 kcal/mol above the –9.3 kcal/mol of the competing transition state **t(7-8)** of the favored path. And any transition state connected to **t14** should be even higher in energy. Thus, a hypothetic mechanism with the involvement of Pd–N bonds was discarded.

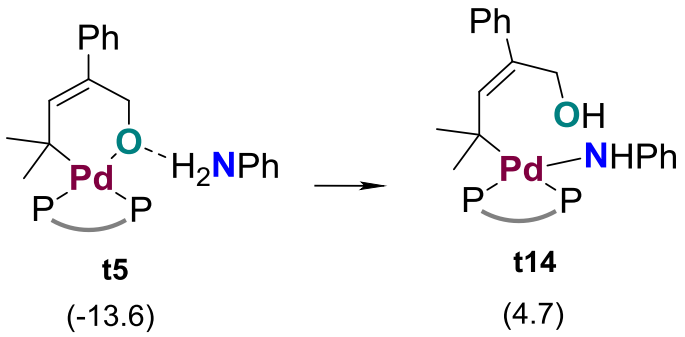

Scheme 5.7. Pathway involving heterolytic N–H cleavage leads to an intermediate with a Pd–N bond. The relative free energies (kcal/mol) are given in parentheses

The branched allylic amine **t8´** shown in Figure 5.5, which could be possibly generated from intermediate **t7** was also taken into consideration. The transition state **t(7-8´)** corresponding to this conversion has a barrier at –0.6 kcal/mol which is much higher in energy than the one (–9.3 kcal/mol) computed for **t(7-8)** which in turn suggests that only linear amine will be observed in this reaction. This again agrees with the experimental results of exclusive formation of linear allylic amines. The geometry of key transition states involved in the formation of Z-allylic amine **p1** is given in Figure 5.6.

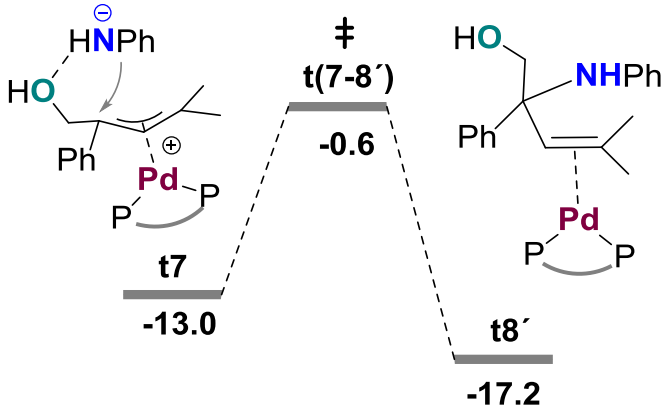

Figure 5.5. Free energy profile (kcal/mol) for the formation of branched product from t7

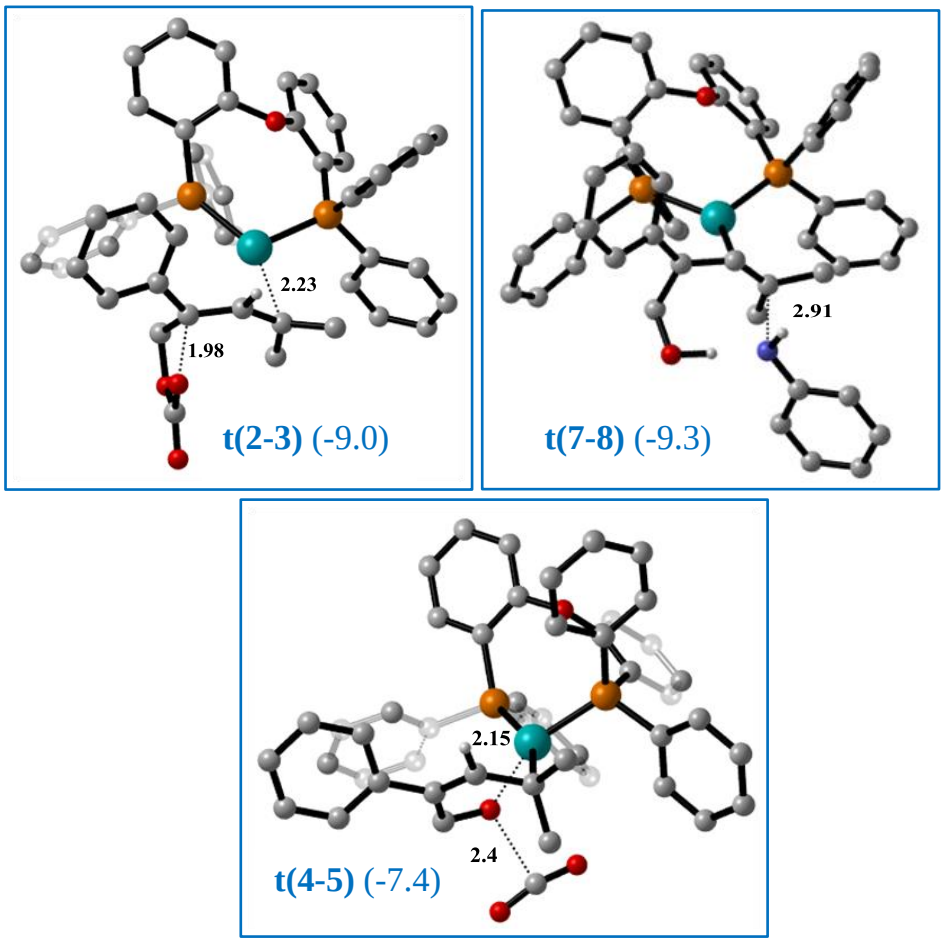

Figure 5.6. Optimized geometries of the key transition states involved in the formation of Z-allylic amines p1. The relative free energies (kcal/mol) are given in parentheses. All distances are in Å

5.3.1.2 Alternative Pathway from t3 Leading to the E-Allylic Amine

The alternative pathway which directly leads to product from intermediate **t3** without involving $\pi-\sigma-\pi$ interconversion process was also studied. This pathway leads to the E-allylic amine **p2**. The computed alternative cycle is given in Scheme 5.8. The geometry of key transition states involved in the formation of E-allylic amine **p2** is shown in Figure 5.7 and the detailed free energy profile is supplied in Figure 5.8. The cycle is identical to the main cycle reported in Scheme 5.6 up to species **t3**. If the system does not undergo the $\pi-\sigma-\pi$ interconversion process, **t3** will

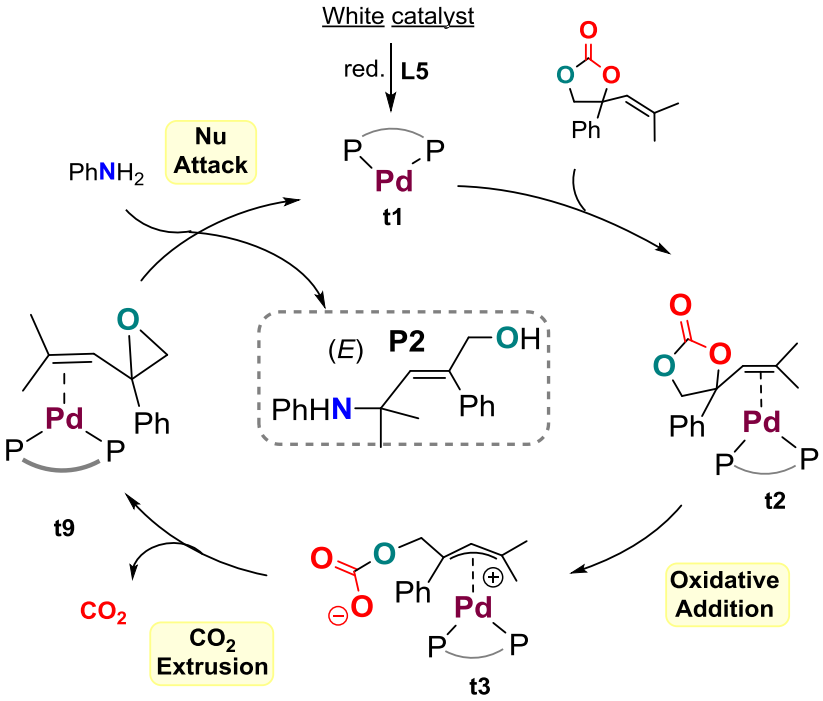

Scheme 5.8. Computed overall mechanism for the formation of E-configured allylic amine p2

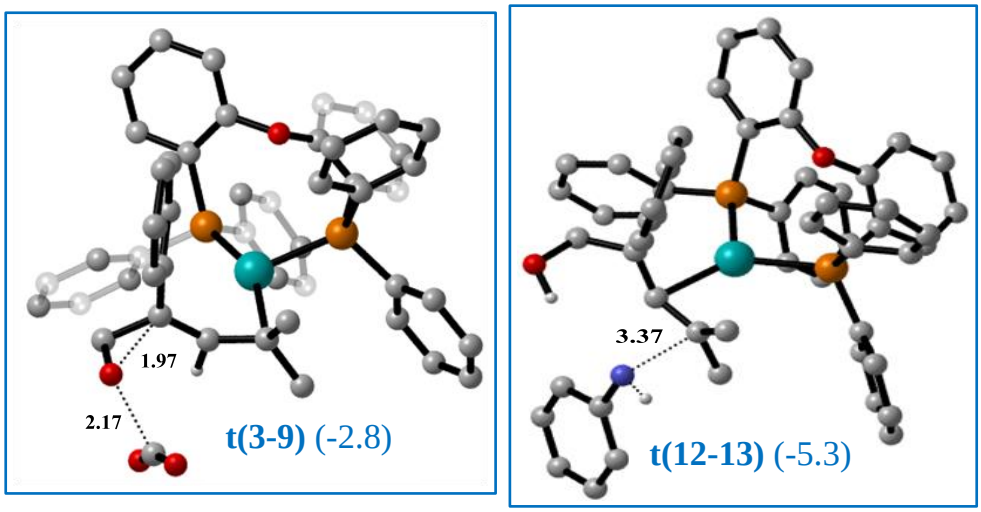

Figure 5.7. Optimized geometries of the key transition states involved in the formation of E-allylic amines p2. The relative free energies (kcal/mol) are given in parentheses. All distances are in Å

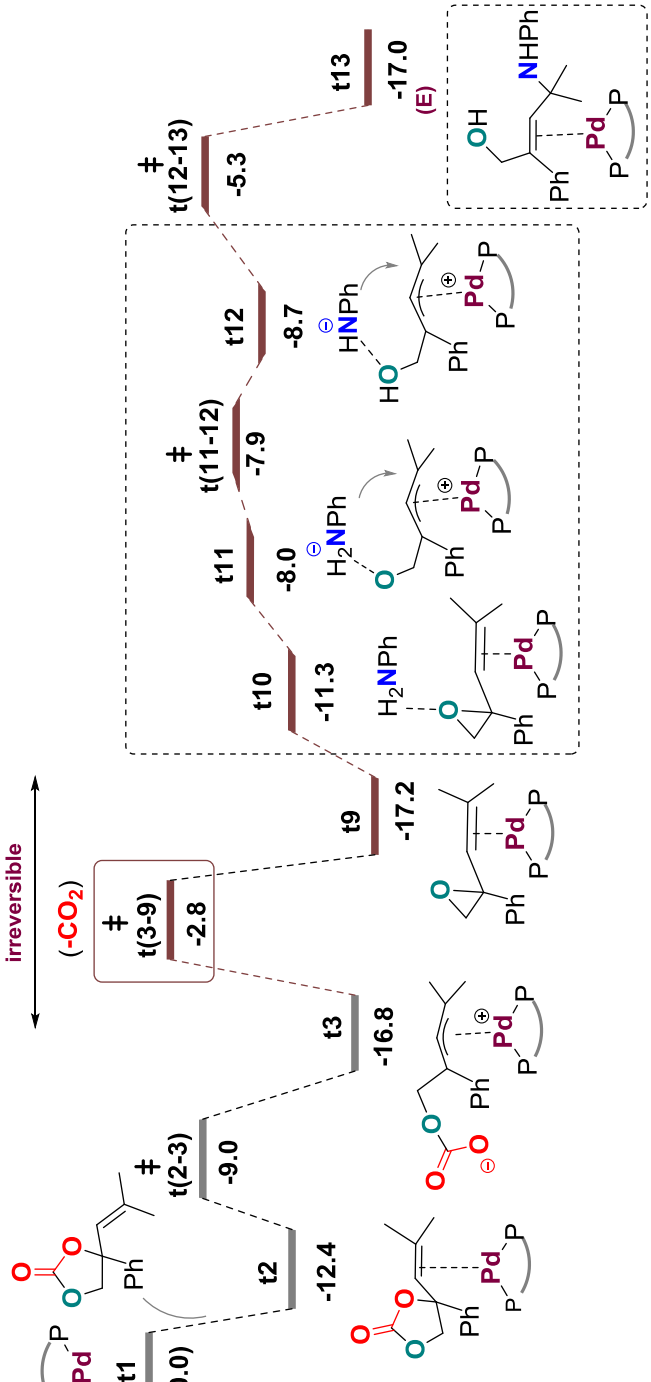

Figure 5.8. Free energy profile (kcal/mol) for the formation of E-allylic amines p2

evolve to a species **t9** containing an epoxide ring, which ultimately leads to a product in the E-configuration, **p2** after the nucleophilic attack.

5.3.1.3. Origin of Stereoselectivily

Since the reaction is characterized by highly stereocontrolled product formation, it is important to find the explanation for the major driving factor for the specific formation of Z-allylic amines **p2** over E-allylic amines **p1.** Close analysis of Figure 5.1 and Figure 5.8 reveals that irreversible CO_2 extrusion plays a key role in controlling the product formation. The key competing transition states are **t(4-5)** for the conversion of **t4→t5** in the **Z-pathway**, and **t(3-9)** for the conversion of **t3→t9** in the **E-pathway**. In the **Z-pathway** this barrier is 4.9 kcal/mol lower in energy, and therefore the formation of Z-allylic amine **p1** at room temperature is favored (28). There is a 6-membered palladacyclic intermediate **t5** in the **Z-pathway** which is absent in the **E-pathway**. The presence of this palladacycle seems the key difference between the two paths. The structural features of **t(4-5)** emphasize the importance of Pd–O chelation (bond length is 2.15 Å) to reduce the energy barrier and plays a key role towards the kinetic differentiation between both pathways leading to the (Z) and (*E*) product respectively. This Pd–O chelation is not feasible going through **t(3-9)** of the **E-pathway.**

Another important aspect here to analyse is the *syn*/*anti* isomerization (29) of the allyl–Pd species involved in the mechanism. The formation of pallacycle ring **t5** happens only because of the favourable $\pi-\sigma-\pi$ interconversion from **t3** to **t4**. This isomerization process has an energy of -7.7 kcal/mol, close to **t(4-5)** and much than **t(3-9)**. Thus, this means that *syn*/*anti* interconversion before CO_2 extrusion is kinetically feasible. Even

though CO_2 extrusion is an irreversible process; the system could still produce the E-allylic amine if the *syn*/*anti* isomerization were favourable after CO_2 extrusion. So it is relevant to make a detailed analysis of the possible *syn*/*anti* isomerization of allylic intermediates in Figure 5.1 to those in Figure 5.8. We investigated the hypothetic conversions **(t5→t9)**, **(t6→t11)** and **(t7→t12)** that could take place after CO_2 extrusion. The resulting profiles are shown in Figures 5.9, 5.10 and 5.11 respectively.

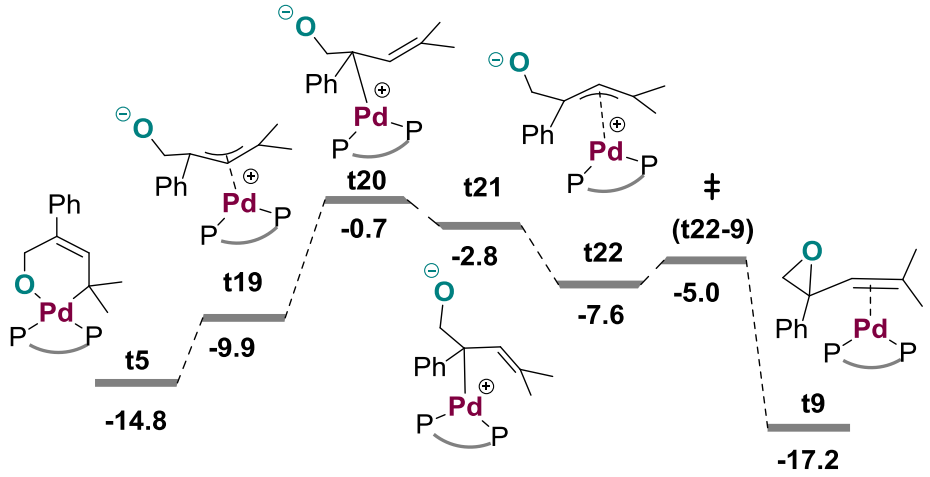

Figure 5.9. Free energy profile (kcal/mol) of *syn*/*anti* isomerization process from t5→t9 through $\pi-\sigma-\pi$ interconversion

It can be seen in Figures 5.9, 5.10 and 5.11 that the corresponding intermediates with the highest free energies, **t20, t24** and **t26** are at -0.7, -3.0 and –3.2 kcal/mol respectively. This is significantly above than the competing transition state to reach **p1**, which is **t(7-8)** with an energy at –9.3 kcal/mol. Thus, with an additional free energy requirement of at least 8.6 kcal/mol, these isomerization reactions are clearly disfavored under the experimental conditions. In short, the optimized catalytic system kinetically favors the Z isomer through a lower energy transition state that results in the formation of a six-membered palladacycle intermediate with Pd–O

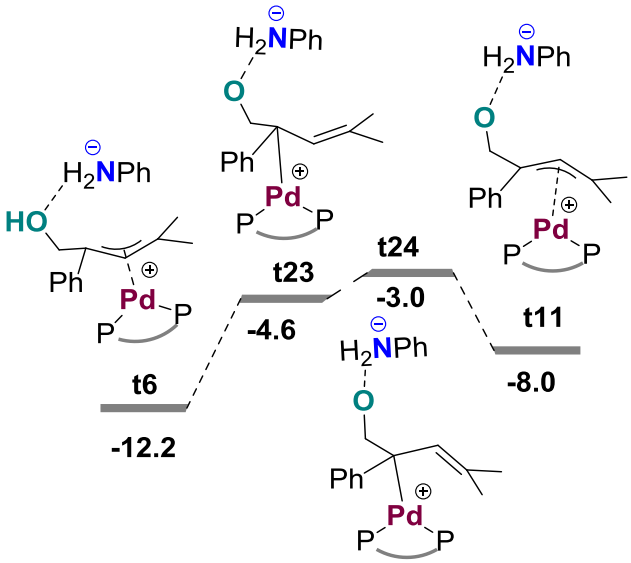

Figure 5.10. Free energy profile (kcal/mol) of *syn*/*anti* isomerization process from t6→t11 through $\pi-\sigma-\pi$ interconversion

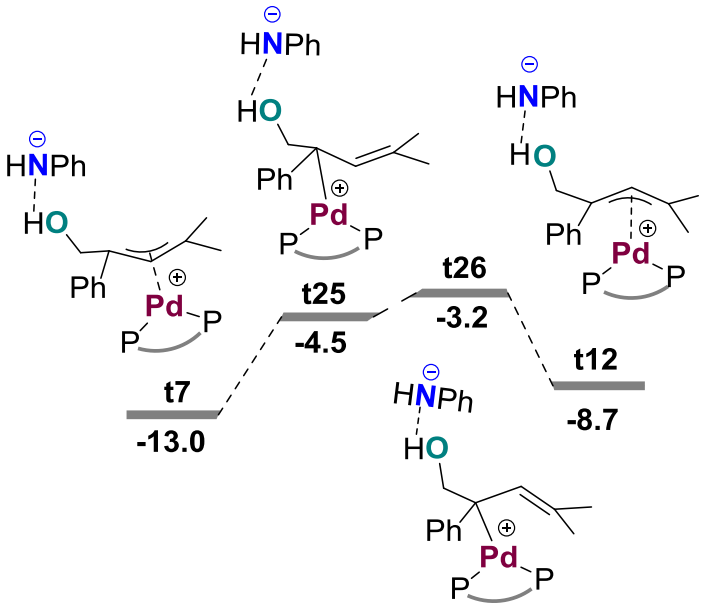

Figure 5.11. Free energy profile (kcal/mol) of *syn*/*anti* isomerization process from t7→t12 through $\pi-\sigma-\pi$ interconversion

chelation. The formation of intermediate **t5** is thus the key to the overall selectivity of the process.

5.3.2 Conclusion

The computed mechanism is in line with all experimental observations. DFT studies were used as a good tool in rationalizing the stereocontrol in these allylic amine formation reactions, and evidence is provided that the formation of a six-membered palladacyclic intermediate leads towards the formation of Z-configured allylic amine products. The current mechanism is more sophisticated than previous proposals focused on zwittterionic species (4), and sheds light on a new mode of stereocontrol. This can facilitate the design of more efficient processes for the functionalization of allylic surrogates.

Part 2

Palladium-Catalyzed Transformation of Cyclic Carbonates to Allylic Aldehydes

5.4 Pd-Catalyzed Transformation of Cyclic Carbonates to Allylic Aldehydes

Quaternary (chiral) carbons are ubiquitous in natural products and pharmaceutically relevant compounds. The construction of highly functionalized all quaternary carbons represents however a challenging task (30). Decarboxylative construction of quaternary carbons has been realized in intramolecular fashion (31), but the more general intermolecular coupling of reaction partners generating highly functionalized quaternary carbons with new Csp^3-Csp^3 bond formation via decarboxylative methodologies under mild conditions is still in its infancy (32). Previous work from the research groups by Tunge, Ooi and Zhang proved the possibility of a Pd-catalyzed additive-free decarboxylative construction of quaternary carbon centers via the reaction of electrophile and vinyl cyclic carbonate/carbamate under quite mild reaction conditions (4).

Kleij and co-workers demonstrated experimentally that the coupling of two vinyl cyclic carbonates can take place upon the extrusion of two CO_2 molecules resulting in a highly functionalized aldehyde product; the formation of this product features the construction of an otherwise synthetically challenging quaternary carbon center, a stereodefined multi-substituted allyl aldehyde fragment and also an aldehyde functionality (Scheme 5.9). Taking into account the high synthetic application potential (33) and interesting chemistry behind these complex scaffolds, this Pd-catalyzed decarboxylative process is an excellent method towards the construction of highly functionalized quaternary carbon centers (Scheme 5.9). Our experimental colleagues found remarkable the dependence of the reactivity on the nature of the substrate. Some substrates ($\mathbf{R_{K1}}$, Scheme 5.9) produce as major product the allylic aldehyde species **1**, where fragments from two molecules of substrate $\mathbf{R_K}$ are integrated into each molecule of product. In

contrast, other substrates ($\mathbf{R_{K2}}$, Scheme 5.9), produce only traces of species **1**, with the major product being aldehyde **2**, resulting from a single molecule of substrate **R**. In this part **2** of this chapter **5**, we will present the complete mechanistic study on this conversion of cyclic vinyl carbonate to allylic aldehydes.

For our calculations in this part 2 of this chapter we used the same method and catalyst (derived from the White precursor and DPEPhos ($\mathbf{L_1}$)) that we used in our study on conversion of cyclic carbonates to allylic amines reported above in part 1.

5.4.1 Results and Discussions

We studied the reaction with two different substrates, taken from the set of species experimentally investigated which are summarized in Scheme 5.9. The first substrate we studied was $\mathbf{R_{K14}}$,

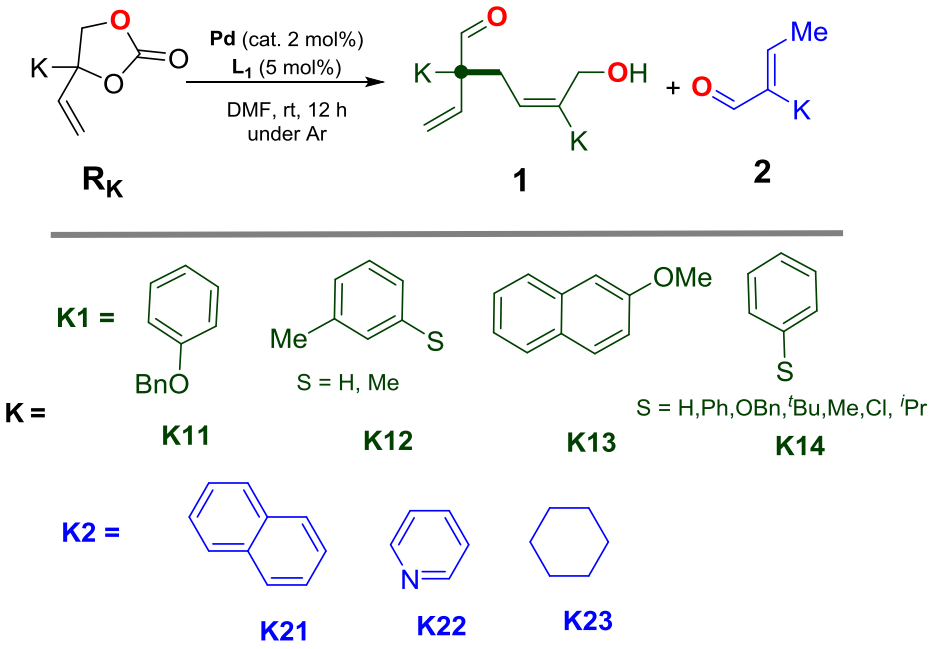

Scheme 5.9. Conversion of cyclic vinyl carbonates to allylic alcohol and aldehydes. Experimental results from the group of Kleij.

S=H (phenyl-substituted, denoted as **Rp** from here on) which gives allylic aldehyde **1** as the major product. The second one was $\mathbf{R_{K21}}$ (naphthyl-substituted, denoted as **Rn** from here on) which gives an aldehyde **2** as the major product.

The computed reaction mechanism happens to be quite complicated. Its main features are shown in a simplified version presented in Scheme 5.10 and Figure 5.12. Figure 5.12 shows the key species in the process. The cyclic vinyl carbonate has been labeled as **R**, The allylic aldehyde **1** has been labeled as **D** (dimer), and the monoaldehyde product **2** has been labeled as **M2** (monomer 2). There is an additional aldehyde species, not observed

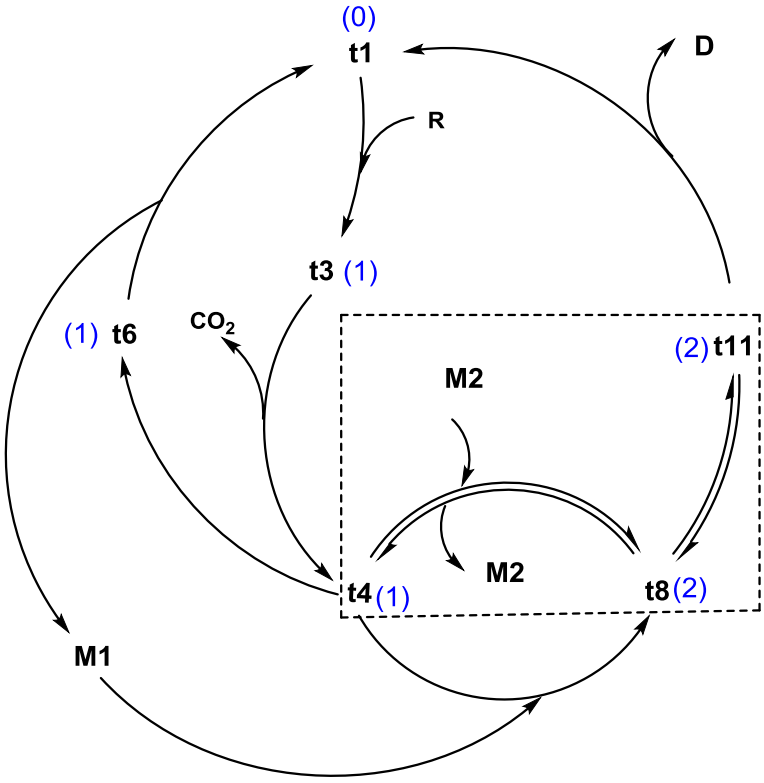

Scheme 5.10. Computed overall mechanism for the formation of allylic aldehyde D and monoaldehyde M2

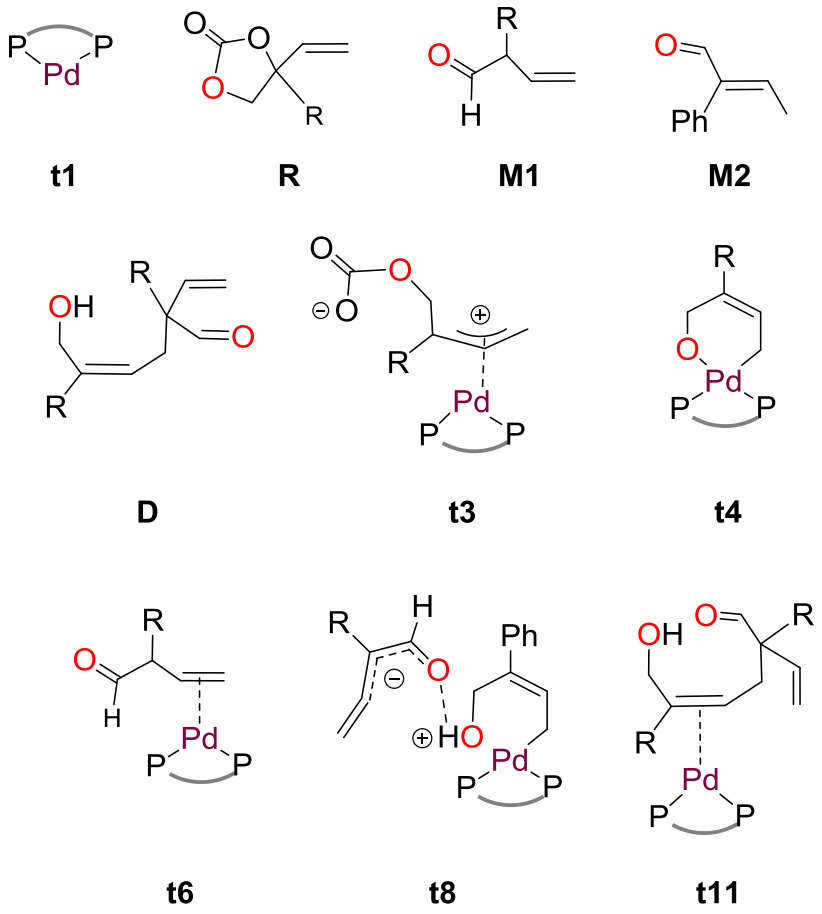

Figure 5.12. Structures of key intermediates in Scheme 5.10

experimentally, which we have labeled as **M1**. The free energy profile will be discussed in three parts outlined in Figures 5.13, 5.14 and 5.15. Figure 5.13 corresponds to the free energy profile for the reaction between **t1** and **R** to produce **M1** (which corresponds to the left part of the cycle in Scheme 5.10). Figure 5.14 corresponds to the second cycle which involves the reaction between **t4** and **M1** to produce **t8**. This corresponds to the bottom part of the cycle in Scheme 5.10. The third part, shown in the Figure 5.15 deals with the conversion of **t8** to either of the two possible products, **D** or **M2**. This corresponds to the boxed part in Scheme 5.10, covering the

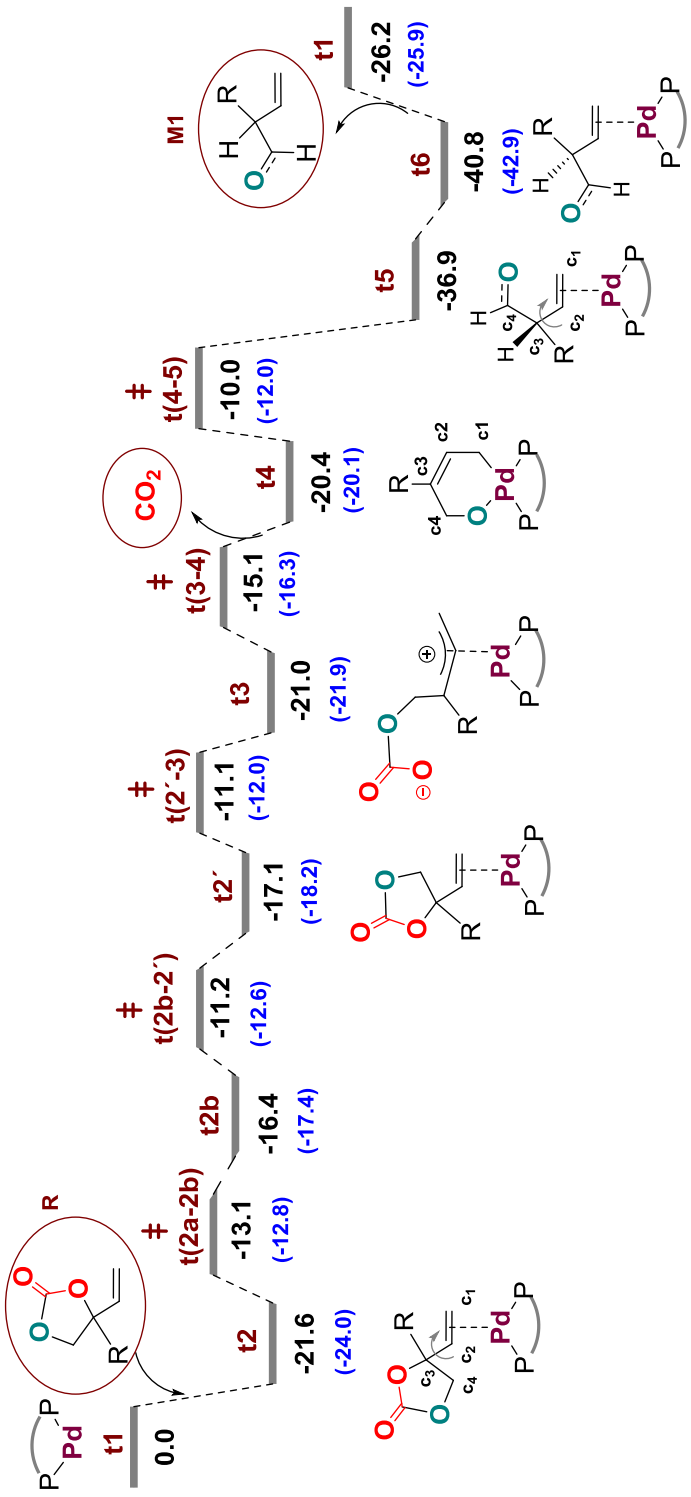

Figure 5.13. Free energy profile (kcal/mol) for the reaction of R with t1 to yield M1 and CO_2. Values in black correspond to reactant Rp (R= Phenyl) and values in blue correspond to reactant Rn (R=Naphthalene)

species in equilibrium. Initially Substrate **R** coordinates to the catalyst **t1** leading to the adduct **t2**. Unlike the favourable and necessary **t3-t4** *syn*/*anti* isomerization in part 1, which is needed for the formation of palladacycle ring, here the isomerization occurs before the oxidative cleavage of cyclic carbonate by the rotation of C_2-C_3 single bond of **t2**. This leads to the formation of **t2´** which is the isomer of **t2**. Further oxidative C-O cleavage takesplace in **t(2'-3)** and carbon dioxide extrusion in **t(3-4)** ends up in the formation of 6-membered palladacycle ring **t4** which follows the same path as discussed in part1. In the amination process, this intermediate **t4** reacted with aniline nucleophile and ended up in the formation of allylic amine products. In the current system there is no such additional nucleophile present. Instead the reactant **R** is present in excess. Even though there is excess of cyclic carbonate present in the system, it is however not nucleophilic enough to attack the **t4** and thus other alternative low energy paths should be considered. Intermediate **t4** can rearrange to **t5** through transition state **t(4-5)**, which implies reversion of Pd(II) to Pd(0). The barrier from **t4** to **t(4-5)** is not high (10.4 kcal/mol for **Rp**, 8.1 kcal/mol for **Rn**), but sufficient to preclude this step from taking place in the presence of a nucleophile. From **t5**, the aldehyde ligand then rearranges by the rotation of the C_2-C_3 single bond to intermediate **t6**, which is more stable than **t5**. Intermediate **t6** will finally release intermediate **M1** from the system to recover **t1**. The overall step is clearly exergonic, 26.2 kcal/mol for **Rp**, 25.9 kcal/mol for **Rn**.

The resulting aldehyde **M1** is sufficiently nucleophilic to attack **t4** in the next cycle. The allylic proton of **M1**, which is quite acidic, is transferred to the alkoxy center in the **t4** complex. The free energy indicated for **t4** in Figure 5.14 (-46.5 and -46.0 kcal/mol for **Rp** and **Rn** respectively) is different from that in Figure 5.13 (-20.4 and -20.1 kcal/mol for **Rp** and **Rn** respectively) because to reach this intermediate in Figure 5.14 an **M1** molecule has been

liberated in the system. The free energy barrier in this step for the transfer of proton from **M1** to **t4** via **t(7-8)** is very low: 2.0 kcal/mol for **Rp**, 0.8 kcal/mol for **Rn**. This barrier is always much lower than that from **t4** to **t5** discussed in Figure 5.13. This shows that **t4** will evolve to **t8** if a nucleophile such as **M1** is available. Thus, a second molecule of **R** is consumed to generate **t4** which then reacts with **M1** to generate intermediate **t8**. The overall step is mildly exergonic.

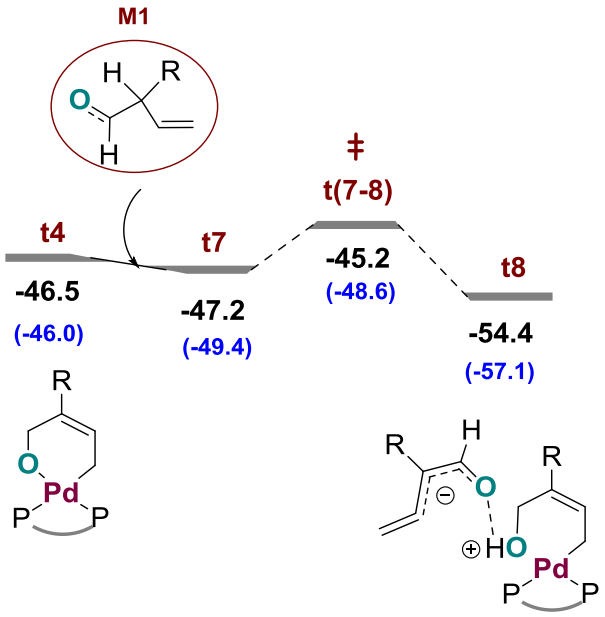

Figure 5.14. Free energy profile (kcal/mol) for the generation of t8 from t4 and M1. Values in black correspond to reactant Rp (R= phenyl) and values in blue correspond to reactant Rn (R= naphthalene)

Intermediate **t8**, which incorporates two molecules of reactant, can rearrange to intermediate **t11**, and then release the allylic aldehyde **D** and recover the catalyst **t1** along with the release of two molecules of CO_2. A catalytic cycle can be made with these steps as showed in the outer circle in Scheme 5.10, going through **t1**, **t4**, **t8** and **t11**. In this evolution towards **D** (green path, Figure 5.15),

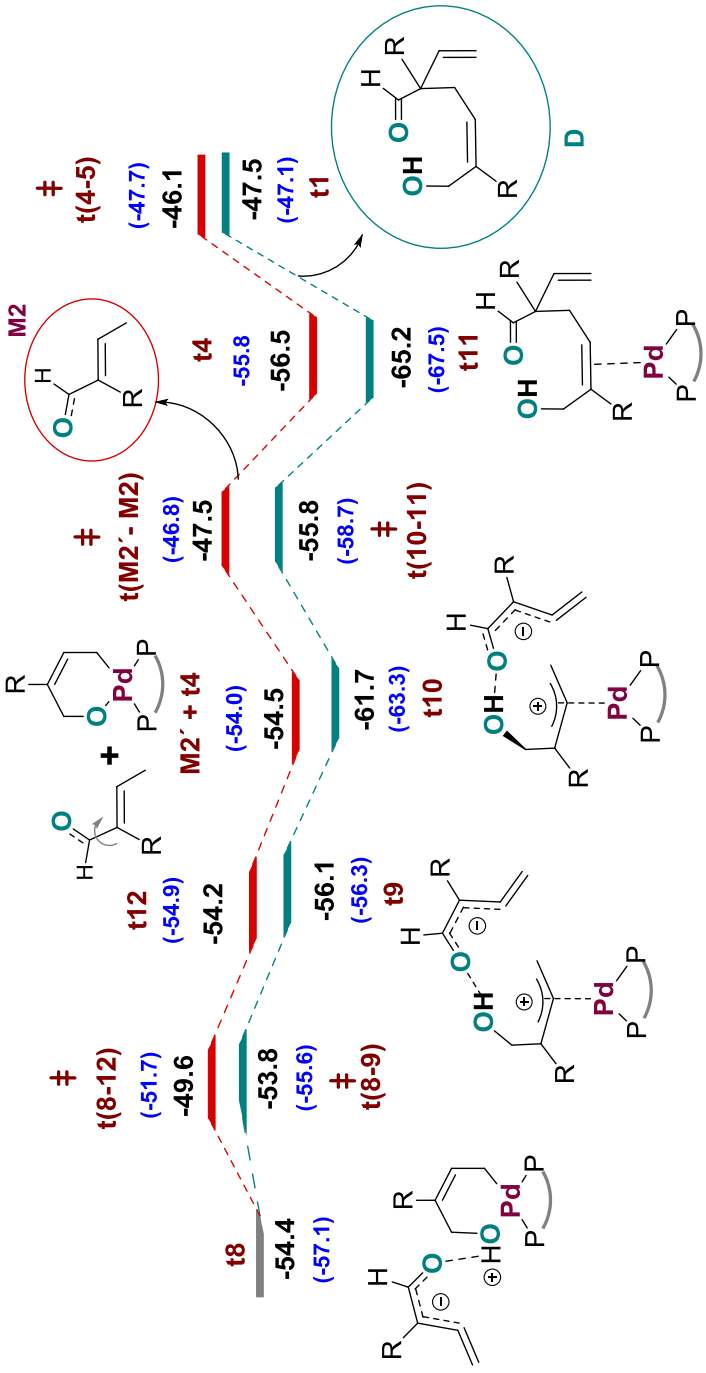

Figure 5.15. Computed free energy profile (kcal/mol) for the two possible evolutions from t8. The red pathway refers to the formation of aldehyde M2 and the green pathway refers to the formation of the allylic aldehyde D. Values in black correspond to reactant Rp (R= phenyl) and values in blue correspond to reactant Rn (R= naphtyl)

the protonation of the alkoxylic oxygen breaks the metallacycle structure. A formally cationic organic fragment coordinates the metallic fragment, and the deprotonated external fragment moves around it until reaching a proper placement to make a carbon-carbon bond in transition state **t(10-11).** Intermediate **t11** has already product **D** in the metal coordination sphere.

There is an alternative evolution for intermediate **t8**. It may release aldehyde **M2**, and return to **t4**. **M2** is significantly more stable than **M1** (34). The palladacyle **t4** then may release a unit of **M1** and return to **t1** to restart the cycle. Thus an alternative cycle can be constructed through **t1**, **t4**, **t8**, **t4** and **t6**. This cycle consumes one molecule of reactant **R** and yields product **M2** and a molecule of CO_2. In this evolution towards **M2** (red path, Figure 5.15), the metallacycle structure is kept, and the deprotonated external fragment moves in the coordination sphere until properly placed to accept a proton and result in the departure of product **M2** and regeneration of the metallacycle **t4**. The geometry of key transition states involved in the formation of allylic aldehyde, **D** and monoaldehyde **M2** for reactant **Rp** is given in Figure 5.16.

There are a lot of intermediates and transition states in Figure 5.15, but it is important to realize that all of them are in a close free energy span, meaning that all these species between **t4**, **t8** and **t11** are in equilibrium. The system can move freely from **t4** to **t11** with a minimum energy cost, and the final state of the system will be decided by the free energy barriers associated to the exit channels from this equilibrium. There are two of these exit channels. The exit channel from **t11** to **t1** yields product **D** and the exit channel from **t4** to **t6** yields product **M2**. If the system leaves the equilibrium through release of **D**, the catalyst **t1** will be regenerated, a new cycle will start and **D** will remain as product. It the system leaves the equilibrium through **t(4-5)**, **M2** will remain, and the

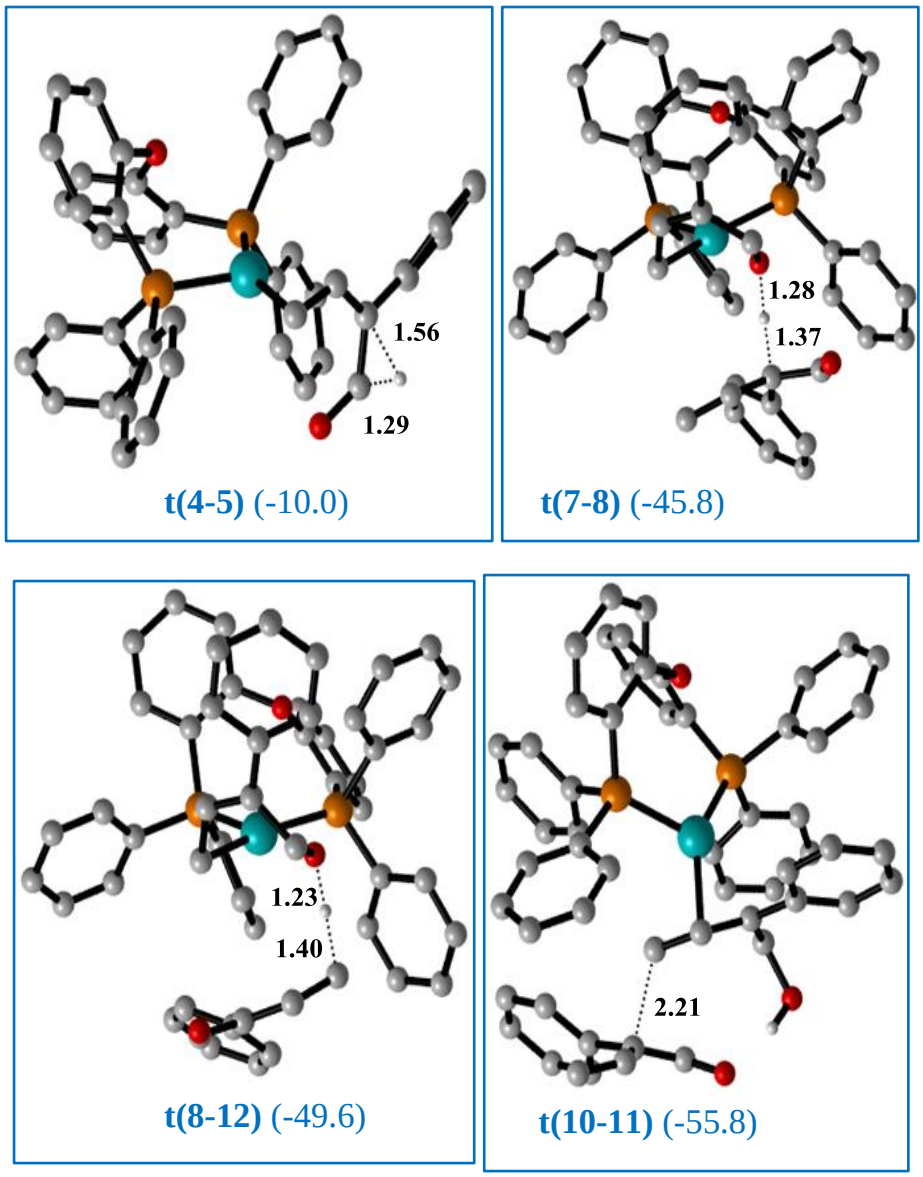

Figure 5.16. Optimized geometries of the important transition states involved in the formation of allylic aldehyde, D and monoaldehyde M2 for reactant Rp. Relative free energies (kcal/mol) are given in parentheses. All distances are in Å

catalyst will be regenerated *via* **t6**. The relative free energies associated to the exit channels are very close for both systems: -46.1/-47.5 kcal/mol for **Rp**, -47.7/-47.1 for **Rn**. This explains why the formation of both products is competitive. It also suggests a preference of product **D** for **Rp**, and a preference of product **M2** for **Rn**. But it is difficult to predict product distribution merely based on the free energy profiles in such a complicated cycle, and because of this we used a microkinetic models to obtain quantitative predictions.

5.4.2 Alternative Equilibrium Through t8'

Figure 5.17 presents an alternative pathway to that reported in Figure 5.15 for the equilibrium connecting **M2** plus **t4** with **t11**. This path differs from the previous one in that it does not go through intermediate **t8** but through an isomeric variation which we have labelled as **t8'**. The path in Figure 5.17 presents lower overall barrier, but it cannot completely replace that in Figure 5.15 because **t8'** is not accessible from the reaction between **t4** and **M1**. This alternative path is not shown in the simplified mechanism in Scheme 5.10 but it has been included in the microkinetic modeling of the process.

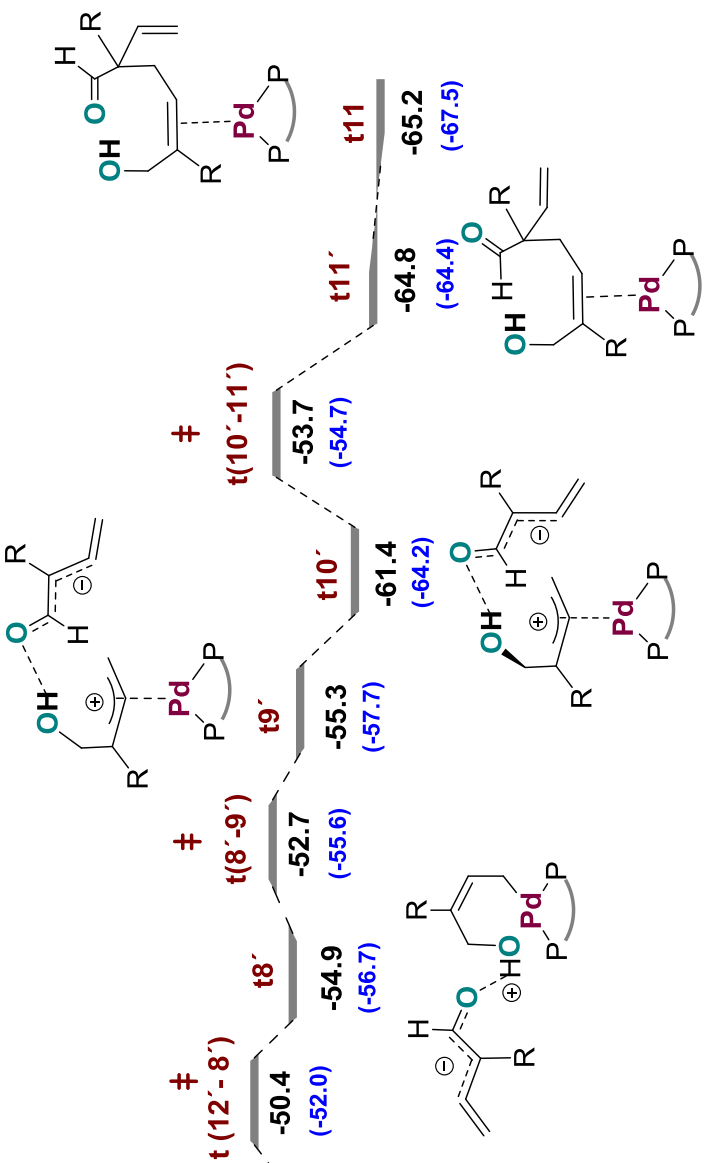

Figure 5.17. Computed free energy profile (kcal/mol) for an alternative equilibrium between M2 plus t4 and t11 going through intermediate t8'. Values in black correspond to reactant Rp (R= Phenyl) and values in blue corresponds to reactant Rn (R= naphthalene)

5.4.3 Microkinetic Modelling

We used the free energy profiles to compute rate constants and equilibrium constants for each step, and ran the calculation from the starting concentrations used in experiment.

5.4.3.1 Microkinetic Modeling for the Reaction of Rp

Table 5.1 collects the rate constants resulting from the application of the Eyring equation to the free energy barriers reported in the previous sections. We ran a simulation with these rate constants and starting concentrations 1.0 mmol/ml for **R** and 0.02 mmol/ml for **t1**. All the reactant was consumed in a very short time (less than sixty seconds). Reaction time was much shorter than in experiment, but this is because the likely rate limiting step is formation of the catalyst from the precursor, a step which is not considered in our model. The significant results were the final concentrations of 0.442 mmol/ml for **D** and 0.112 for **M2**. This means that 88% of **R** was converted into **D**, and 12% was converted into **M2**, thus a ratio of 88:12, close to experiment.

5.4.3.2 Microkinetic Modeling for the Reaction of Rn

Table 5.2 collects the rate constants resulting from the application of the Eyring equation to the free energy barriers reported in the previous sections. We ran a simulation with these rate constants and starting concentrations 1.0 mmol/ml for **R** and 0.02 mmol/ml for **t1**. All the reactant was consumed in a short time (nine hundred seconds). Reaction time was much shorter than in experiment as discussed in in the previous section. The significant results here were the concentrations of 0.0562 mmol/ml for **D** and 0.728 for **M2** and 0.159 for **M2'**. This means that 11% of **R** was converted into **D**, and 89% was converted into **M2** + **M2'**, thus a ratio of 11:89, close to experiment.

Table 5.1. Rate constants for each of the reaction steps considered in the microkinetic modeling of the reaction of Rp

Reaction	Barrier (kcal/mol)	Rate constant
t1 + R = t2	0.01	6.1056E+12
t2 = t3	10.5	123084.754
t3 = t2	9.9	339131.0763
t3 = t4 + CO_2	5.8	345263220.9
t4 = t6	10.4	145735.3191
t6 = t1 + M1	14.6	120.8986726
t4 + M1 = t8	2.0	2.1176E+011
t8 = t11	0.6	2.2537E+12
t11 = t8	11.4	26912.82408
t11 = t1 + D	17.7	0.643049414
t8 = t4 + M2´	4.8	1869630832
t4 + M2´ = t8	4.9	1579047909
M2´= M2	7	45480336.06
M2 = M2´	9	1551002.785

M2 + t4= t10´	6.1	208002547.7
t10´ = M2 + t4	11	52893.40068
t10´ = t11	7.7	13941188.02
t11= t0´	11.5	22729.96245

Table 5.1. Rate constants for each of the reaction steps considered in the microkinetic modeling of the reaction of Rn

Reaction	Barrier (kcal/mol)	Rate constant
t1 + R = t2	0.01	6.1056E+12
t2 = t3	12.0	9767.78173
t3 = t2	10.0	286422.4359
t3 = t4 + CO_2	5.6	484029048.7
t4 = t6	8.1	7093450.9
t6 = t1 + M1	17.0	2.097820029
t4 + M1 = t8	0.8	1.6076E+12
t8 = t11	1.5	4.9278E+11
t11 = t8	11.9	11565.28929

t11 = t1 + D	20.4	0.006722168
t8 = t4 + M2´	5.4	678566687.3
t4 + M2´ = t8	3.2	27894895024
m2´= M2	8.1	7093450.9
M2 = M2´	9	1551002.785
M2 + t4= t10´	5	1333628146
t10´ = M2 + t4	12.2	6967.465671
t10´ = t11	9.5	666514.8128
t11= t10´	12.8	2528.782698

5.4.4 Dependence of Reactivity on the Nature of the Substrate

We examined the optimized structures in search of a qualitative explanation for the product selectivity. There is no obvious steric influence from the phenyl/naphtyl replacement in any of them, as the extra ring in naphtyl points in all cases away from the rest of the atoms. In contrast, electronic effects are very likely having an effect in the structure of transition state **t(4-5)** in the exit channel leading to product **M2**. In this transition state, shown in Figure 5.16 for the system containing naphtyl, there is a hydrogen transfer between two carbon centers. One of these carbon centers, changing thus hybridization, is adjacent to the napthyl group, and this should account for a strong electronic influence. There is no such obvious electronic dependence in the exit channel leading to product **D** (Figure 5.15). Thus, electronic effects are likely the key to the selectivity between the two products. This

is indeed consistent with the experimental results reported above, where reactant **K13**, with a MeO-naphthyl substituent, was shown to behave similarly to **Rp** despite the large steric difference.

5.4.5 Conclusion

DFT calculations provide a complex mechanism that is able to reproduce with the help of microkinetic models the non-trivial dependence between the identity of the product and the nature of the substituents in the substrate. The ratios of products are close to the experimental observation suggesting the validity of our mechanistic proposal. These mechanistic insights can be further applied to develop new synthetic methodology to further construct highly functionalized quaternary carbon centers.

5.5. References

(1) Flynn, A. B.; Ogilvie, W. W. *Chem. Rev*. **2007**, *107*, 4698

(2) (a) Zhang, Y. J.; Yang, J. H.; Kim, S. H.; Krische, M. J. *J. Am. Chem. Soc*. **2010**, *132*, 4562 (b) Laserna, V.; Fiorani, G.; Whiteoak, C. J.; Martin, E.; Escudero-Ad, E. C.; Kleij, A. W. *Angew. Chem., Int. Ed.* **2014**, *53*, 10416

(3) (a) Khan, A.; Yang, L.; Xu, J.; Jin, L. Y.; Zhang, Y. J. *Angew. Chem., Int. Ed*. **2014**, 53, 11257 (b) Khan, A.; Zheng, R.; Kan, Y.; Ye, J.; Xing, J.; Zhang, Y. J. *Angew. Chem., Int. Ed*. **2014**, *53*, 6439 (c) Ohmatsu, K.; Imagawa, N.; Ooi, T. *Nat. Chem*. **2014**, *6*, 47 (d) Khan, A.; Xing, J.; Zhao, J.; Kan,Y.; Zhang, W.; Zhang, Y. J. *Chem. Eur. J*. **2015**, *21*, 120 (e) Yang, L.; Khan, A.; Zheng, R.; Jin, L. Y.; Zhang, Y. J. *Org. Lett.* **2015**, *17*, 6230 (f) Khan, A.; Zhang, Y. J. *Synlett* **2015**, *26*, 853

(4) (a) Guo, W.; Martínez-Rodríguez, L.; Kuniyil, R.; Martin, E.; Escudero-Adán, E. C.; Maseras, F.; Kleij, A. W. *J. Am. Chem. Soc.* **2016**, *138*, 11970 (b) Gómez, J. E.; Guo, W.; Kleij, A. W. *Org. Lett.* **2016**, *18*, 6042 (c) Guo, W.; Martínez-Rodríguez, L.; Martin, E.; Escudero-Adán, E.

C.; Kleij, A. W. *Angew. Chem., Int. Ed*. **2016**, *55*, 11037 (d) Cai, A.; Guo, W.; Martínez-Rodríguez, L.; Kleij A. W. *J. Am. Chem. Soc.* **2016**, *138*, 14194

(5) (a) Rintjema, J.; Epping, R.; Fiorani, G.; Martín, E.; Escudero-Adan, E. C.; Kleij, A. W. *Angew. Chem., Int. Ed*. **2016**, *55*, 3972 (b) Guo, W.; Gonzalez-´ Fabra, J.; Bandeira, N. A. G.; Bo, C.; Kleij, A. W. *Angew. Chem., Int. Ed.* **2015**, *54*, 11686

(6) Kang, S.-K.; Kim, S.-G.; Lee, J.-S. *Tetrahedron: Asymmetry* **1992**, *3*, 1139

(7) Li, T.-R.; Tan, F.; Lu, L.-Q.; Wei, Y.; Wang, Y.-N.; Liu, Y.-Y.; Yang, Q.-Q.; Chen, J.-R.; Shi, D.-Q.; Xiao, W.-J. *Nat. Commun.* **2014**, *5*, 5500

(8) (a) Sperger, T.; Sanhueza, I. A.; Kalvet, I.; Schoenebeck, F. *Chem. Rev.* **2015**, *115*, 9532 (b) Mora, G.; Piechaczyk, O.; Le Goff, X. F.; Le Floch, P. *Organometallics* **2008**, *27*, 2565

(9) Balcells, D.; Maseras, F. *New J. Chem.* **2007**, *31*, 333

(10) (a) Whiteoak, C. J.; Nova, A.; Maseras, F.; Kleij, A. W. *ChemSusChem* **2012**, *5*, 2032 (b) Schmeier, T. J.; Nova, A.; Hazari, N.; Maseras, F. *Chem. - Eur. J.* **2012**, *18*, 6915 (c) Castro-Gomez, G.; Salassa, G.; Kleij, A. W.; Bo, C. *Chem. - Eur. J.* **2013**, *19*, 6289 (d) Jover, J.; Maseras, F. *J. Org. Chem.* **2014**, *79*, 11981 (e) Li, H.; Hall, M. B. *J. Am. Chem. Soc*. **2014**, *136*, 383 (f) Li, H.; Hall, M. B. *J. Am. Chem. Soc.* **2015**, *137*, 12

(11) Ref.1, Appendix

(12) Ref.2, Appendix

(13) Ref.3, Appendix

(14) Ref.4, Appendix

(15) Ref.5, Appendix

(16) Ref.6, Appendix

(17) Ref.7, Appendix

(18) Braun, W.; Herron, J. T.; Kahaner, D. K. *Int. J. Chem. Kinet*. **1988**, *20*, 51

(19) (a) Trost, B. M.; Crawley, M. L. *Chem. Rev*. **2003**, *103*, 2921 (b) Johannsen, M.; Jørgensen, K. A. *Chem. Rev*. **1998**, *98*, 1689 (c) Trost, B. M.; Van Vranken, D. L. *Chem. Rev*. **1996**, *96*, 395 (d) Huang, L.; Arndt, M.; Gooßen, K.; Heydt, H.; Gooßen, L. J. *Chem. Rev*. **2015**, *115*, 2596 (e) Müller, T. E.; Beller, M. *Chem. Rev*. **1998**, *98*, 675 (f) Hong, S.; Marks, T. J. *Acc. Chem. Res*. **2004**, *37*, 673 (g) Müller, T. E.; Hultzsch, K. C.; Yus, M.; Foubelo, F.; Tada, M. *Chem. Rev*. **2008**, *108*, 3795

(20) (a) Butt, N. A.; Zhang, W. *Chem. Soc. Rev.* **2015**, *44*, 7929 (b) Arnold, J. S.; Zhang, Q.; Nguyen, H. M. *Eur. J. Org. Chem*. **2014**, 4925 (c) Trost, B. M.; Zhang, T.; Sieber, J. D. *Chem. Sci*. **2010**, *1*, 427 (d) Leitner, A.; Shu, C.; Hartwig, J. F. *Org. Lett.* **2005**, *7*, 1093 (e) Moreno-Mañas, M.; Morral, L.; Pleixats, R. *J. Org. Chem*. **1998**, *63*, 6160 (f) Leitner, A.; Shekhar, S.; Pouy, M. J.; Hartwig, J. F. *J. Am. Chem. Soc.* **2005**, *127*, 15506 (g) Shekhar, S.; Trantow, B.; Leitner, A.; Hartwig, J. F. *J. Am. Chem. Soc.* **2006**, *128*, 11770 (h) Plietker, B. *Angew. Chem., Int. Ed.* **2006**, *45*, 6053 (i) Das, K.; Shibuya, R.; Nakahara, Y.; Germain, N.; Ohshima, T.; Mashima, K. *Angew. Chem., Int. Ed*. **2012**, *51*, 150 (j) Gumrukcu, Y.; de Bruin, B.; Reek, J. N. H. *ChemSusChem* **2014**, *7*, 890 (k) Yang, S.-C.; Tsai, Y.-C. *Organometallics* **2001**, *20*, 763 (l) Kinoshita, H.; Shinokubo, H.; Oshima, K. *Org. Lett.* **2004**, *6*, 4085 (m) Ghosh, R.; Sarkar, A. *J. Org. Chem.* **2011**, *76*, 8508 (n) Ohshima, T.; Miyamoto, Y.; Ipposhi, J.; Nakahara, Y.; Utsunomiya, M.; Mashima, K. *J. Am. Chem. Soc.* **2009**, *131*, 14317 (o) Pace, V.; Martínez, F.; Fernádez, M.; Sinisterra, J. V.; Alcántara, A. R. *Org. Lett.* **2007**, *9*, 2661 (p) Dubovyk, I.; Watson, I.

D. G.; Yudin, A. K. *J. Org. Chem.* **2013**, *78*, 1559 (q) Adak, L.; Chattopadhyay, K.; Ranu, B. C. *J. Org. Chem*. **2009**, *74*, 3982

(21) (a) Banerjee, D.; Junge, K.; Beller, M. *Angew. Chem., Int. Ed.* **2014**, *53*, 1630 (b) Banerjee, D.; Junge, K.; Beller, M. *Org. Chem. Front.* **2014**, *1*, 368 (c) Yi, C. S.; Yun, S. Y. *Org. Lett.* **2005**, *7*, 2181 (d) Minami, T.; Okamoto, H.; Ikeda, S.; Tanaka, R.; Ozawa, F.; Yoshifuji, M. *Angew. Chem., Int. Ed.* **2001**, *40*, 4501 (e) Qin, H.; Yamagiwa, N.; Matsunaga, S.; Shibasaki, M. *J. Am. Chem. Soc.* **2006**, *128*, 1611

(22) (a) Reed, S. A.; White, M. C. *J. Am. Chem. Soc.* **2008**, *130*, 3316 (b) Yin, G.; Wu, Y.; Liu, G. *J. Am. Chem. Soc.* **2010**, *132*, 11978 (c) Sharma, A.; Hartwig, J. F. *J. Am. Chem. Soc*. **2013**, *135*, 17983 (d) Paradine, S. M.; Griffin, J. R.; Zhao, J.; Petronico, A. L.; Miller, S. M.; White, M. C. *Nat. Chem*. **2015**, *7*, 987 (e) C. C. Pattillo, I. I. Strambeanu, P. Calleja, N. A. Vermeulen, T. Mizuno, M. C. White, *J. Am. Chem. Soc.* **2016***, 138*, 1265

(23) (a) Martínez, C.; Martínez, L.; Kirsch, J.; Escudero-Adán, E. C.; Martin, E.; Muñiz, K. *Eur. J. Org. Chem*. **2014**, 201 (b) Lishchynskyi, A.; Muñiz, K. *Chem. Eur. J.* **2012**, *18*, 2212

(24) (a) Hikawa, H.; Yokoyama, Y. *Org. Biomol. Chem.* **2011**, *9*, 4044 (b) Yokoyama, Y.; Takagi, N.; Hikawa, H.; Kaneko, S.; Tsubaki, N.; Okuno, H. *Adv. Synth. Catal.* **2007**, *349*, 662 (c) Ramanathan, B.; Odom, A. L. *J. Am. Chem. Soc.* **2006**, *128*, 9344 (d) Zeng, X.; Soleilhavoup, M.; Bertrand, G. *Org. Lett.* **2009**, *11*, 3166 (e) Trost, B. M.; Malhotra, S.; Chan, W. H. *J. Am. Chem. Soc.* **2011**, *133*, 7328 (f) Fang, X.; Li, H.; Jackstell, R.; Beller, M. *J. Am. Chem. Soc.* **2014**, *136*, 16039

(25) (a) Hussain, N.; Hussain, M. M.; Ziauddin, M.; Triyawatanyu, P.; Walsh, P. J. *Org. Lett.* **2011**, *13*, 6464 (b) Tonogaki, K.; Itami, K.; Yoshida, J. *J. Am. Chem. Soc.* **2006**, *128*, 1464 (c) Xie, M.; Sun, Y.; Zhang, W.; Gu, X.; Zhao, X.; Xie, F.; Wang, S. *Synth. Commun.* **2008**,

38, 3785 (d) Patel, S. J.; Jamison, T. F. *Angew. Chem., Int. Ed*. **2004**, *43*, 3941 (e) By non-catalytic allylic substitutions: Sen, S. E.; Roach, S. L. *Synthesis*, **1995**, *7*, 756 (f) Anumandla, D.; Littlefield, R.; Jeffrey, C. S. *Org. Lett.* **2014**, *16*, 5112

(26) (a) Taillemaud, S.; Diercxsens, N.; Gagnon, A.; Charette, A. B. *Angew. Chem., Int. Ed.* **2015**, *54*, 14108 (b) Chen, H.; Kaga, A.; Chiba, S. *Org. Biomol. Chem.* **2016**, *14*, 5481 (c) He, Z.; Wibbeling, B.; Studer, A. *Adv. Synth. Catal*. **2013**, *355*, 3639 (d) Rama, R. N; Soni, V. K. *Adv. Synth. Catal*. **2015**, *358*, 276 (e) He, Z.; Kirchberg, S.; Fröhlich, R.; Studer, A. *Angew. Chem., Int. Ed*. **2012**, *51*, 3699 (f) Zhang, C.; Santiago, C. B.; Crawford, J. M.; Sigman, M. S. *J. Am. Chem. Soc*. **2015**, *137*, 15668 (g) Zhang, C.; Santiago, C. B.; Crawford, J. M.; Sigman, M. S. *J. Am. Chem. Soc*. **2015**, *137*, 15668 (h) Zhu, S.; Niljianskul, N.; Buchwald, S. L. *Nat. Chem*. **2016**, *8*, 144

(27) (a) Akermark, B.; Bäckvall, J.-E.; Löwenborg, K.; Zetterberg, K. *J. Organomet. Chem*. **1979**, *166*, C33 (b) Bäckvall, J. E. *Acc. Chem. Res*. **1983**, *16*, 335

(28) Note that experimentally the formation Z-allylic amine **p1** requires longer reaction times than suggested by the energetic span (12.0 kcal/mol) computed for its formation (Figure 8). However, the calculation starts off with a Pd(0) catalyst and the formation of the latter from Pd(II) acetate precursor in the presence of excess phosphine has been reported previously to be more energy demanding. See: (a) Amatore, C.; Carré, E.; Jutand, A.; M'Barki, M. A. *Organometallics* **1995**, *14*, 1818 (b) Amatore, C.; Jutand, A.; Thuilliez, A. *Organometallics* **2001**, *20*, 3241 (c) Wei, C. S.; Davies, G. H. M.; Soltani, O.; Albrecht, J.; Gao, Q. *Angew. Chem., Int. Ed*. **2013**, *52*, 5822

(29) (a) Trost, B. M.; Machacek, M. R.; Aponick, A. *Acc. Chem. Res*. **2006**, *39*, 747 (b) Ogasawara, M.; Takizawa, K.; Hayashi, T. *Organometallics* **2002**, *21*, 4853 (c) Tsuji, J. *Pure Appl. Chem*. **1982**, *54*,

197 (d) Hayashi, T.; Kawatsura, M.; Uozumi, Y. *J. Am. Chem. Soc.* **1998**, *120*, 1681

(30) (a) Zeng, X.-P.; Cao, Z.-Y.; Wang, Y.-H.; Zhou, F.; Zhou, J. *Chem. Rev*. **2016**, *116* (b) Fuji, K. *Chem. Rev*. **1993**, *93*, 2037 (c) Mei, T.-S.; Patel, H. H.; Sigman, M. S. *Nature* **2014**, *508*, 340 (d) Murphy, J. J.; Bastida, D.; Paria, S.; Fagnoni, M.; Melchiorre, P. *Nature* **2016**, *532*, 218 (e) Masarwa, A.; Didier, D.; Zabrodski, T.; Schinkel, M.; Ackermann, L.; Marek, I. *Nature* **2014**, *505*, 199 (f) Krautwald, S.; Sarlah, D.; Schafroth, M. A.; Carreira, E. M. *Science* **2013**, *340*, 1065

(31) (a) Behenna, D. C.; Liu, Y.; Yurino, T.; Kim, J.; White, D. E.; Virgil, S. C.; Stoltz, B. M. *Nat. Chem*. **2012**, *4*, 130 (b) Chen, Z.-S.; Duan, X.-H.; Zhou, P.-X.; Ali, S.; Luo, J.-Y.; Liang, Y.-M. *Angew. Chem., Int. Ed*. **2012**, *51*, 1370 (c) Trost, B. M.; Xu, J.; Schmidt, T. *J. Am. Chem. Soc.* **2009**, *131*, 18343 (d) Ghosh, S.; Bhunia, S.; Kakde, B. N.; De, S.; Bisai, A. *Chem. Commun*. **2014**, *50*, 2434

(32) (a) Weaver, J. D.; Recio, III, A.; Grenning, A. J.; Tunge, J. A. *Chem. Rev*. **2011**, *111*, 1846 (b) Cornella, J.; Larrosa, I. *Synthesis* **2012**, *44*, 653 (c) Satoh, T.; Miura, M. *Synthesis* **2010**, 3395 (d) Rodríguez, N.; Goossen, L. J. *Chem. Soc. Rev.* **2011**, *40*, 5030 (e) Li, C.; Breit, B, *J. Am. Chem. Soc.* **2014**, *136*, 862 (f) Shintani, R.; Tsuji, T.; Park, S.; Hayashi, T. *J. Am. Chem. Soc.*, **2010**, *132*, 7508

(33) (a) Huang, X.; Wu, S.; Wu, W.; Li, P.; Fu, C.; Ma, S. *Nat. Commun.* **2017**, 12382 (b) Kimura, M.; Mukai, R.; Tamaki, T.; Horino, Y.; Tamaru, Y. *J. Am. Chem. Soc.* **2007**, *129*, 4122 (c) Araki, S.; Usui, H.; Kato, M.; Butsugan, Y. *J. Am. Chem. Soc.* **1996**, *118*, 4699

(34) The isomerization from **M1** to **M2** has also been noted by others for instance: Newcomb, M.; Chestney, D. L. *J. Am. Chem. Soc.* **1994**, *116*

Chapter 6

Conclusion

We have shown that the mechanism of the relevant transition metal catalyzed CO_2 activation can be successfully characterized by computational chemistry using the DFT approach. The B97D has been found to be a sufficient choice as functional. Geometry optimization with a double-zeta plus polarization basis set was found sufficient, as far as the results are refined by single point calculations with a larger basis set. The usage of multilayer method was successful in terms of computational cost without compromising the qualitative result for the systems with bulkier ligands. Microkinetic models were necessary to reproduce the ratio of products in selected cases with convoluted reaction mechanisms.

Concerning the specific reactions covered in this thesis, an in depth discussion on the conclusion has been covered in their respective chapters. In this section only the main points are summarized.

Regarding the allene carboxylation reaction:

- The reaction takes place through two interlinked catalytic cycles, one of them activates carbon dioxide, and the other one activates allene. The two cycles are interconnected by shared palladium intermediates and by the transfer of a formate intermediate between them.
- $AlEt_3$ assists all the important steps in the mechanism including allene insertion and CO_2 activation

On the reaction of carbon dioxide with siloxy silane:

- The seemingly innocent counterion Cs^+ in the fluoride salt plays a critical role lowering the free energy barriers in the reaction.
- The reproduction of the experimental results requests the explicit introduction of the counterion and the solvent molecules in its first coordination sphere.

Concerning the conversion of cyclic carbonates to Z-allylic amines and aldehydes:

- Stereocontrol is ruled by the formation of a six-membered palladacyclic intermediate that leads towards the formation of Z-configured products. The reaction is complex and involves many competing steps. *Syn-Anti* isomerization of the contributing intermediates has been in particular studied in detail, and found to be possible before the selectivity-determing step but not after it.
- The non-trivial dependence between the identity of the product and the nature of the substituents in the substrate requires the introduction of microkinetic models for its proper reproduction.

Appendix

(1) Koch, W.; Holthausen, M. C. *A Chemist's Guide to Density Functional Theory*, *2nd Edition*, Wiley New York, **2001**

(2) Grimme, S. *J. Comput. Chem.* **2006**, *27*, 1787 (b) Becke, A. D. *J. Chem. Phys.* **1997**, *107*, 8554

(3) Frisch, M. J.; Trucks, G. W.; Schlegel, H. B.; Scuseria, G. E.; Robb, M. A.; Cheeseman, J. R.; Scalmani, G.; Barone, V.; Mennucci, B.; Petersson, G. A.; Nakatsuji, H.; Caricato, M.; Li, X.; Hratchian, H. P.; Izmaylov, A. F.; Bloino, J.; Zheng, G.; Sonnenberg, J. L.; Hada, M.; Ehara, M.; Toyota, K.; Fukuda, R.; Hasegawa, J.; Ishida, M.; Nakajima, T.; Honda, Y.; Kitao, O.; Nakai, H.; Vreven, T.; Montgomery, J. A., Jr.; Peralta, J. E.; Ogliaro, F.; Bearpark, M.; Heyd, J. J.; Brothers, E.; Kudin, K. N.; Staroverov, V. N.; Kobayashi, R.; Normand, J.; Raghavachari, K.; Rendell, A.; Burant, J. C.; Iyengar, S. S.; Tomasi, J.; Cossi, M.; Rega, N.; Millam, J. M.; Klene, M.; Knox, J. E.; Cross, J. B.; Bakken, V.; Adamo, C.; Jaramillo, J.; Gomperts, R.; Stratmann, R. E.; Yazyev, O.; Austin, A. J.; Cammi, R.; Pomelli, C.; Ochterski, J. W.; Martin, R. L.; Morokuma, K.; Zakrzewski, V. G.; Voth, G. A.; Salvador, P.; Dannenberg, J. J.; Dapprich, S.; Daniels, A. D.;Farkas, O.; Foresman, J. B.; Ortiz, J. V.; Cioslowski, J.; Fox, D. J. *Gaussian 09*, Revision D.01; Gaussian, Inc. Wallingford, CT, **2009**

(4) Marenich, A. V.; Cramer, C. J.; Truhlar, D. G. *J. Phys. Chem. B.* **2009**, *113*, 6378

(5) Andrae, D.; Haeussermann, U.; Dolg, M.; Stoll, H.; Preuss, H.; *Theor. Chim. Acta.* **1991**, *78*, 247 (b) Andrae, D.; Haeussermann, U.; Dolg, M.; Stoll, H.; Preuss, H.; *Theor. Chim. Acta.* **1990**, *77*, 123

(6) Hariharan, P. C.; Pople, J. A. *Theoret. Chim. Acta.* **1973**, *28*, 213 (b) Francl, M. M.; Petro, W. J.; Hehre,W. J.; Binkley, J. S.; Gordon, M. S.;

DeFrees, D. J.; Pople, J. A. *J. Chem. Phys*. **1982**, *77*, 3654

(7) (a) Krishnan, R.; Binkley, J. S.; Seeger, R.; Pople, J. A. *J. Chem. Phys*. **1980,** *72*, 650 (b) Clark, T.; Chandrasekhar, J.; Spitznagel, G. W.; Schleyer, P. V. R. *J. Comp. Chem*. **1983**, *4*, 294

(8) Hay, P. J.; Wadt. W. R. *J. Chem. Phys.* **1985**, *82*, 270 (b) Hay, P. J.; Wadt, W. R. *J. Chem. Phys.* **1985**, *82*, 284 (c) Hay, P. J.; Wadt, W. R. *J. Chem. Phys.* **1985**, *82*, 299

(9) (a) Warshel, A. J.; Levitt, M. *J. Mol. Biol*. **1976**, *103*, 227 (b) Dapprich, S.; Komromi, I.; Byun, K.; Morokuma, K.; Frisch, M. J. *J. Mol. Struct. (THEOCHEM)* **1999**, *461462*, 1

(10) Rappé, R. K.; Casewit, C. J.; Colwell, K. S.; Goddard III, W. A.; Skiff, W. M. *J. Am. Chem. Soc.* **1992**, *114*, 10024

UNIVERSITAT ROVIRA I VIRGILI
COMPUTATIONAL MECHANISTIC STUDIES ON THE TRANSITION METAL CATALYZED ACTIVATION OF CARBON DIOXIDE
Rositha Kuniyil

UNIVERSITAT
ROVIRA i VIRGILI